DISCRETE FRACTURE NETWORK MODELING OF ALAŞEHIR
GEOTHERMAL FIELD

A THESIS SUBMITTED TO
THE GRADUATE SCHOOL OF NATURAL AND APPLIED SCIENCES
OF
MIDDLE EAST TECHNICAL UNIVERSITY

BY

HAKKI AYDIN

IN PARTIAL FULFILLMENT OF THE REQUIREMENTS
FOR
THE DEGREE OF MASTER OF SCIENCE
IN
PETROLEUM AND NATURAL GAS ENGINEERING

JUNE 2018

Approval of the Thesis:

DISCRETE FRACTURE NETWORK MODELLING OF ALAŞEHİR GEOTHERMAL FIELD

Submitted by **HAKKI AYDIN** in partial fulfillment of the requirements for the degree of **Master of Science in Petroleum and Natural Gas Engineering Department, Middle East Technical University** by,

Prof. Dr. Halil Kalıpçılar
Dean, Graduate School of **Natural and Applied Sciences** _____

Prof. Dr. Serhat Akın
Head of Department, **Petroleum and Natural Gas Engineering** _____

Prof. Dr. Serhat Akın
Supervisor, **Petroleum and Natural Gas Eng. Dept., METU** _____

Examining Committee Members:

Asst. Prof. İsmail Durgut
Petroleum and Natural Gas Engineering Dept., METU _____

Prof. Dr. Serhat Akın
Petroleum and Natural Gas Engineering Dept., METU _____

Assoc. Prof. Dr. Ali Bülbül
Geological Engineering Dept., Pamukkale Universty _____

Date: 27.06.2018

I hereby declare that all information in this document has been obtained and presented in accordance with academic rules and ethical conduct. I also declare that, as required by these rules and conduct, I have fully cited and referenced all material and results that are not original to this work.

Name, Last name: Hakkı Aydın

Signature:

ABSTRACT

**DISCRETE FRACTURE NETWORK MODELING IN ALASEHIR
GEOTHERMAL FIELD**

Aydin, Hakki

M.S., Department of Petroleum and Natural Gas Engineering

Supervisor: Prof. Dr. Serhat Akin

June 2018, 107 pages

Understanding of fractures network and fracture characteristic properties is essential for an effective geothermal reservoir management. Discrete Fracture Network (DFN) is one of the widely used approach to characterize fractured reservoirs. DFN modeling approach uses fracture geometry, conductivity and connectivity to create a fracture network. In this study, DFN modeling is used to characterize Alaşehir geothermal reservoir, which consists from heavily fractured marble and schist. Fracture parameters such as fracture permeability, aperture, intensity and fracture radius are conditioned for model calibration. Most of the required fracture parameters are retrieved from different data sources. Stochastic correlations related with known parameters are used to estimate unavailable parameters. The dynamic model results are verified with pressure transient buildup tests conducted in the field. Upscaled fracture properties are in accord with well test analysis and tracer test results. DFN model shows that all wells are interconnected by strong fractures network. Fractures network is validated with a tracer test and reservoir monitoring in the field.

Keywords: Natural Fractures, Discrete Fracture Network Modeling, Marble, Schist

ÖZ

ALAŞEHİR JEOTERMAL SAHASININ AYRIK ÇATLAK AĞ MODELLEMESİ

Aydın, Hakkı

Yüksek Lisans, Petrol ve Doğal Gaz Mühendisliği Bölümü

Tez Yöneticisi: Prof. Dr. Serhat Akın

Haziran 2018, 107 sayfa

Çatlak ağ sisteminin ve çatlaklı kayaçların karakteristik özeliklerinin iyi anlaşılması, etkili bir rezervuar yönetimi için elzemdir. Ayrık Çatlak Ağı (AÇA), çatlaklı rezervuarları karakterize etmek amacıyla yaygın olarak kullanılan bir yaklaşımdır. AÇA, çatlakların geometrisini, geçirimliliğini ve birbirleri ile olan iletişimini kullanarak bir çatlak ağı yaratır. Bu çalışmada, AÇA modeli kullanılarak çok çatlaklı, mermer ve şistlerden oluşan Alaşehir jeotermal rezervuarı karakterize edilmiştir. Model kalibrasyonu için çatlak parametrelerinden çatlak geçirgenliği, açıklığı, yoğunluğu ve yarıçapı koşullandırılmıştır. Gerekli çatlak parametrelerinin büyük bir kısmı daha önce sahada yapılan çalışmalardan referans alınmıştır. Çatlak özeliklerinden bilinmeyenler ise değeri bilinen parametrelerden faydalanılarak olasılıklı korelasyonlar ile tahmin edilmiştir. Dinamik model sonuçları kısa süreli basınç yükselim testleri ile doğrulanmıştır. Model çakışması sonucu elde edilen çatlak özelikleri, sahada yapılan kuyu testleri ve izleyici testi sonuçları ile uyumludur. AÇA modeli bütün kuyuların güçlü bir çatlak ağ sistemi ile bağlantılı olduğunu göstermiştir. İzleyici testi ve rezervuar takibinde kullanılan, ayrıca doğal izleyici olarak da bilinen ve enjeksiyon suyunun girişimlerini gösteren klor ve kondense olmayan gazların üretim kuyularındaki oranları kullanılarak çatlak ağ sistemi doğrulanmıştır.

Anahtar Kelimeler: Doğal Çatlaklar, Ayrık Çatlak Ağ Modeli, Mermer, Şist

vi

To My Beloved Family

ACKNOWLEDGEMENT

I would like to thank my thesis advisor Prof. Dr. Serhat Akın for his valuable encouragement and guidance throughout this study.

Special thanks to Neal Josephson for his helps in using the software which is called FracMan.

Lastly, I would like to thank to İnanç Alptuğ Hıdıroğlu for his helps to reach my goal.

TABLE OF CONTENTS

LIST OF TABLES

TABLES

LIST OF FIGURES

FIGURES

xiii

NOMENCLATURE

P_L=Probability function of Levy Model

L=Distance to fracture center, m

$L^{'}$= Derivative of the distance to fracture center

D= Fractal Dimension

P_x= Probability function of Nearest Neighbor Model

b=Empirical constant

C=Empirical constant

P_{32}= Fracture intensity 1/m

P_{33}= Volume intensity 1/m

P_{10}=Linear intensity 1/m

K_f= Hydraulic Conductivity,

2b= Aperture, mm

Ƥ= Density, kg/m^3

µ=Viscosity, cp

g=Gravity, m/s^2

N=Number of box

r=Size of box

d_E= Euclid dimension

Ø=Effective porosity

I_{max}= Maximum fracture length, m

I_{mim}= Minimum fracture length, m

A_p= Total fracture area, m^2

A=Area of given cell, m^2

I_{total}= Total length of all fractures, m

β=Proportionality coefficient

ɑ=Fracture azimuth

θ= Fracture Dip, ^{o}

K=fracture permeability, Darcy

r_w=Wellbore radius, m

V_m=Mud loss, bbl

r_s=Invasion radius, m

w=Fracture width, mm

$\frac{\Delta p}{\mathcal{T}_y}$= Overpressure ratio

W= Peclet number

L=Model parameter

t_m=Mean arrival time, day

e=Flow contribution coefficient

m=Tracer mass, kg

D_l=Dispersion coefficient, m^2s^{-1}

CHAPTER 1

INTRODUCTION

Geothermal resources are usually discovered in tectonically active areas. During the tectonic movement of brittle rock blocks, natural faults and fractures are created. Natural fractures constitute the major fluid flow paths in the geothermal reservoirs. Production wells which are drilled into these fractures usually provide high flow rates. Reinjection of waste fluid into geothermal reservoir support reservoir pressure and enhance more heat extraction from reservoir rock. However, the main concern of long-term reinjection is the risk of dramatic temperature drop in production wells.

Since the study is related with fracture system, it is worth to mention how fractures are created in the subsurface. Fractures are created as a result of tectonic motions which are forced by overburden weight and stresses, formation pressure or thermal activities. The scale of fractures may vary from micrometers to kilometers in length. Brittle rocks such as sedimentary rocks, volcanic rocks and metamorphic rocks are the main components of naturally fractured reservoir (Kuchuk et al., 2015). Fractures are preferential pathways in the subsurface for all reservoir fluids. Specifically, in geothermal reservoirs, geothermal fluid flows through discontinuities such as interconnected fractures and conductive faults. Unlike fractures, reservoir rock matrix has small permeability due to compaction and cementation during sedimentation process. Therefore, fracture permeability controls the overall permeability in the geothermal reservoir. Most of the geothermal reservoirs in the world produce from naturally fractured systems.

1

In the hot reservoirs that does not have natural fracture system, in other words the reservoir rock which has very limited permeability, EGS (Enhanced Geothermal System) is applicable. In EGS, artificial fractures are created by using hydraulic fracturing technology. However, Alaşehir geothermal field is naturally fractured reservoir similar to most of the geothermal reservoirs in Turkey. Therefore, artificial fractures are not included in this study. The scope of the study is to investigate characteristics of natural fractures. Natural fractures can be quantified by several methods**:**

- Borehole imaging tools such as FMI log (Full-bore Formation Micro imager) and FMS log (Formation Micro Scanner) are applicable in water based mud to scan fracture orientation, fracture aperture and fracture porosity in the bore hole (Gaillot et al., 2007).

- Taking core sample is another way for fracture evaluation in geothermal applications. Core samples are usually taken during drilling in the wildcat fields or in EGS projects to have an idea about reservoir rock mechanics for fracture propagation. Core sample analysis can also be used to confirm borehole imaging tools.

- During drilling, one of the most important indication of natural fractures is partial or total mud loss into formation. Mud loss can be associated with fracture aperture, thus fracture permeability. Type curve matching technique and analytical models are used to estimate natural fracture permeability qualitatively and quantitatively (Akin, 2013 and Huang et al., 2011).

- Outcrops are used as an analogue to the subsurface. Especially, in wildcat areas where there is no available drilling well data or well test data, outcrops are very useful to estimate characteristic properties of reservoir rock. In geothermal exploration studies, fractures found on the outcrops are analyzed to make analogy about subsurface reservoir fracture properties such as fracture connectivity, fracture permeability and fracture density.

- Seismic reflections are used to understand the structure and stratigraphy of the particular geothermal field. Faults and fractures can be detected through seismic lines. However, the resolution of the seismic data may not be sufficient to detect small fractures that are not associated with faults. In geothermal

exploration, the target depth of wells and well drilling program is usually prepared based on the near well data and seismic interpretations (Howell et al., 2018).

- Well testing is a widely used technique that provide detail information about reservoir and well properties. Pressure transient tests conducted in geothermal application are build-up test, fall off test, injection test, interference test and drawdown test. As opposed to geological models, well test describes the reservoir in dynamic condition. Thus, it is possible to describe reservoir heterogeneity that includes boundaries (sealing and conductive faults) in other words extend of the reservoir can be determined by well testing. Permeability anisotropy and layering in the reservoir can also be determined by conducting a particular well test (Bourdet et al, 2002).

- Another special technique to describe geothermal reservoir is tracer testing. Tracer testing is one of the most reliable ways to confirm connection between injection and production wells in geothermal reservoir management. By conducting a tracer test, several quantitative and qualitative results can be obtained such as conductive flow paths, mean fluid velocity, thermal breakthrough time and recovery. If a tracer test is designed and executed properly, existence of compartmentalization in the reservoir can also be detected.

- Chemical properties of geothermal fluid can be used for evaluating flow system (Hartle et al., 2013). Reservoir temperature directly affects the amount of chemicals dissolved in the geothermal fluid. The mineral composition of the reservoir rock is in equilibrium with geothermal fluid. Concentration of some minerals such as SiO_2, Na, and K change with temperature. Premature temperature decline in geothermal production wells can be detected by monitoring concentration of these reactants. However, there is a group of minerals whose equilibrium concentration does not change with temperature. These nonreactive minerals are Cl and B (Padilla et al., 2016). Cl is considered as a natural tracer that is sensitive to arrival of injected brine. Therefore, change of Cl concentration is analyzed to identify conductive flow paths in reservoir.

CO_2 (g) production is also monitored as a complementary to Cl spatial distribution. In addition, SiO_2 (silica) concentration change may provide valuable information on interpretation of temperature decline as a result of cold reinjection brine.

Dual porosity approach (DP) or discrete fracture network (DFN) modeling may be used to simulate naturally fractured reservoirs (NFR). DP modeling is a good representative model for oil reservoirs since both fracture and rock matrix play an effective role to contribute total oil rate. However, high fluid velocity in heavily fractured geothermal reservoirs indicates that major contribution of total flow rate is provided by fractures and contribution of rock matrix can be considered negligible. DP model has some restrictions, which make it unsuitable for description of geothermal reservoirs. For example, it does not take account the disconnected fractures (Kuchuk et al., 2015). The equation for fluid flow between fracture and rock matrix is not fully evaluated with DP model (Soltanieh, 2015). It is also limited to be used in simulation of complex geometric system. On the other hand, by using DFN model, fluid flow in fractured and complex system can be simulated without limitation of evaluating flow equation. Therefore, characterization of natural fractures with DFN approach can address most of the questions about characteristics of natural fracture in geothermal reservoirs.

Characterization of fractures in geothermal reservoirs is necessary for an effective production and injection program that enable more heat extraction from the reservoir rock. In this study, Alaşehir geothermal field is characterized by using a special tool which is Discrete Fracture Network (DFN). A software, Fracman7.6 (Golder Associates Inc., 2009) which is developed by Golder Associates, is used to construct a representative fracture network system for Alaşehir geothermal field.

CHAPTER 2

LITERATURE REVIEW

It is challenging to model Naturally Fractured Reservoirs (NFR) because of high uncertainity and anisotropy in their hydraulic properties. In order to better understand behaviour of NFR, several studies have been conducted since the early 1900s. Versluys (1915) investigated anisotropic permeabillity by using arbitrarily-oriented bundles of tubes. He stated that high number of arbitrary sets can be reduced to three mutually conductors as K_x, K_y, K_z. Ferrandon (1948) further developed the bundle of tubes model by introducing permeability tensor. He noted that flow contribution of each conductor to total flow rate is proportional to the potential gradient along a unit area of tubes. Snow (1965) considered parallel plate openings, which is called aperture of real fractures. He proposed that discharge of each fracture is proportional to cube of its aperture for a given gradient. This is called cubic law. Long and Witherspoon (1985) proved that fracture geometry fluctuates the fluid flow significantly. They reported the most important fracture geometric parameters as fracture aperture, fracture shape, density, orientation and fracture size. With development of computing power and algorithms in 1980s, the modeling approaches have become the most attractive way for evaluating complex fracture systems. Fluid flow simulation in fractured rocks has been accomplished by using continuum model, dual porosity model and discrete fracture network model.

2.1   Continuum Approach

In continuum approach, fluid flow in fractures is considered as similar to fluid flow in porous media. Long and Witherspoon (1985) stated that fracture systems behave like a porous medium as the number of intersected fractures increase. For simplicity, fractures in a rock mass are considered as an equivalent porous medium (EPM), therefore predicted hydraulic properties are averaged values (Lee et al., 1995). It is not possible to distinguish hydralic properties of fractures from that of porous media in continuum model. The advantage of continuum approach is that simulation takes short run times compare to other approaches. Some investigators used DFN model incorporating with continuum model. Snow (1968) formed a cubic network between fractures. Oda (1986) proposed a mathematical model of equivalent permeability tensor. Continuum approach has been coupled with DFN model in several geothermal and carbonate oil reservoirs.

Lee et al. (1995) used equivalent porous approach to estimate permeability of naturally fractured reservoir. They introduced fracture permeability tensor, which is related with fracture geometry. In order to estimate permeability tensor, system properties were sampled statistically. They also used hydromechanic and rock mechanics to present permeability of Andesite rock with depth in Lan Yu site in Taiwan. They confirmed model results with a tracer test and in situ hydraulic tests.

Hull and Clemo (1987) developed a computer model that simulate the hydraulic behaviour of a system consisting from matrix permeability and discrete fracture permeability. They studied the effects of equivalent porous medium approach in dual permeability system. They developed a code at the Idaho National Engineering Laboratory to simulate fluid flow, heat transport and solute flow in a two dimensional and dual permeable reservoir. They assumed that maximum number of fractures converging at a node was eight and aperture was taken constant between two nodes. However, aperture can change between the next nodes. Constant head, flow rate and conductivity was assumed. They performed several combination of simulation for a geothermal reservoir consisting from an interconnected injection and production well. They increased matrix permeability and removed some of the fractures to test the compensation effect of matrix on total system. They concluded that pressure

6

ditribution does not change significantly as small fractures are replaced with matrix permeability however larger fractures should be explicitly simulated. Tracer mean arrival times changed when fractures are replaced with matrix permeability. Active porosity increased thus fluid swept pore volume increased and the effect of dominant fluid paths decreased. Thermal front moves very slowly in matrix as opposed to fractures. Thus replacing fractures with porous media resulted in great overestimate of thermal breakthrough time.

2.2   Dual Porosity Approach

The concept of fluid flow in double porosity system was first delineated by (Barrenblatt et al. 1960) and (Warren and Root, 1963). Barrenblatt et al. (1960) conducted laboratory studies on fissured strata and they proved that description of transient flow of liquids in fissured system with homogeneous porous system leads to wrong interpretations. According to Barrenblatt et al. (1960), fissures have greater width compare to pores, thus permeability of fissure system is much greater than that of pores. However, matrix porous media occupy much more volume than fissures. They proposed the motion of liquid between porous media and fissures by defining pressure and velocity in individual void and cases at which their theory is applicable are given in details in Barrenblatt et al. (1960). Primary and secondary porosity were defined by Warren and Root (1963). According to them, primary porosity is formed as results of deposition and lithification processes and primary porosity has good interconnection. Thus, it is possible to derive a correlation between primary porosity and permeability. Secondary porosity is formed as results of tectonic motions or solution of circulating water. Secondary porosity is not highly interconnected which makes it unsuitable to correlate with permeability. Secondary porosity is usually developed in brittle formations like carbonate oil reservoirs and geothermal reservoir rocks such as marble and calcshist. Warren and Root (1963) provided an actual reservoir and a model reservoir of heterogeneous porous system in Figure-1

7
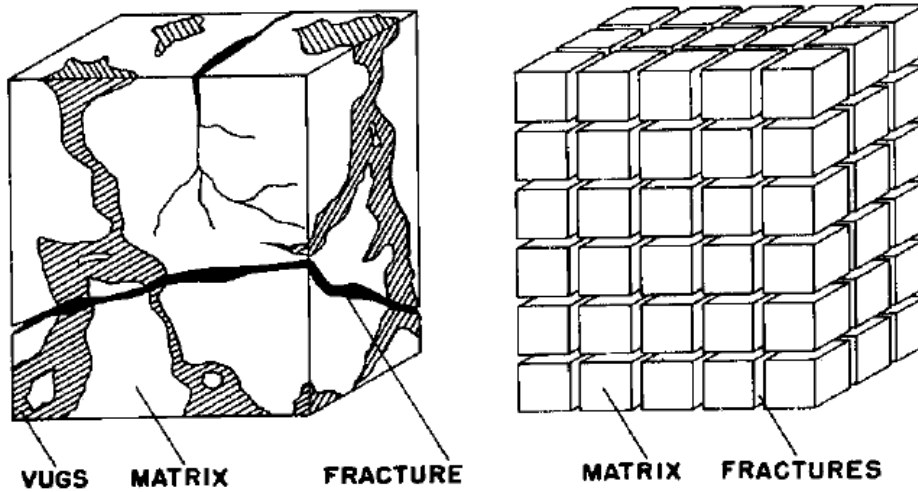
Figure 1: Heterogeneous porous medium (Warren and Root, 1963)

Warren and Root (1965) analyzed double porosity system analytically with buildup tests. They stated that capacitence of secondary porosity and interporosity flow term are sufficient to characterize double porosity systems.

Double porosity model was first used in a numerical simulation of oil reservoir by Kazemi et al. (1976). They developed a three dimensional, multiple-well simulator for a fractured oil reservoir. Two phase flow extensions of single phase flow equations derived by (Warren and Root, 1963) were used in the simulator. They assumed that the fractures act as flow boundaries of matrix blocks. The simulator was tested in quadrant of a five spot model and a five well fractured reservoir model. They used 13 nodes, 5 nodes and 1 nodes in x,y,z directions respectively. Distance between nodes was 500 ft and each node had 25 matrix blocks. They ploted capillary pressure graph and water oil ratio was also calculated to discuss the effect of imbibition, gravity and viscous forces in fractured and unfractured reservoirs. Since Kazemi et al. (1976), several simulation programs have been developed to model fractured reservoirs.

Dual porosity model is a representative model for fractured and vuggy geothermal reservoirs. However, it does not meet all requirements of high flow rates found in geothermal wells. Therefore, discrete fracture network model is usually applicable in geothermal reservoirs.

8

2.3 Discrete Fracture Network Approach

Discrete Fracture Network (DFN) model describes fluid flow in fractures by considering fracture geometry and connectivity. Unlike dual porosity model and continuum approach, DFN takes into consideration the contribution of individual fracture to the total system. Therefore, DFN model represents fractured systems more realistic and it enables us to examine effects of individual fracture parameter on flow respond. The DFN concept was started in 1980s for both 2D and 3D systems (Long et al. 1982; Andersson, 1984; Dershowtz and Einstein, 1987). The disadvantage of DFN is that it requires fracture geometry to describe flow behaviour. There is a need for definition of fracture geometry within acceptable range of uncertainty. Einstein and Baecher, (1983) proposed statistical methods to decrease geological uncertainty. They sampled field data and plotted their cumulative density function. Joint spacing was verified as exponential distribution with 5 % confidence level. Trace length showed lognormal distribution. Orientation data was recorded to behave as exponential distribution. With new correlations and algorithms DFN approach has been continously developed and applied in natural fracture reservoir and hydraulic fracturing operations such as development of enhanced geothermal system (EGS) and shale oil and shale gas.

Dershowitz et al. (2010) used DFN approach in FracMan software to simulate hydraulic fracturing propagation in naturally fractured low permeable reservoir with an emprical algorithm. Interaction of natural fractures and hydraulic fractures were evaluated by distributing frac fluid in natural fractures. Model was calibrated with microseismic activities and results were compared with geomechanical simulation.

Xu and Dowd (2008) developed a computer code that generate 2D and 3D fractures network stochastically in FracSim3D. They populated their model with data collection from scanlines of outcrops, core analysis and logging. In the case of no correlation, monte carlo sampling was applied for model construction. They used point process models to locate fractures and other fracture properties were generated by their probability density function with monte carlo sampling. The software was capable of ploting statistics such as histogram, rose diagram and probability density function.

Shiriyev (2014) studied DFN modeling by using FracMan Software to increase oil recovery in heavy oil reservoir by carbon dioxide flooding. He constructed a conceptual model based on analysis of core scanner and structural map of the studied field. In model calibration, he obtained good matches between actual well test data and simulation data. Once calibration process completed, he calculated permeability and porosity tensors for each grid cell in FracMan, which were then exported to CMG Stars software to obtain oil production history in Double Porosity model. Carbon dioxide injection was started and calibrated with field data.

Soltanieh (2015) characterized a fractured carbonate oil reservoir in South East Turkey by using DFN modeling in FracMan software. Pressure build up test data was used for model calibration. Good matches were obtained only at initial and last points of simulated well test results. He exported FracMan results to CMG Stars to simulate polymer injection as a water shutoff technique. DP model was calibrated with history match of production.

Doe et al. (2014) investigated feasibility of EGS (Enhanced Geothermal Systems) based on geometry, connectivity and heat transport phenomena. They developed Gringarten's solutions by using DFN approach. Role of fracture geometry on thermal breakthrough was studied. They constructed a complex fracture network with non-uniform intensity and aperture in FracMan's hydraulic fracturing module. The model was then exported to Hydro Geosphere for simulation. They concluded that low fracture density causes early thermal breakthrough but temperature declines more slowly. Higher fracture density postpones temperature breakthrough but falls off sharply as the thermal front in the matrix less behind thermal front in fractures. Further increase of fracture intensity does not affect temperature behavior of outlet once matrix depletion controls the thermal breakthrough.

CHAPTER 3

STATEMENT OF PROBLEM

Geothermal reservoirs are naturally fractured complex systems. It is extremely important to characterize fracture system for understanding reservoir heterogeneity. Reservoir outcrops located in the field may roughly represent the reservoir rock properties. However, outcrops are not much reliable because they are not at the reservoir conditions. In addition, outcrops may be exposed to erosion and dissolution which may cause misunderstanding about reservoir characteristics. On the other hand, fracture modeling can provide more realistic results. Discrete fracture network (DFN) modeling is a practical and widely used technique to characterize fractured reservoirs. The main goal of this study is to characterize heavily fractured Alaşehir geothermal reservoir by using DFN modeling. In DFN modeling, initially a static model is constructed. The model is populated with stochastic fracture data retrieved from several sources. The static model for each well is then conditioned to dynamic model. Dynamic model results are matched with actual well test data. After model calibration, stochastic fracture properties such as fracture permeability and porosity are upscaled. Shortest and highest conductance pathways between wells are determined. Upscaled fractures can be used as input file to reservoir simulators such as Tough2 and Eclipse.

CHAPTER 4

CHARACTERISTICS OF ALAŞEHİR GEOTHERMAL FIELD

Alaşehir geothermal field has become the most attractive target for geothermal exploration activities and constructing power plants for last decade. The field lies on a graben which is called Alaşehir Graben, which is 6-10 km wide for the particular study area and the graben becomes wider through Aegean Sea in Western Turkey (Figure-2). Geothermal exploration activities started in 1989 by TPAO (Turkish Petroleum Corporation). More than 100 wells have been drilled in the field by six different operator companies. There are 6 binary power plants and a combined flashing-binary power plant actively generate electricity from the field with total installed capacity of 150 MWe. Meteoric origin reservoir fluid is liquid dominated and Paleozoic aged reservoir rock consists from marble, mica schist, calcshist and quartz. The field has reservoir temperature ranges from 140 ºC to 250 ºC, average gross and net reservoir thickness are reported as 1200 m and 650 m respectively by Gurel, (2016).

Ciftci and Bozkurt (2009) defined the stratigraphic units of Alaşehir field (Figure-4). They stated that, Paleozoic age metamorphic constitutes the basement of the field and the Tertiary fillings are overlaid the basement. All stratigraphic units are available on the surface as reported by Bozkurt (2007) (Figure-3). Conceptual model of the field area is given in Ciftci and Bozkurt (2009) (Figure-5). According to their conceptual model, geothermal fluid is meteoric origin and there are conductive faults which make connection between surface and subsurface. Meteoric water and spring water travel along conductive faults to the reservoir rock.

13

Because of its acidity, it dissolves calcite minerals in marble and vuggy developed in fractures. After being warmed, pressurized and dissolved minerals, it is now called geothermal brine which is captured by impermeable sediment units overlaid by metamorphics.

This study includes 13 km^2 area of the field and only 10 production wells are included in DFN modeling. However, injection wells are also included in remaining part of the study for further reservoir characterization.

Figure 2: Study Area
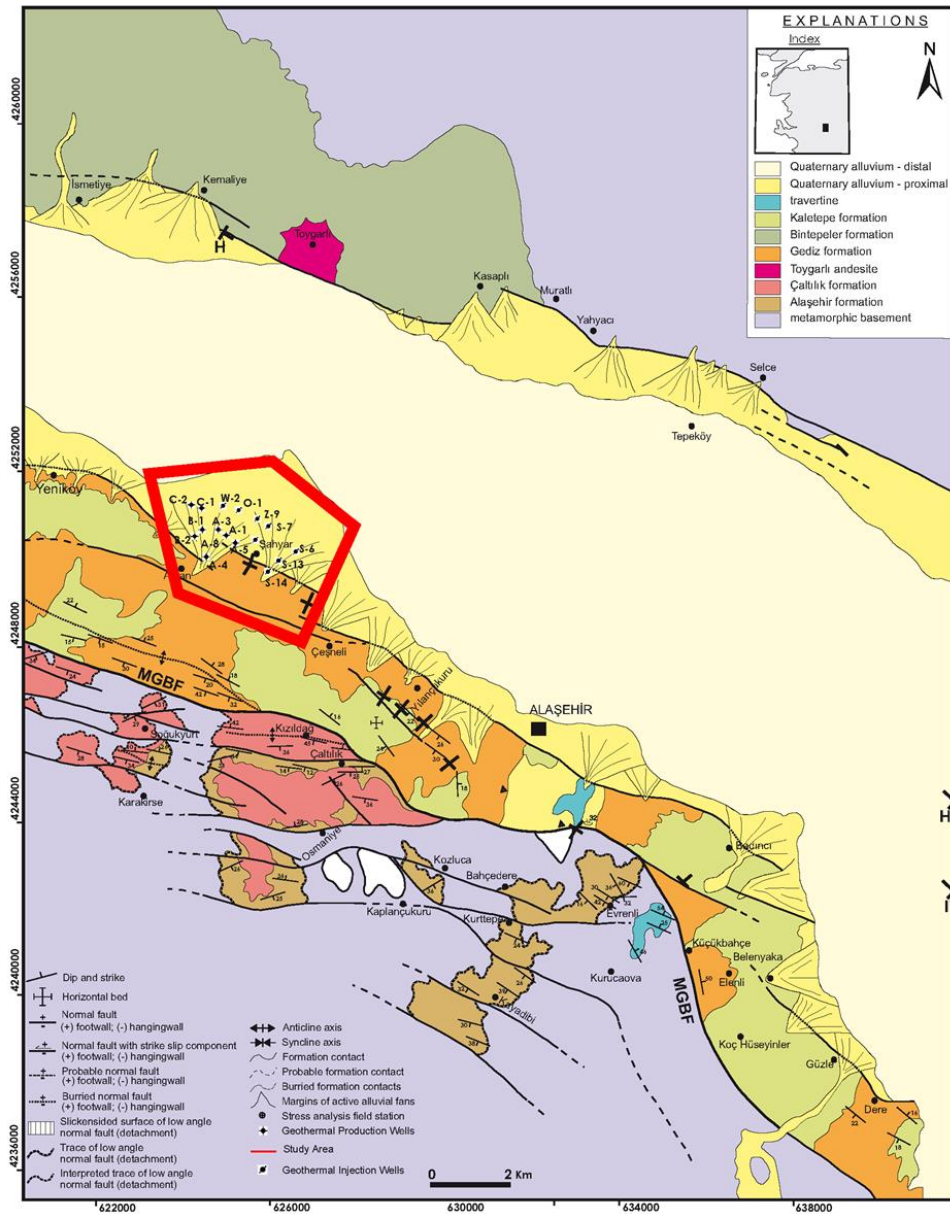
Figure 3: Study area in Geological Map of Alaşehir Geothermal Field (Bozkurt, 2007)
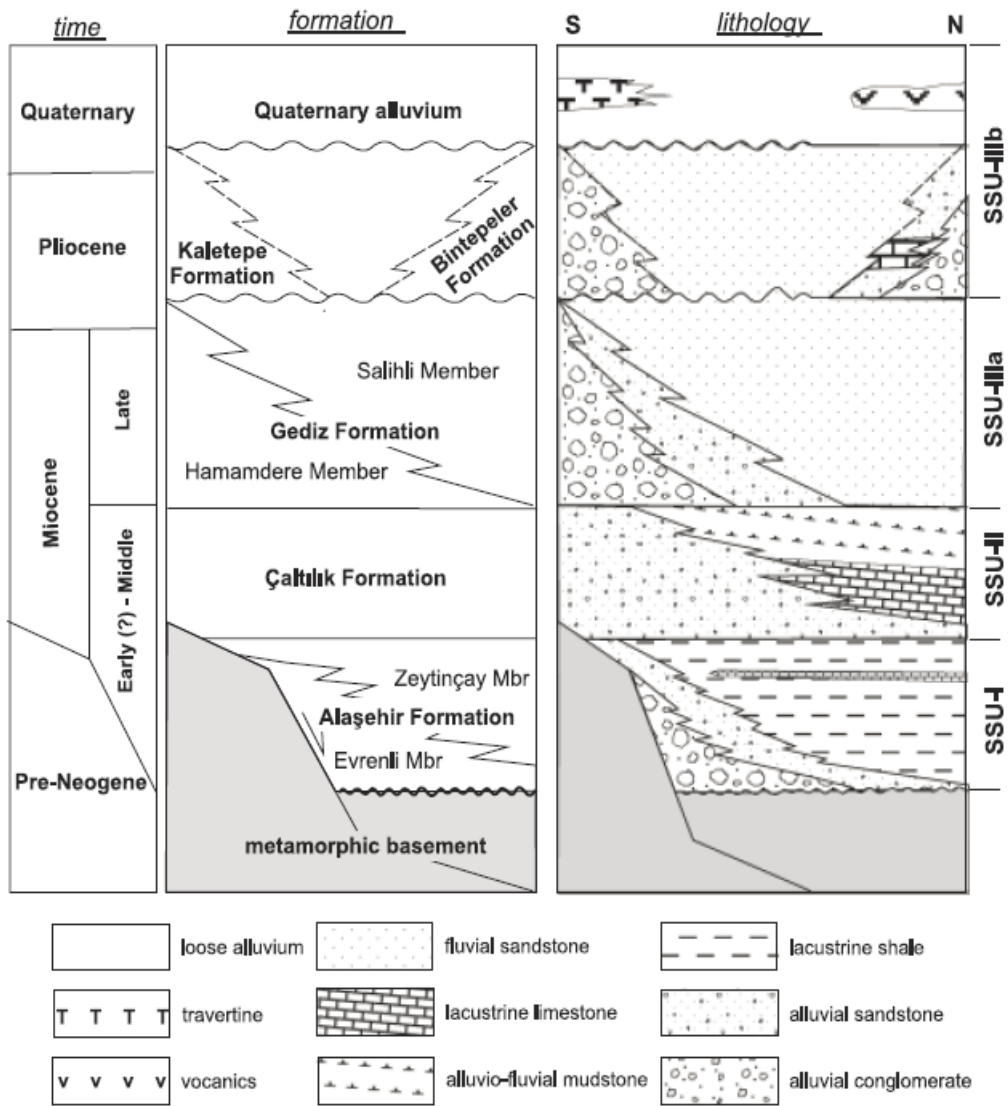
Figure 4: Stratigraphic Units in Alaşehir Field (Çiftçi and Bozkurt, 2009)
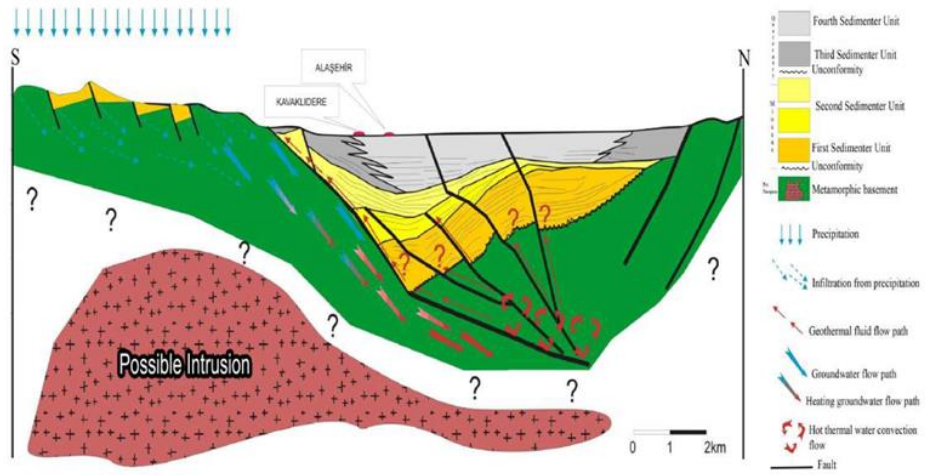
Figure 5: Conceptual Model of Alaşehir Geothermal Field (Çiftçi and Bozkurt,2009)

CHAPTER 5

METHODOLOGY

The study started with gathering data for static model construction. Reservoir parameters are retrieved from different data sources such as seismic, outcrops, drilling mud loss, well test, tracer test, geochemistry and well correlations. FracMan creates fractures stochastically based on their distribution function. In FracMan, fracture set can be generated based on geometric, geocellular, geologic, trace map, stratigraphic methods. In this study, fracture set is generated by using geocellular method. In geocellular method, fractures are generated into specified grid blocks. FracMan requires fracture features to generate fracture set. These features include fracture orientation, location, intensity, size, permeability, aperture and shape.

Once the static model is constructed, stochastic fractures are generated. After that, wells are conditioned to dynamic analysis. The static model is reconstructed and populated with updated data until dynamic well test results are matched with actual well test data. As the dynamic model calibration achieved, fractures are upscaled (Figure-6). The dynamic model results are compared and populated with interference test results, tracer test results and geochemical interpretations for further reservoir characterization.
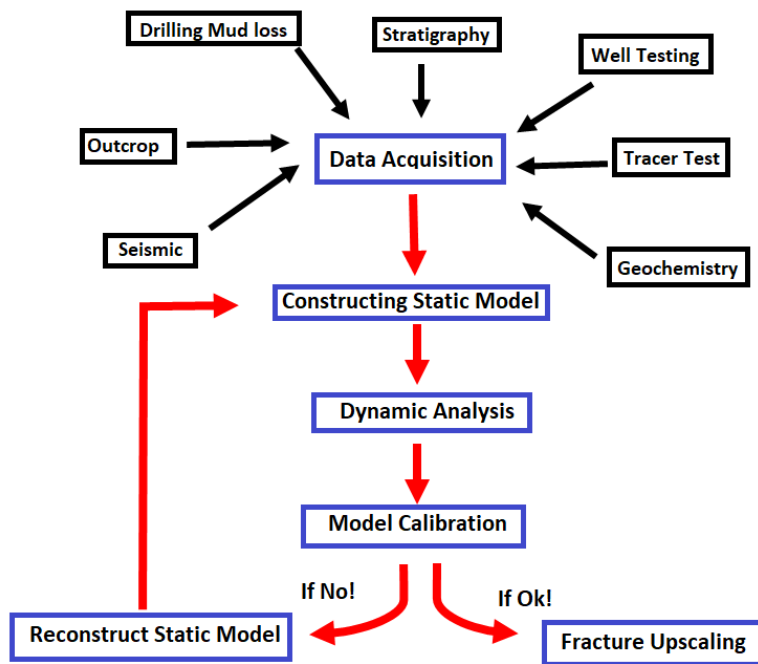
Figure 6: Workflow Diagram

5.1 Fracture Geometry

It is apparent that fracture geometry and connectivity have significant effects on projects, which include fracture systems. Therefore, it is crucial to understand fracture geometry for such heterogeneous systems. Fracture properties will be defined and data attainment for fracture geometry

5.1.1 Fracture Location

The models used for fracture location in the FracMan7.6 are Levy Lee, Enhanced Baecher and Nearest Neighbor.

5.1.1.1 Levy Lee Model

Levy Lee model is based on fractal dimension of the fracture centers. The model assumes that fractures centers are fractal however fracture networks may or may not be fractal. Levy flight process is used to create fracture centers by relating fracture size to its distance to the next fracture (Figure-7).

The probability function of Levy model is given in equation 2.1 (Dershowitz et al., 1998).

$$P_L(L' > L) = L^{-D}$$ (5.1)

Where D represents fractal dimension of point of fracture centers and L is the distance of fracture centers to the next created one.
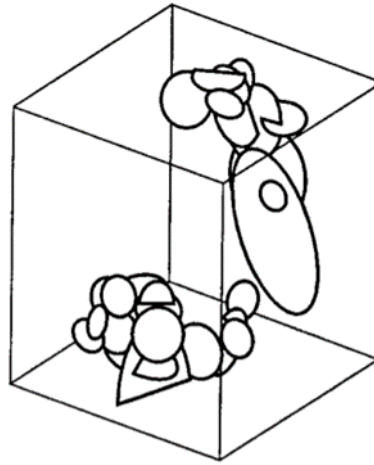
Figure 7: Levy Lee Model (Dershowitz et al, 1998)

5.1.1.2   Enhanced Baecher Model

Enhanced Baecher model is a developed form of Baecher disk model, which is introduced by Baecher et al. (1978). In order to generate fracture network, the model requires the fracture geometry such as fracture density, orientation, size, aperture and shape of fractures. Disk shape fractures are generated by using a Poisson process in which fracture centers are located by a uniform distribution. The orientation and radius of fractures need to be given in Baecher model. In Enhanced Baecher model, fracture shapes may vary from three to six sides polygons (Staub et al., 2002).
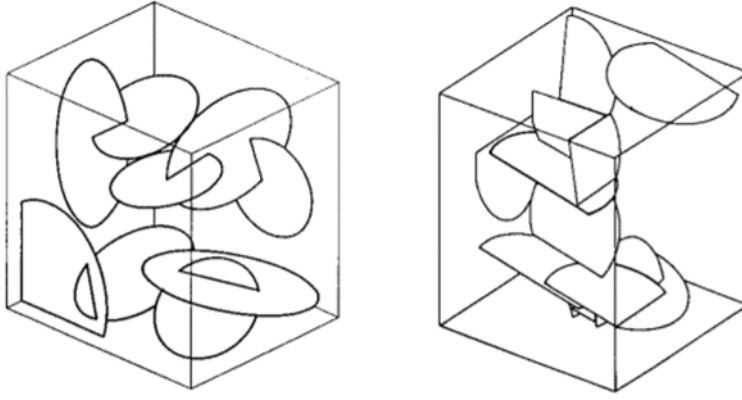
Figure 8: Disks shape Model and Enhanced Baecher Model (Geier et al., 1989)

5.1.1.3 Nearest Neighbor Model

In this model, fractures are concentrated near to the initially generated major fractures. The fracture intensity of new fractures decreases exponentially with distance to the major fractures. The model provides a good fracture connection as it is compared with disk shape model. The probability function of the nearest neighbor model is given as:

$$P_x(x) = CL^{-b} \qquad (5.2)$$

where L is the distance between new fracture and the previous one, b and C are empirical constants.
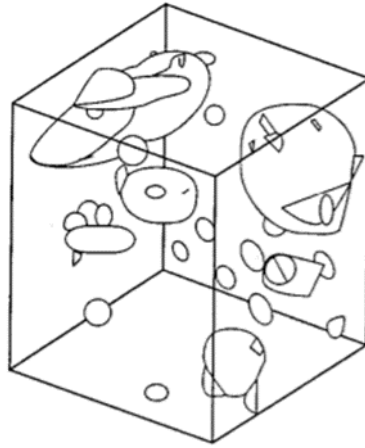
Figure 9: Nearest Neighbor Model (Dershowitz et al, 1988)

5.1.2   Fracture Orientation

Fracture orientation is represented in terms of dip and direction of fracture. Dershowitz, (1980) defined the fracture dip as the angle between the joint plane and a horizontal plane and dip direction is defined as the angle between y axis in a horizontal plane and dip angle (Figure-10). It can be measured from outcrops or by image well log. Einstein and Baecher (1983) and Dershowitz (1979) studied the distribution of joint orientation based on several statistical approaches such as Fisher, Bingham, Uniform and Elliptical on the sphere. The Fisher distribution was found as the most flexible and simple model providing fracture orientation because its parameters can be derived from in-situ data. In addition, Fisher distribution is regarded as the analog to the normal distribution for orientation data.
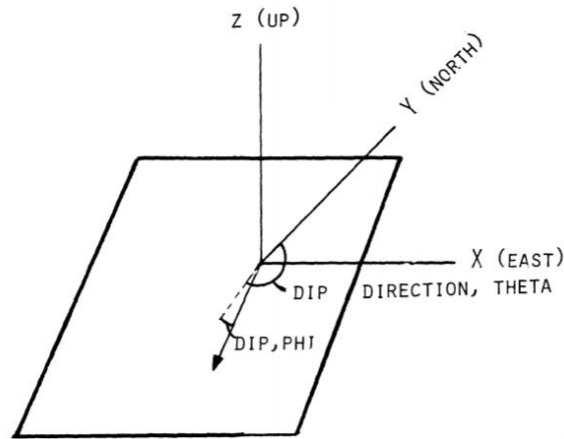
Figure 10: Dip and Dip Direction (Dershowitz, 1980)

5.1.3 Fracture Intensity

Fracture intensity can be defined as areal intensity (P_{32}), volume intensity (P_{33}), or linear intensity (P_{10}) which are function of the distribution of fracture size.

5.1.4 Areal Intensity

Dershowitz, (1984) defined the areal intensity as ratio of the total area of fractures to its unit volume. The unit of the areal intensity is number of fractures per unit area:

$$\frac{Total\ Area\ of\ Fractures}{Unit\ Volume} \qquad (5.3)$$

5.1.5 Volume Intensity

It is a portion of the total fracture volume in a given volume of reservoir:

$$\frac{Total\ Fractures\ Volume}{Total\ Volume}$$

5.1.6 Linear Intensity

Linear intensity is quantified as number of fractures per unit length of the reservoir. Outcrops and image logs can provide useful information about linear fracture intensity by scanning borehole or core sample on the surface.

24

5.1.7 Fracture Size

Fracture size may vary from micro scale to several meters based on the features of structure. It can be assumed as uniform or stochastic when there is no available data about fracture shape. However, it is better to consider probability distribution rather than deterministic one because fracture size usually depends on joint sizes and shapes.

5.1.8 Fracture Permeability and Aperture

Snow (1965) stated that fluid flows in the opening of the two plates of fractures which is called fracture aperture (Figure-11). Fracture aperture may range from millimeters to centimeters. In flow simulation, aperture is usually considered as it has an exponential distribution. The cubic law is used for aperture and permeability relation. The cubic law assumes that laminar flow of viscous and incompressible fluid occurs in the region bounded by two smooth parallel plates (Equation 5.4).
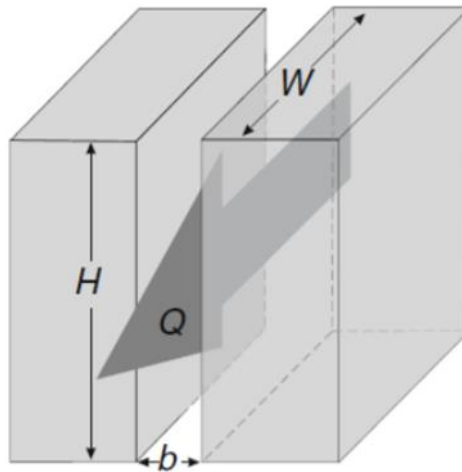
Figure 11: Flow in Parallel Plates (Dershowitz, 2012)

$$K_f = \frac{(2b)^2 g \rho}{12 * \mu} \qquad (5.4)$$

Where K_f is hydraulic conductivity and 2b is aperture, g is gravity and ρ represents density and μ is viscosity.

5.1.9 Fracture Shape

In Baecher model, fracture shapes are defined as polygons which has three to six sides. Davy et al. (2006) noted that in the case of small anisotropy in the fracture plane, fracture shape does not affect flow simulation results. However, if there is no information about fracture shape, it can be assumed as a disk.

5.2 Data Attainment for DFN Model

Required fracture properties for DFN modeling can be obtained from several data sources such as outcrops on the surface, drilling mud loss, core sample, seismic data, well testing, and geochemistry, geology and well logs. These sources have different data quality and measurement scale (Figure-12). For example, seismic can provide information about the whole reservoir area, however resolution of seismic is too low to capture small fractures. On the other hand, imaging well log can detect micro fractures at a small scale; however, it is limited with wellbore cross section.
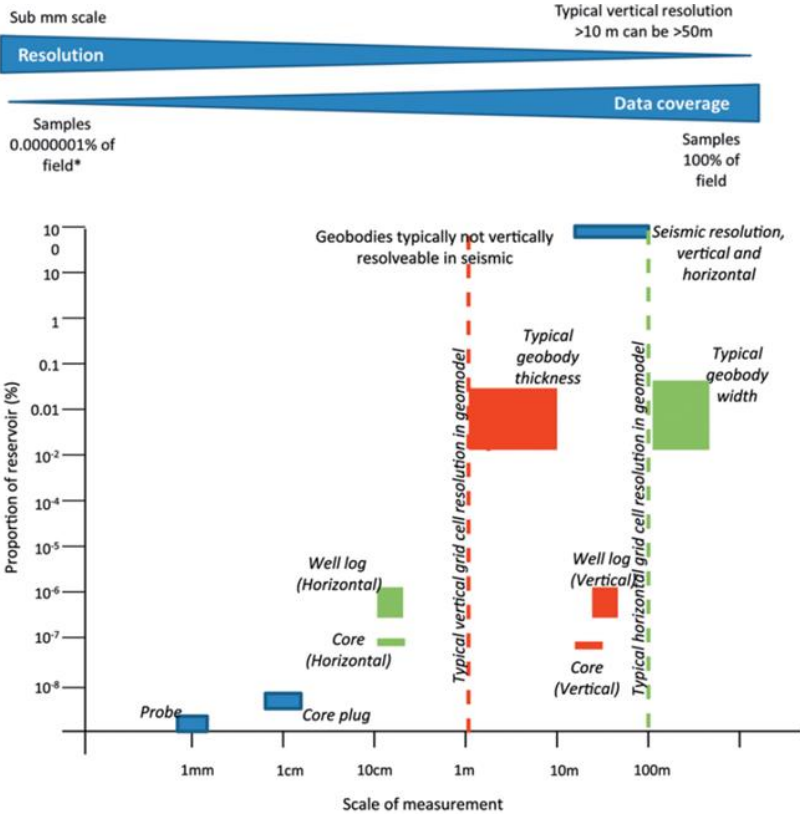
Figure 12: Quantification of Data Quality of Variety Sources (Hower et al., 2018)

5.2.1 Outcrop Analysis

In geothermal exploration phase, it is difficult to obtain information about characteristics of subsurface rock without drilling a well in a given field area. One of the easiest way of obtaining information about reservoir rock is to analyze outcrop which is already available on surface. Outcrop is usually considered as analogue to reservoir rock. In outcrop studies, fractal analysis has been found efficient and useful by several scientists to estimate reservoir characteristics such as fracture permeability, fracture porosity and aperture. Fractal dimension can be calculated by several methods which are: Box Counting Method, R/S Analysis Method, Yard Stick Method, Variation Method, Root Mean Square Method and Structure Function Method. The comparison of these methods can be found in Liang et al. (2012). They concluded that Box Counting Method is much reliable and efficient compare to other methods. Miao et al. (2015) predicted fracture permeability and fracture density by using fractal approach and cubic law. They found that interconnected fractures permeability increases with fracture density and porosity enhancement. Babadagli (2001) defined fractal analysis as estimation of fractal dimension which is non-integer number. He used the box counting method to estimate fractal dimension of fracture network in microscale to gigascale in Menderes graben of South Western Turkey. The box counting method uses relation of number of boxes (N) containing fractures with the size of square box(r). The data (r, N) is analyzed on log-log scale by using linear regression method to determine fractal dimension (D):

$$N = constant * r^D \qquad\qquad (5.5)$$
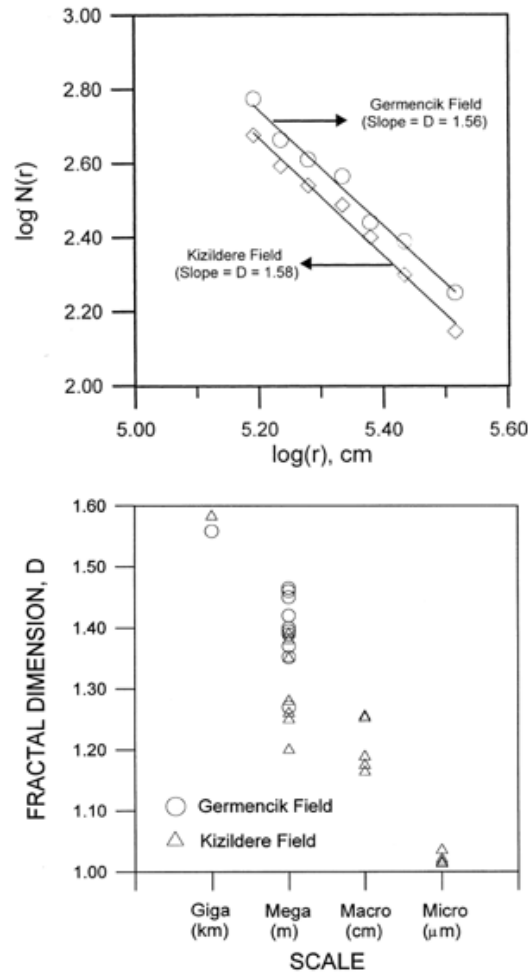
Figure 13: Fractal Dimension of Fractures in South Western Turkey (Babadagli, 2001)

Babadagli (2001) concluded that the higher fractal dimension was obtained for the denser fracture network. He also noted that fractal dimension of microscale samples was lower than that of larger scale samples and fractal dimension was close to unity for microscale samples.

Miao et al. (2015) proposed a relationship between fractal dimension, fracture length distribution, fracture area porosity and ratio of maximum length to minimum length of fracture. The fractal theory and cubic law were used to determine fracture permeability by assuming laminar flow in fractures.

$$\mathfrak{a} = \beta * I^n \qquad (5.6)$$

$$D_f = d_E + \frac{ln\text{Ø}}{ln(\frac{I_{max}}{I_{min}})} \qquad (5.7)$$

$$\text{Ø} = \frac{A_p}{A} \qquad (5.8)$$

$$D = \frac{I_{total}}{A} \qquad (5.9)$$

$$D = \frac{(2-D_f)\text{Ø}[1-\left(\frac{I_{min}}{I_{max}}\right)^{1-D_f}]}{(1-D_f)\beta I_{max}[1-\left(\frac{I_{min}}{I_{max}}\right)^{2-D_f}]} \qquad (5.10)$$

$$K = \frac{\beta^3 D(1-D_f)I_{max}^3(1-cos^2\alpha\,sin^2\theta}{128(4-D_f)[1-\text{Ø}^{\frac{1-D_f}{2-D_f}}} \qquad (5.11)$$

Where D_f is fractal dimension, d_E is Euclid dimension which is 2 in 2D and 3 in 3D, Ø is effective porosity, maximum fracture length and minimum fracture length are denoted as I_{max} and I_{min} respectively, A_p is the total fracture area, A is the area of a given cell, I_{total} is the total length of all fractures, D represents fracture density, **β** and n is proportionality coefficient, ɑ is fracture aperture, **α** is the fracture azimuth and the dip is represented by θ, K is the fracture permeability.

In Alaşehir geothermal field, Paleozoic age metamorphic reservoir rock consists of schist, marble and quartz. Outcrops of the reservoir rock are available on North and South of Gediz graben (Figure-14). Gurel et al., (2016) studied fractal of outcrops in Alaşehir geothermal area to characterize subsurface reservoir rock. In their study, fracture density, permeability and effective porosity were calculated by using box counting method and equations proposed by Miao et al., (2015). They calculated average fractal dimension of marble as 1.32 and it was 1.29 for schist. Vertical linear fracture density was calculated as 3.97 for minimum and 8.88 for maximum value. Horizontal linear fracture density was found somewhat higher than vertical fracture density.

Minimum, maximum and average horizontal fracture density were 4, 14.59 and 7.56 respectively. Gurel, (2016) found volumetric fracture density from outcrop study as 0.0934 ± 0.04 m^{-1} in direction of X and volumetric fracture density was found 0.0898 ± 0.03 m^{-1}. They provided histogram of fracture aperture in (Figure-15). Other results of the study are given in (Table-1). They found that average fracture porosity changed from 0.03 to 0.12 and average permeability of schist was reported as 362 mD while it was 1564 mD for marble. Fracture length was reported to change from 1.6m to 25.9 m.
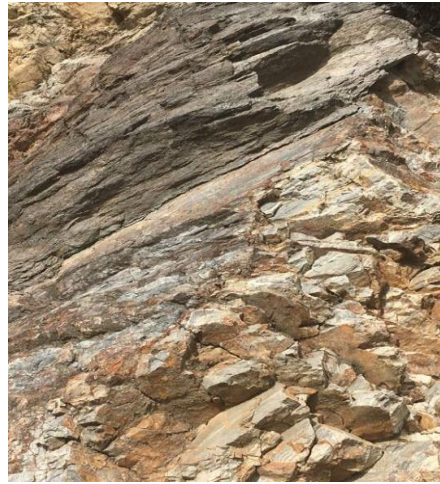

Figure 14: Schist and Marble Outcrop in Alaşehir Area
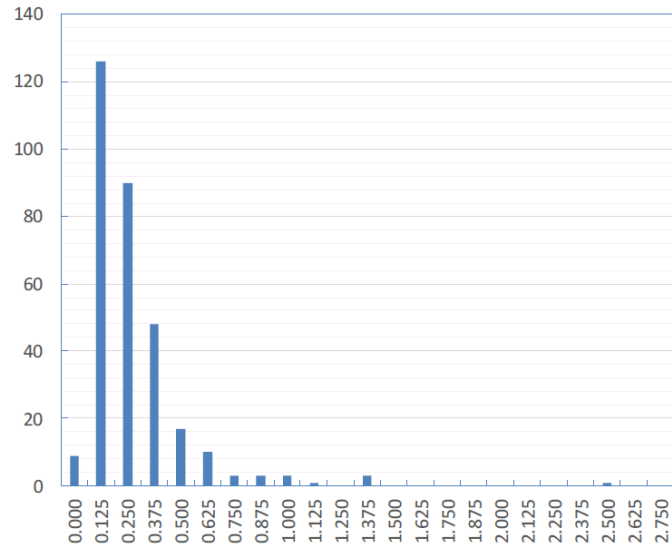
Figure 15: Histogram of Fracture Aperture (mm) in Alaşehir Area (Gürel et al., 2015)

Table 1: Results of Outcrop Analysis (Gürel et al. 2015)

Sample	S-1	S-2	S-3	S-4	S-5	M-1	M-2	M-3	M-4	M-5
Total Fracture Length (L_{total}) (m)	13.62	6.06	9.72	4.85	1.61	7.32	31.81	13.67	6.04	25.93
Unit Area (A) (m^2)	4.62	3.40	2.00	2.09	1.06	0.93	2.22	0.97	0.83	13.13
Fracture Porosity (ϕ)	0.02	0.08	0.06	0.12	0.11	0.07	0.07	0.03	0.05	0.04
Areal Fracture Density (D) (m/m^2)	2.95	1.78	4.85	2.32	1.52	7.83	14.33	14.11	7.30	1.97
Permeability (mD)	76.25	806.40	501.12	119.21	24.70	2536.03	4037.44	523.00	370.77	355.49

Apart from small scale fractured outcrop, large scale faults are also available in Alaşehir geothermal area. Ciftci, (2007) reported high angle normal faults and low angle North dipping detachment faults in the South of the graben (Figure-16). He noted that low angle (0-20°) North dipping detachments bound the southern margin of the graben and they constitute the contact between Menderes Metamorphic and sedimentary overlain rocks.

31
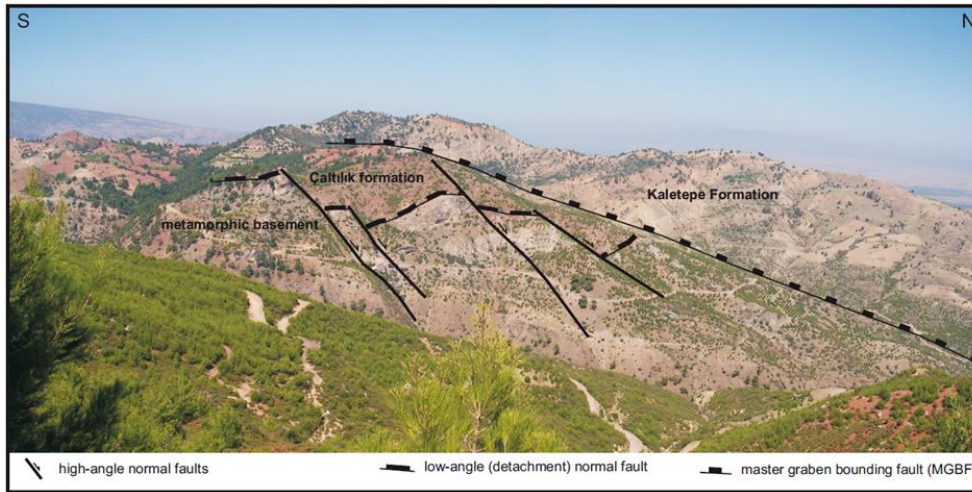
Figure 16: Fault Outcrops in Southern Gediz Graben (Ciftci, 2007)

Bozkurt and Sözbilir, (2004) provided dip angle and dip direction of the inactive low angle (5-11°) detachment fault which cut the metamorphic and Miocene sedimentary rocks (Table-2). They also provided the direction and dip of Pliocene age high angle normal faults which are younger than detachment fault (Table-3 and Table-4). They proposed that high angle normal faults have cross cutting relation with detachment fault. However, Seyitoglu et al. (2010) think that these faults are merged to the detachment fault which they consider as an indication of Rolling Hinge mechanism.

Table 2: Presently Low Angle Normal Fault (Bozkurt and Sözbilir, 2004)

No	Dip direction (°N)	Dip amount (°)
1	020	11
2	360	05
3	360	08
4	002	08
5	005	11

Table 3: High Angle Normal Faults (Bozkurt and Sözbilir, 2004)

No	Dip direction (°N)	Dip amount (°)
1	016	43
2	033	40
3	027	40
4	035	40
5	004	62
6	196	54
7	184	64
8	180	51
9	034	50
10	350	44
11	017	79
12	003	81

Table 4: Growth Faults (Bozkurt and Sözbilir, 2004)

No	Dip direction (°N)	Dip amount (°)
1	188	43
2	210	72
3	200	74
4	035	67
5	210	77
6	030	80
7	160	64

In this study, dip angle of fault calculated from wells correlation. Total mud loss depth of two wells which are believed to target the same fault are used to estimate dip angle. Dip angle of north dipping fault is calculated as 10 ° (Figure-17).
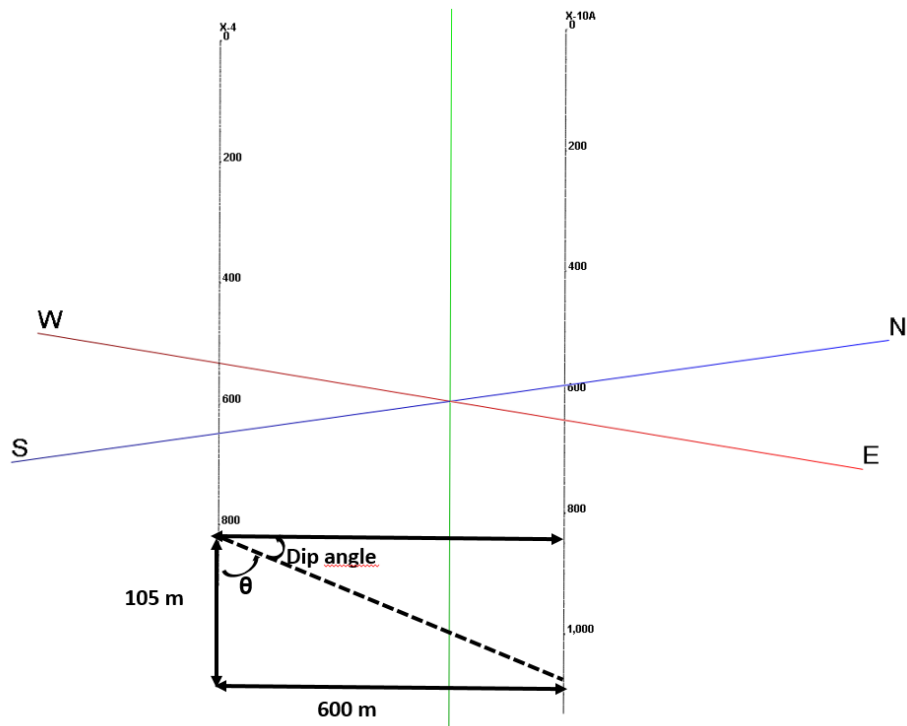
Figure 17: Direction and Dip Angle of Fault from Well Correlation

5.2.2 Drilling Mud Loss

One of the strongest indication for existence of natural fractures in geothermal reservoir is the partial or total mud loss during drilling. Invasion of large drilling fluid volume into productive pay zone is not desired because of solid particles related, skin effect near wellbore. However, mud losses provide a good insight about fracture characteristics before conducting a well test. Association of mud loss with fracture permeability was first introduced by Drummond, (1964). Since then, several qualitative and quantitative models have been proposed. These models were initially based on compressible Newtonian mud invasion in a fracture with a constant aperture. To illustrate, Sanfillippo et al. (1997) developed an analytical solution to estimate hydraulic fracture aperture by considering diffusivity equation with a constant pressure boundary. Later on, Lietard et al. (1999) introduced a non-Newtonian Bingham plastic mud and type curve matching method to estimate hydraulic fracture aperture. Their work was further developed by Majidi et al. (2008) by using yield-power law to include the effect of formation fluid.

34

Lastly, Huang et al. (2011) used cubic equation which is a simpler and direct method as an alternative to type curve matching. The cubic equation is derived from the transient radial invasion of mud loss which can be found in Lietard et al. (1999).

$$(r_s)_{max} = 1 + \frac{w\Delta p}{3 r_w \mathcal{T}_y} \tag{5.12}$$

$$(V_m)_{max} = \pi w [\, (r_s)_{max}{}^2 - r_w{}^2] \tag{5.13}$$

$$(\frac{\Delta p}{\mathcal{T}_y})^2 w^3 + 6 r_w \left(\frac{\Delta p}{\mathcal{T}_y}\right) w^2 - \frac{9}{\pi} (V_m)_{max} = 0 \tag{5.14}$$

Where is $\frac{\Delta p}{\mathcal{T}_y}$ overpressure ratio, r_w is wellbore radius, $(V_m)_{max}$ represents the maximum mud loss, r_s is invasion radius, fracture width is denoted as w.

Investigation of the fracture width and permeability from mud loss data can be found in Akin, (2013). He used the cubic equation proposed by Huang et al. (2011) coupled with an artificial neural network model (ANN). His study includes drilling mud loss data of three wells and results are given in (Table-5).

Table 5: Results of Cubic Law and ANN (Akin, 2013)

Well	1	2	3
Drill bit diameter, inch	8.5	8.5	8.5
Mud-loss Volume, bbl	1666	1147	1264.9
Number of Events	36	22	138
Overpressure ratio	641777.8	684000	684000
Calculated aperture, m	3.71×10^{-4}	3.7×10^{-4}	2.07×10^{-4}
Calculated permeability, mD	745.12	1100.23	83.37
Well Test Derived permeability, mD	517.21	968.35	255
ANN aperture, m	3.87×10^{-4}	$4.45 \times 10^{-}$	1.68×10^{-4}
ANN permeability, mD	846.26	1286.62	44.5

5.2.3 Seismic Study

Exploration for geothermal potential of Gediz graben started in 1989 with TPAO (Turkish Petroleum Corporation). 2D seismic lines, magnetic and gravity studies conducted in the field. Several scientists have been interpreted the seismic data (Yilmaz and Gelişli, 2003; Bozkurt and Sözbilir, 2004; Çiftçi, 2007; Demircioğlu et al., 2010). Although seismic sections provide large scale of information about subsurface, it has low resolution which may lead wrong interpretations. After oil discovery in Alaşehir field, most of the studies focused on the fillings overlaid the metamorphic. They estimated tectonic evaluation of the field by interpreting outcrop and seismic data. The consensus about the field is as follow:

-   Alaşehir Graben developed as the result of N-S extensional tectonic.

-   There are some major normal faults system which are low angle (0-20°) detachment and high angle (various synthetic and antithetic faults).

-   North dipping low angle detachment fault is older than high angle normal faults

-   Southern detachment fault controlled the structure of the field.

The controversy raised from the relation of normal faults and detachment. Another controversy is the structural driving mechanism of the graben. Çiftçi and Bozkurt (2009) stated that the younger high angle normal faults and inactive low angle detachment faults are superimposed. They concluded that high angle faults cross-cutting the low angle detachment fault and displace it. Therefore, low angle detachment fault had high angle in the beginning which suggested the episodic extension of the graben. On the other hand, Demircioglu et al. (2010) proposed that normal faults and detachment fault are merged (Figure-19) and there is no cross cutting. Based on this consideration they argue rolling hinge mechanism.

In Alaşehir field, geothermal wells, which are located in the southern margin, are targeted to intersection of E-W trending high angle normal faults and north dipping detachment fault.
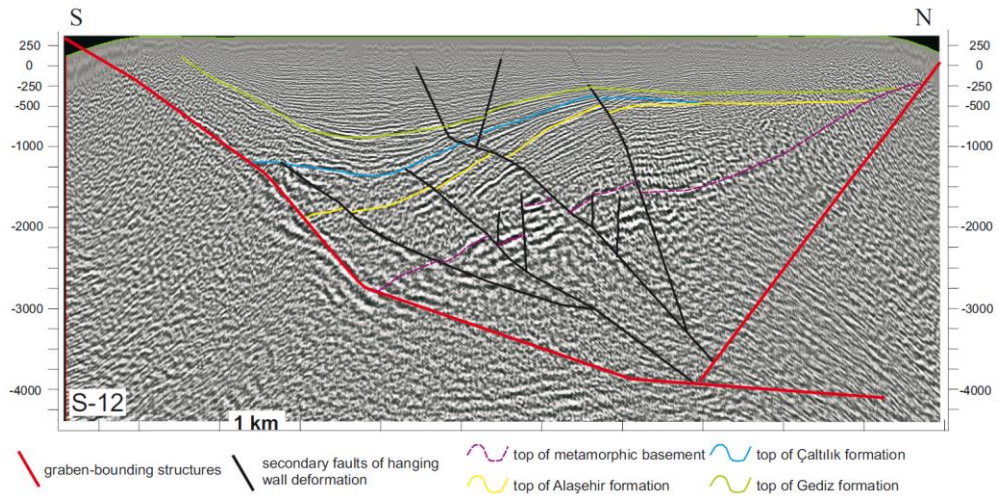
Figure 18: South-North Seismic Section (Çiftçi, 2007)
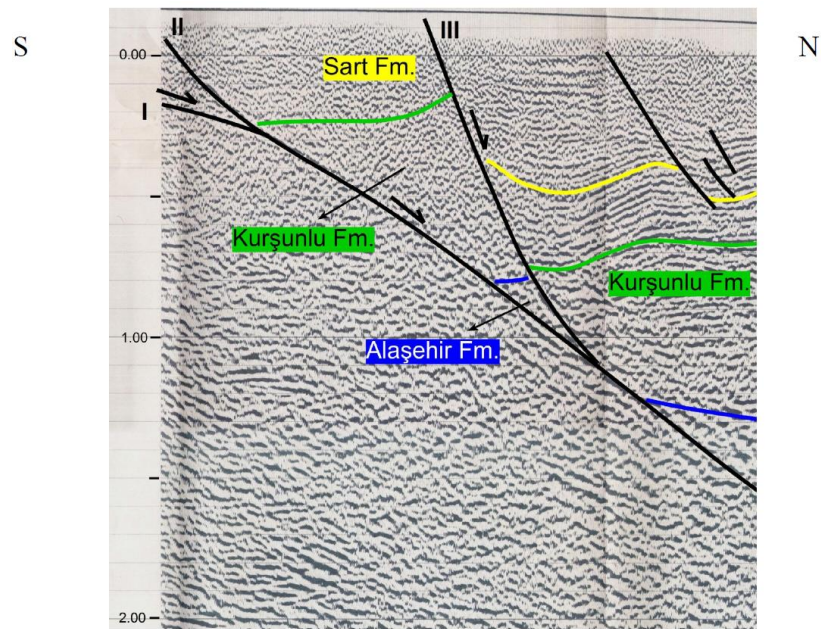
Figure 19: N- NE Trending Seismic Section (Demircioglu et al., 2010)

5.3 Static Model

In constructing the static model for a particular field area, Fracman7.6 required fracture parameters which are fracture aperture, permeability, length, orientation and fracture density. These parameters are usually considered as distribution instead of taking average value. Therefore, the static model is populated from different data sources to make it more reliable. The Enhanced Beacher model is used to generate fractures in constructing static model of Alaşehir reservoir. In FracMan7.6, geocellular fractures are generated based on grid blocks. There are ten production wells in DFN model. Each well was assumed to produce from a rectangular shape boundary with 1200 m length-side and the height of the particular area is taken as the penetrated thickness of the metamorphic. Input parameters are given in (Table-6). The constrained area is divided into 10x10x10 (1000 grids) for each well (Figure-20). Stochastic fractures are generated in these grid blocks based on the fracture parameters introduced to the software. (Figure-21).

Table 6: Fracture Characteristics for Static Model

|	Mean Fracture length (m) (exponential)	Mean Volumetric Fracture Intensity(1/m) (exponential)	Reservoir pay zone (m) Uniform distribution	Mean Permeability(md) Lognormal distribution	Mean Fracture Aperture(mm) Exponential distribution
Well X-1	20	0.06	200	1360	1.6
Well X-2	20	0.065	300	570	1.3
Well X-3	25	0.073	56	3600	1.6
Well X-4	25	0.06	214	5600	1.5
Well X-5	20	0.08	50	216	1.5
Well X-8	25	0.065	117	220	1.6
Well B-1	25	0.045	250	340	1.8
Well B-2	25	0.055	586	420	1.7
Well W-2	20	0.055	170	500	1.6
Well C-3	25	0.06	200	38	1.6
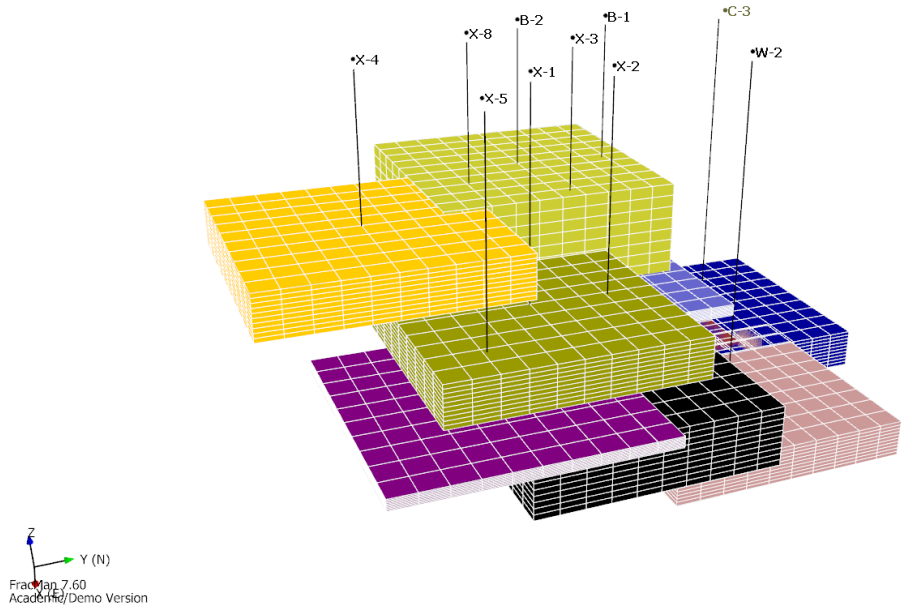
Figure 20: Grid Blocks for DFN Modeling
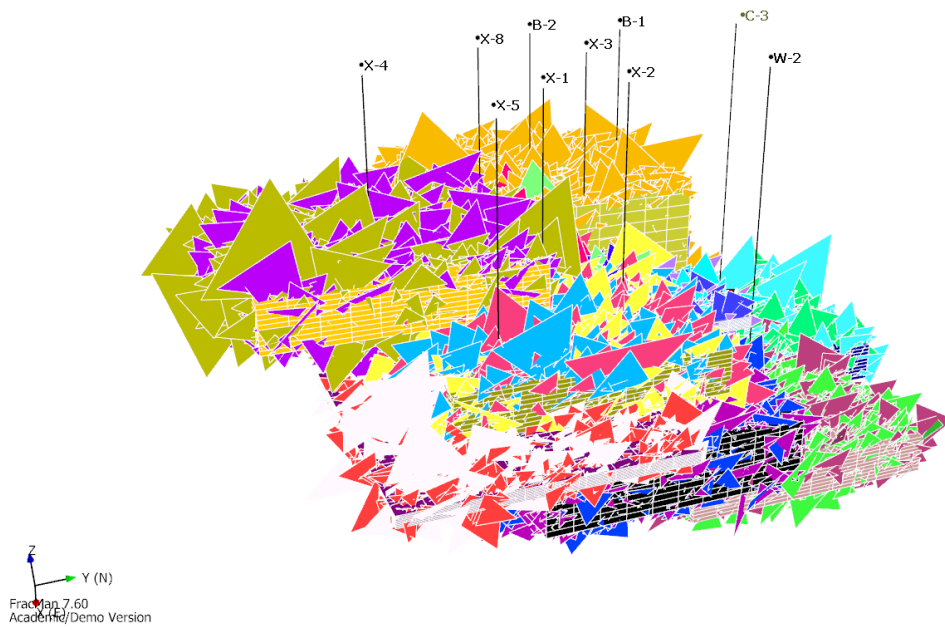
Figure 21: Stochastic Fractures Set

39

5.4 Dynamic Model Analysis and Calibration

FracMan7.6 enables us to simulate fracture sets for a transient test of single phase and slightly compressible fluid. The software provides the flow calculation for both injection and production events. Galerkin's finite element method is used in fluid flow calculation. The method subdivides fractures into smaller triangular elements (Figure-22). The networks between these triangular elements are generated by meshing process for fluid flow simulation. In well test simulation, mesh size, initial pressure, fracture set, production pay zone, test duration and fluid properties need to be specified. Small mesh size provides more accurate simulation results but the simulation run time takes longer. In this study, mesh size is taken in the range of 20 to 50 meters based on fracture density and pay zone thickness which affect the simulation run time. Fluid properties are calculated from empirical correlations. To illustrate, formation volume factor and density of water is calculated from correlation given in Gould, (1974). Water viscosity was estimated from Meehan, (1980) correlation. Brill and Beggs, (1973) correlation is used to find water compressibility
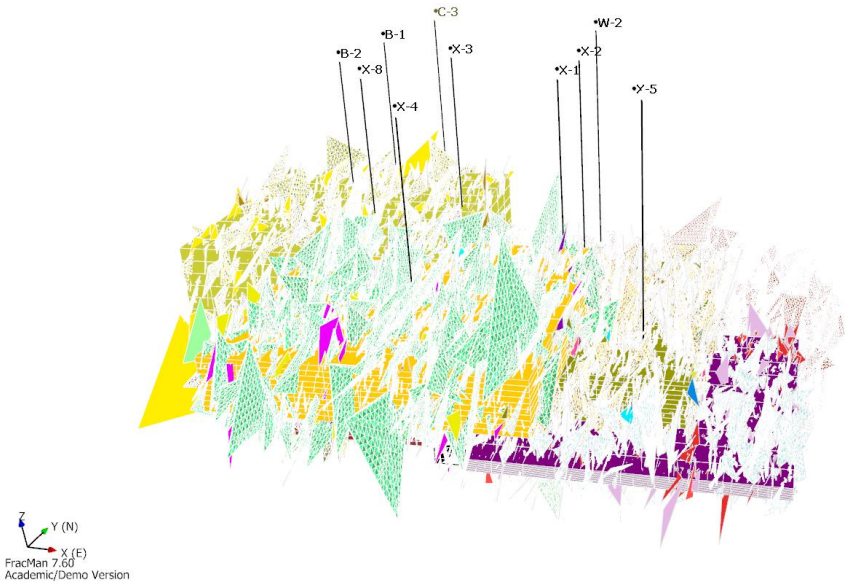

Figure 22: Meshed Fractures Set

The dynamic model calibration is achieved by tuning fracture length, fracture aperture and fracture density. Fracture permeability is taken as the results obtained from pressure transient well test analysis and it was not considered as a tuning parameter.

However, instead of taking one deterministic value of permeability, it was considered as log normal distribution in the model. Well effect was also included in well test simulation to account for skin effect in early time of pressure buildup test. The procedure given in workflow scheme was applied until a good match obtained between actual test data and simulation results (Figure-23).

In order to test goodness of fit between simulation result and actual test data, chi-square test is applied. The test uses the following equation:

$$X^2 = \sum \frac{(O-E)^2}{E} \tag{5.15}$$

Where;

X^2: Chi-square test statistic

O: Actual Test Data

E: Simulation Test Data

Null hypothesis defined as there is a good match if p-value of X^2 is higher than α=0.05. To calculate p-value, number of degrees of freedom need to be known. Generally, number of degrees of freedom is taken as number of samples minus one. Microsoft Excel has a function called CHITEST (Actual_range; expected range) to calculate p-value of data set which must have the same dimension and not correlated to each other. In this study, p-value of all simulation results are 1.0 which is higher than 0.05. This means that the goodness of match is significant with 95 % confidence. A good visual match was also obtained for all simulations (Figure-23).
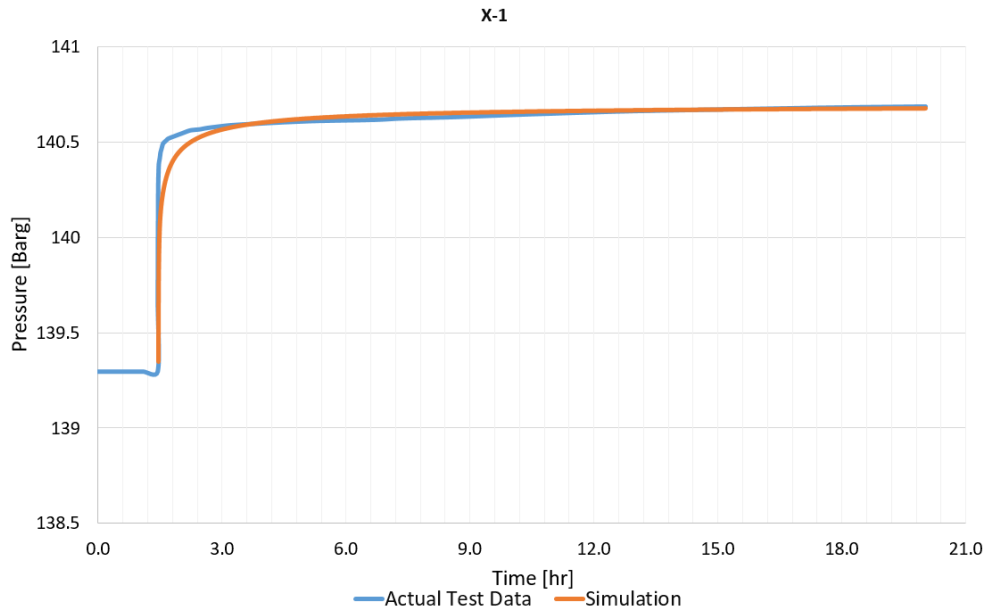
Figure 23: Match between Actual Test Data and Simulated Data for Well X-1

5.5 Fracture Upscaling

FracMan7.6 provides number of analyses on grids and fractures to upscale fracture properties. The analyses included in this study are cluster analysis, pathway analysis and Oda analysis. The upscaling properties from these analyses are proper for flow simulators such as Eclipse Petrel and CMG Stars.

The main target of cluster analysis is to identify compartmentalization by processing fracture sets and find out isolated groups of self-connected fractures. Fractures set of each well is selected and cluster analysis was performed. In the analysis, minimum number of fractures in a cluster was considered as 20. The total number of clustered fractures and total volume of clustered fractures are given in (Table-7). There was no identified compartmentalized fracture set in this particular study area in Alaşehir.

Table 7: Cluster Analysis

	X-1	X-2	X-3	X-4	X-5	X-8	W-2	B-1	B-2	C-3
Number of Clustered Fractures	15963	16287	3112	6949	2587	6316	7596	5419	6825	6598
Total Volume of Clustered Fractures, m³	818982	712821	267316	538404	147329	530631	431857	437356	731095	566625

By performing pathway analysis, geometric connections between wells can be identified. FracMan7.6 is able to compute geometry of the connected fractures between sources and sink wells defined by users. The software reports geometry of shortest and the highest conductance pathways between wells such as path length, number of fractures and total volume of fractures. The pathway analysis for wells near to each other performed and result is given in (Table 8). The shortest pathways are responsible for early breakthrough of tracers or cold water. In Alaşehir geothermal field, shortest pathways are denser in production well which are closer to the injection area. Highest conductance pathways dominate the flow direction and production rate of wells. It was found that fracture volume increases from East to west and from North to south of the field. Therefore, production wells on the eastern and northern part of the field may be affected negatively in terms of temperature and CO_2 decline

Table 8: Shortest Flow Paths and Highest Conductance Flow Paths

	Shortest Flow Paths			Highest Conductance Paths	
	Fracture Length	Number of fractures	Fracture Volume,m^3	Number of fractures	Fracture Volume,m^3
X-1 to X-2	657	12	324	223	36765
X-1 to X-3	1020	21	291	215	21150
X-1 to X-4	1373	24	226	200	30524
X-1 to X-5	708	16	72	100	11847
X-1 to X-8	1522	24	296	278	49533
X-4 to X-8	885	12	181	79	20475
X-4 to X-5	2535	38	718	153	25451
X-8 to X-3	830	16	281	212	29940
X-8 to B-2	520	12	15	127	44853
B-2 to X-3	1005	16	623	467	68956
B-2 to B-1	2620	42	726	1229	137729
B-1 to C-3	657	10	75	118	14138
B-1 to W-2	1931	23	376	98	11932
C-3 to W-2	1965	21	760	20	24663
X-3 to X-2	1485	27	628	915	70243

Permeability is an anisotropy rock parameter which changes with direction in reservoir. FracMan7.6 has Oda analysis to account for directional permeability variation. The analysis calculates permeability tensors in x, y and z directions for each grid block. Oda permeability assumes that there is no flow in a direction parallel to their unit normal. The analysis, does not need flow simulations for calculation but the disadvantage is that it does not consider fracture size and connectivity, which limit it to wells connected fractures networks.

Thus, permeability obtained from Oda's analysis is over-estimated compared to dynamic well test analysis. Fracture porosity is denoted as P_{33} (dimensionless) and calculated as multiplication of one-sided surface area of fracture with fracture aperture for a given unit volume. Oda analysis results are given in (Table-9 and Table-10). It was found that vertical permeability of wells in Western of the particular study area is higher than permeability of X and Y direction. Wells located in Eastern of the field have higher permeability in direction of X and Y. It can be concluded that Western of the field produces from deeper depths while the flow contributions of horizontal directions are dominant in Eastern wells. Mean fracture porosity is less than 3 % for all wells. There are no significant porosity variations in the field. However, the metamorphic rock is at shallower depth in South of the field, which may be an indication for higher reservoir thickness. The spatial distribution of porosity is given in (Figure-24).

Table 9: Results of Fracture Upscaling

	Well-X1	Well-X2	Well-X3	Well-X4	Well-X5
Number of Grids	1000	1000	1000	1000	1000
Max Porosity,%	7.1	4.1	5.8	3.4	4.3
Min Porosity,%	0.2	0.3	0.6	0.2	0.2
Mean Porosity,%	2.9	1.5	2.6	1.37	1.4
Max Permeability in X direction	1861	627	2169	878	1005
Min Permeability in X direction	56	11.4	170	18	21
Mean Permeability in X direction	429	81	657	235	203
Max Permeability in Y direction	6207	3301	6680	3068	5022
Min Permeability in Y direction	329	65	1186	202	102
Mean Permeability in Y direction	2155	417	3257	1218	984
Max Permeability in Z direction	5793	3133	6672	3179	4903
Min Permeability in Z direction	328	61	1170	207	102
Mean Permeability in Z direction	2026	398	3068	1149	927

Table 10: Results of Fracture Upscaling

	Well-X8	Well-B1	Well-B2	Well-W2	Well-C3
Number of Grids	1000	1000	1000	1000	1000
Max Porosity,%	6.9	5.1	5.9	5.6	5.2
Min Porosity,%	0.4	0.4	0.02	0.4	0.44
Mean Porosity,%	3.1	1.7	1.4	1.8	2.1
Max Permeability in X direction	1094	949	1136	943	997
Min Permeability in X direction	24	19	2	36	24
Mean Permeability in X direction	352	365	166	227	274
Max Permeability in Y direction	5343	3928	4781	4399	4266
Min Permeability in Y direction	247	275	9	227	143
Mean Permeability in Y direction	1815	1766	828	1152	1345
Max Permeability in Z direction	4814	3789	4263	4134	4022
Min Permeability in Z direction	240	263	8	215	137
Mean Permeability in Z direction	1708	1662	785	1084	1258
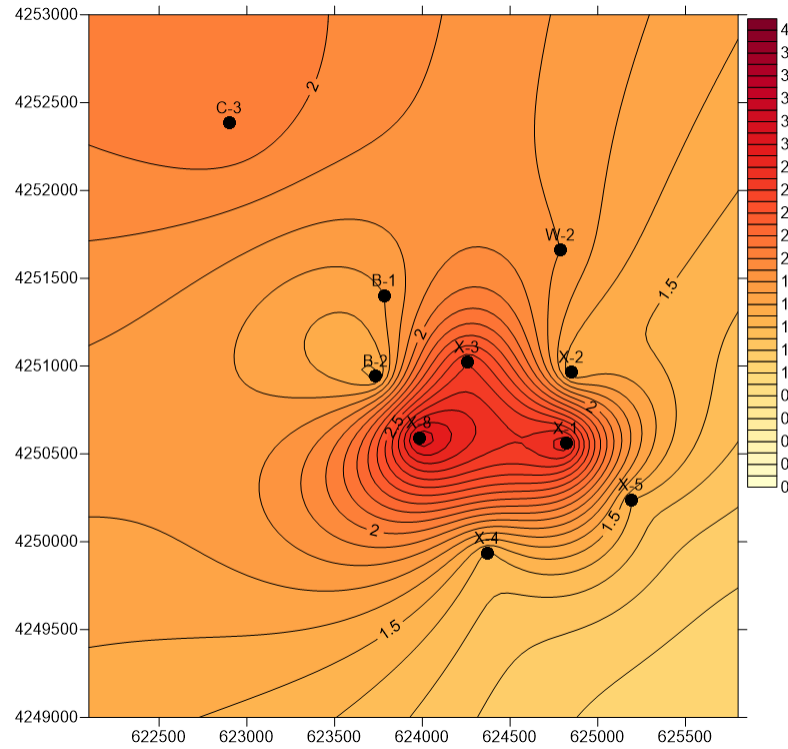
Figure 24: Porosity Distribution

CHAPTER 6

RESERVOIR MONITORING

6.1 Geochemical Analysis

In geothermal energy utilization, produced fluid and waste reinjection brine have different properties such as temperature, pH, EC (Electrical Conductivity) and concentration of chemical components including chloride, total hardness, silica and bicarbonate. Since the nature of the hosted reservoir fluid changes with reinjection brine, monitoring the changes in geochemical properties of the production wells is usually very useful in evaluating a geothermal system. Therefore, CO_2 (Carbon dioxide), Cl (Chloride) and SiO_2 (Silica) concentration of the production wells have been monitored to understand the reservoir reaction to long term reinjection in Alaşehir geothermal field.

Chloride is considered as a nonreactive and conservative chemical component and it is not controlled by reservoir temperature. Unlike other components, Cl does not tend to precipitate in the reservoir and surface conditions. Especially, in flashing type power plants Cl content of the reinjection brine increases continuously. Therefore, elevation in Cl concentration of production wells can be considered as the indication of arrival of reinjection fluid which makes Cl a natural tracer. In Alaşehir geothermal field, Cl is used to understand the effect of reinjection wells on production. It was observed that Cl concentration was slightly increased from 220-225 ppm to 240-250 ppm in the first year of production. In the second year, a new power plant put on production. Four new reinjection wells were used in this binary type power plant at injection side of the

existing injection wells. As new injection wells started to reinject, wellhead pressure of existing injection wells increased at least 3.5 barg which shows that all injection wells are in the same fracture network system. Chloride concentration of production wells increased to 260-290 ppm in a very short time (Figure-25). Although, elevation in Cl concentration of injection wells in the binary power plant is lower than flashing system, it was considered that equilibrium Cl concentration occurs at the reservoir and as the new reinjection wells introduced to the system, circulation of the re-injection fluid in the reservoir became faster than before. Thus elevation in Cl concentration accelerated. Spatial distribution of Cl content at different time shows the conductive flow paths in the field. It can be clearly identified that there is a conductive path from S-13 to X-4 and X-8 from the South of the field (Figure-26 and Figure-27). Another target of the reinjection fluid is found as center of production area which probably produce from intersection of N-S and E-W trending faults.
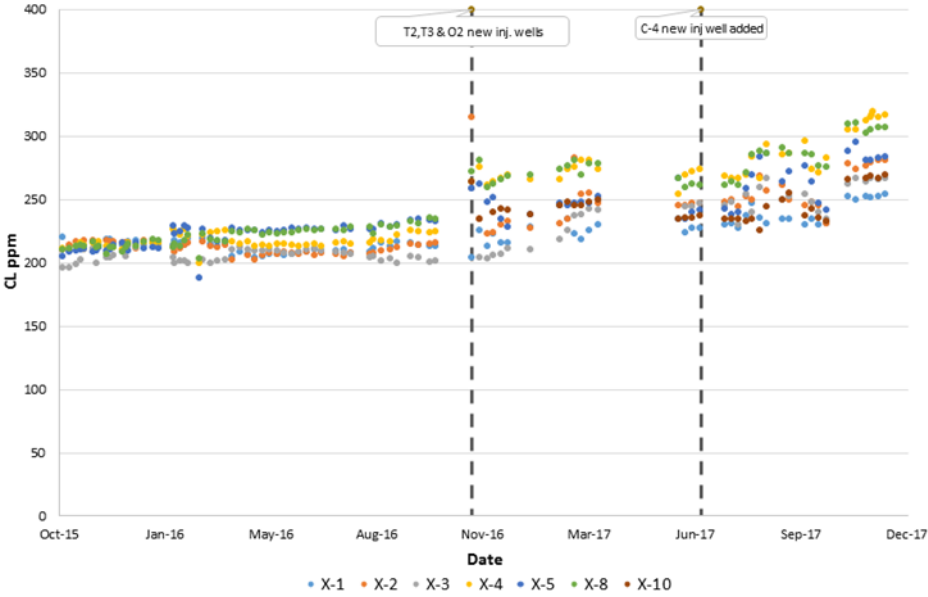
Figure 25: Change of Chloride Concentration

Figure 26: Spatial Distribution of Chloride Concentration, November 2015

Figure 27: Spatial Distribution of Chloride Concentration, May 2016

Geothermal fields in Western Turkey contains significant amount of non-condensable gases (NCG) dissolved in the liquid dominated reservoir fluid. Some investigators reported NCG content of geothermal fields in Turkey as follows: Haizlip et al. (2013)

reported NCG content of the reservoir ranging from 1.5% to 3.4%. Akin (2017) reported NCG content of Alaşehir geothermal field as 2 % to 4 % by weight in the reservoir. Since more than 99 % of non-condensable gases consists from CO_2, it is worth to consider CO_2 instead of NCG. Haizlip et al. (2016) investigated the origin of CO_2 in Western Turkey. They concluded that origin of carbon dioxide is calcite dissolution. They also stated that carbon isotope analysis suggested no indication for magmatic origin CO_2. Therefore, equilibrium of calcite mineral with geothermal fluid plays the main role in CO_2 production. Temperature, pressure, pH and salinity are the main parameters affecting the calcium equilibrium in water. The reactions and equilibrium constants that carry CO_2 in different forms are given in Haizlip et al. (2016) in detail. To summarize, reinjection brine has higher pH which has basic property and dissolve less amount of CO_2 while travelling to production wells. Therefore, decline of CO_2 production is common in geothermal production wells. In Alaşehir geothermal field, a sharp decline of CO_2 has been observed which shows that there is a strong connection between injection and production wells. The CO_2 production decreased by 60 % in two years. Spatial distribution of CO_2 with time is given in Figure-28, Figure-29 and Figure-30.

Figure 28: Spatial Carbon Dioxide Distribution (wt %) at September 2015
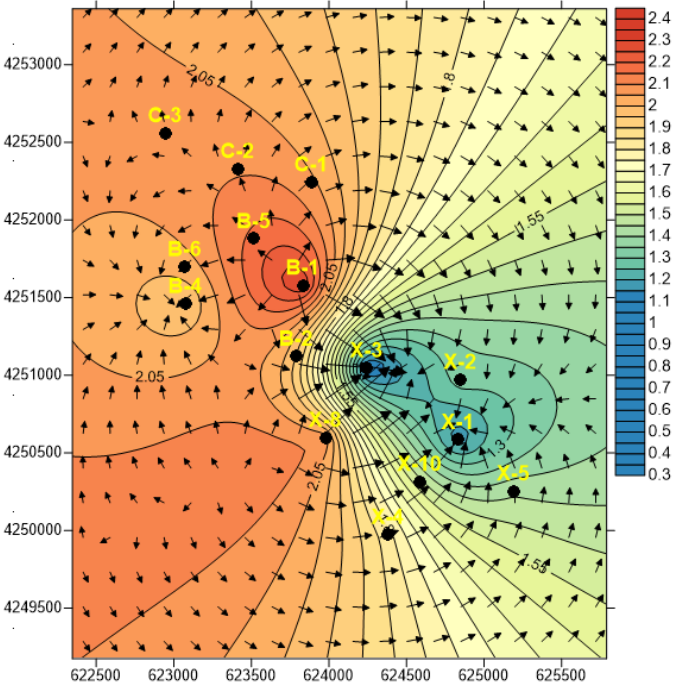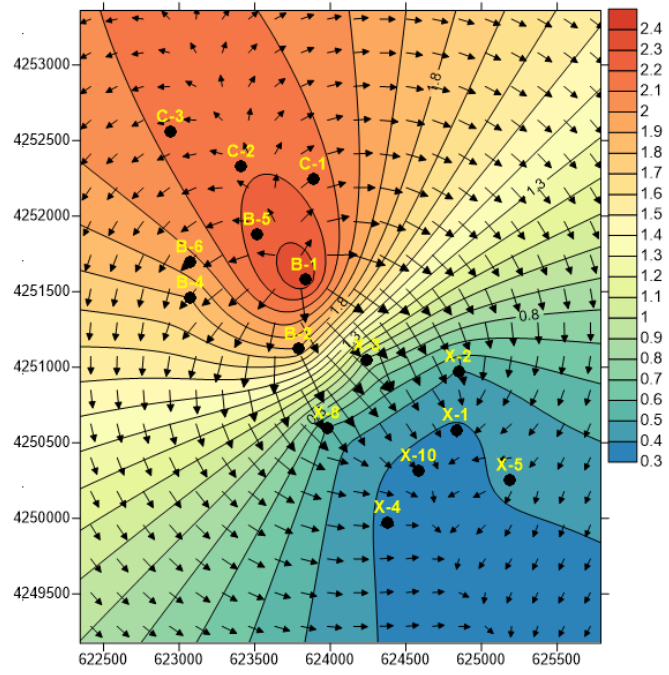
Figure 29: Spatial Distribution of Carbon Dioxide (wt %) at May 2016
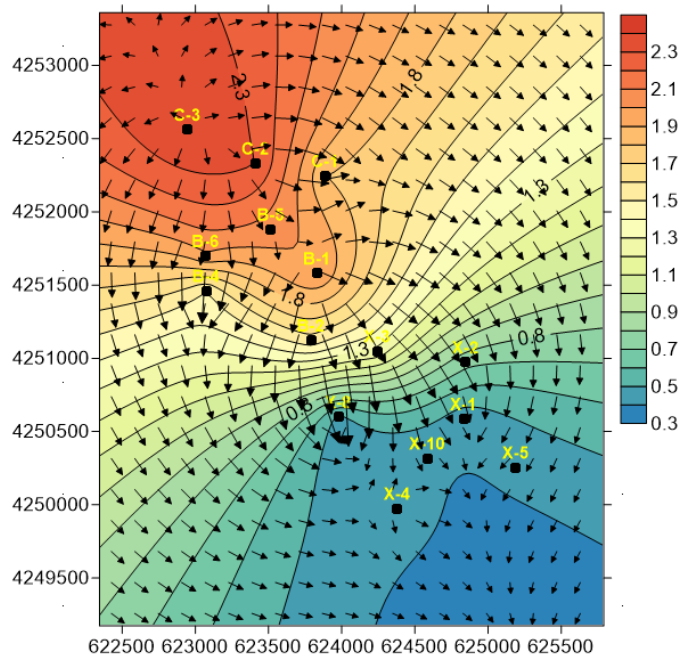
Figure 30: Spatial Distribution of Carbon Dioxide (wt %) at January 2017

Silica is one of the most reactive geochemical component that is controlled by temperature. Fournier (1989) stated that solubility of silica decreases as temperature decreases. Therefore, it is usually monitored to estimate temperature reduction in production wells. In addition, silica is used as a geothermometer to estimate reservoir temperature. In Alaşehir geothermal field, silica concentration decreased slightly in production wells which are closer to injection area. However, as new reinjection fluid is introduced in the field, decline of silica concentration accelerated, which is an indication of premature temperature decline (Figure-31).
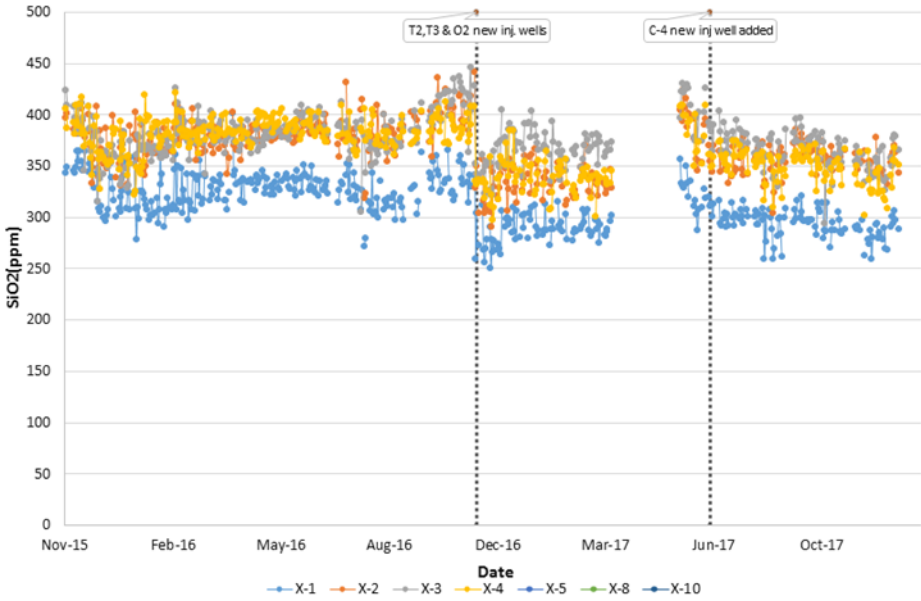
Figure 31: Change of Silica Concentration in Production Wells

6.2 Tracer Test

In Alaşehir geothermal field, a comprehensive tracer test conducted to identify interconnection between production and injection wells (Akin, 2017). It was also aimed to quantify fracture pore volume, mean fluid velocity in the reservoir, recovery of the injected brine and reservoir heterogeneity. To achieve these purposes, four different naphthalene sulfonates: 2ns (Naphtalenesulfonic Acid Sodium Salt), 1,3,6 nts (Naphtalenetrisulfonic Acid Trisodium Salt), 1,6 nds (Naphtalenedisulfonic Acid Disodium Salt) and 2,6 nds (Naphtalenedisulfonic Acid Disodium Salt) were injected into four different injection wells simultaneously.

It was observed that all injected tracers were detected in all of the production wells with different tracer return curves. This shows a strong connection between injection and production wells (Figure-32). N-S and E-W trending faults were considered as intersected and there is no compartmentalization in the study area. The amounts of recovered tracers are given in (Table-11).

Table 11: Recovered Tracer Amount (Akin, 2017)

Wells	S-6	O-1	Z-9	W-1
	2 ns, 100 kg	1,3,6 nts, 100 kg	1,6 nds, 100 kg	2,6 nds, kg
X-1	1.33	19.94	11.52	0.36
X-2	1.23	16.33	7.62	
X-3	1.84	4.43	3.35	6.39
X-4	34.38	8.21	11.79	0.20
X-5	3.80	1.28	6.47	0.03
X-8	23.42	5.58	9.23	0.12
X-10	0.31	0.16	0.08	
X-10A	6.37	24.41	21.24	0.34
B-1		1.32	0.85	4.23
B-2	3.00	0.44	0.86	0.67
B-4	0.93	0.03	0.22	0.03
B-5	0.26	0.01	0.08	0.02
B-6			0.06	0.33
C-1			0.01	0.09
C-2				0.07
C-3				0.19
Total	76.87	82.15	73.38	13.07

Akin (2017) performed momentum analysis to quantify tracer swept pore volume, flow geometry and their heterogeneity. Dykstra Parsons and Lorentz coefficients are usually used for heterogeneity purposes Shook (2003).

Zero value of coefficients means a homogeneous reservoir and one represents heterogeneous reservoir. In all tracer types, the highest coefficient value was observed in well X-1. This means that well X-1 produces from a highly heterogeneous fracture system, which may have formed due to intersection of conductive faults. Lorentz and Dykstra Parsons coefficients of other wells are similar (Table-12, Table-13 and Table-14). Swept pore volume between well S-6 and well X-1 was 5 times smaller than others. This means that while traveling to well X-1 fluid flows mainly through major faults instead of entering fault related fractures. Pore volumes calculated from moment analysis are in a good agreement with fractures pore volume of DFN modeling (Figure-32, Figure-33 and Figure-34).
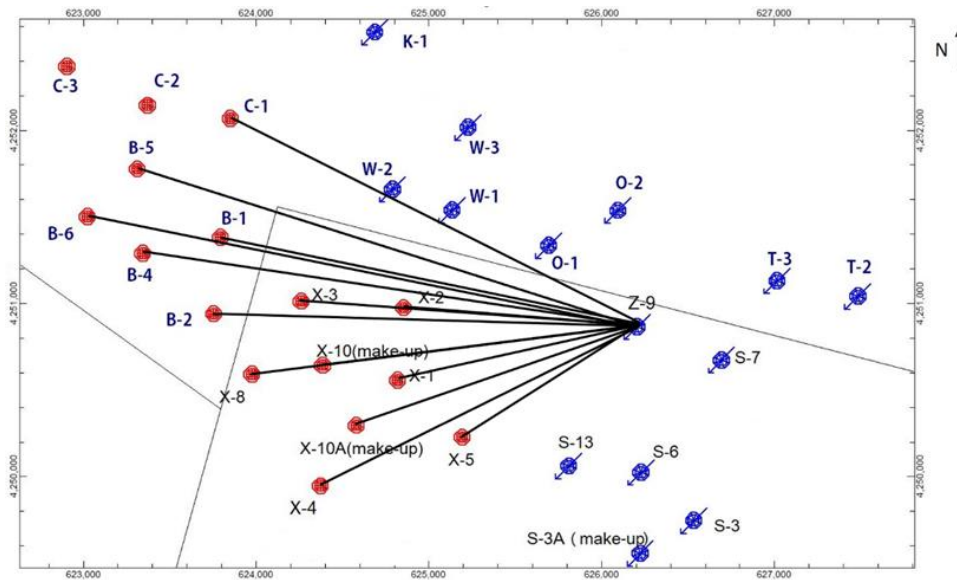
Figure 32: Communication between Z-9 and Production Wells

Table 12: Swept Pore Volume and Heterogeneity Coefficients of NTS 1,3,6

Well-O1 nts-1,3,6							
	Well X-1	Well X-2	Well X-3	Well X-4	Well X-5	Well X-8	Dimenssion
Swept Pore Volume	72694	76293	22398	81434	28044	37522	M^3
Lorentz Coefficient	0.469	0.027	0.161	0.139	0.139	0.136	Dimensionless
Dykstra-Parsons Coefficient	0.532	0.22	0.20	0.174	0.181	0.158	Dimensionless

Table 13: Swept Pore Volume and Heterogeneity Coefficients of NDS 1,6

Well-Z9 nds-1,6							
	Well X-1	Well X-2	Well X-3	Well X-4	Well X-5	Well X-8	Dimenssion
Swept Pore Volume	63804	67100	153598	92478	114040	61631	M^3
Lorentz Coefficient	0.337	0.137	0.154	0.181	0.196	0.025	Dimensionless
Dykstra-Parsons Coefficient	0.369	0.239	0.176	0.214	0.217	0.209	Dimensionless

Table 14: Dykstra-Parsons and Lorentz Coefficients of NS-2

Well-S6 ns-2							
	Well X-1	Well X-2	Well X-3	Well X-4	Well X-5	Well X-8	Dimenssion
Swept Pore Volume	9731	46256	20536	79125	33560	71238	M^3
Lorentz Coefficient	0.316	0.289	0.201	0.232	0.270	0.230	Dimensionless
Dykstra-Parsons Coefficient	0.307	0.301	0.139	0.258	0.299	0.237	Dimensionless
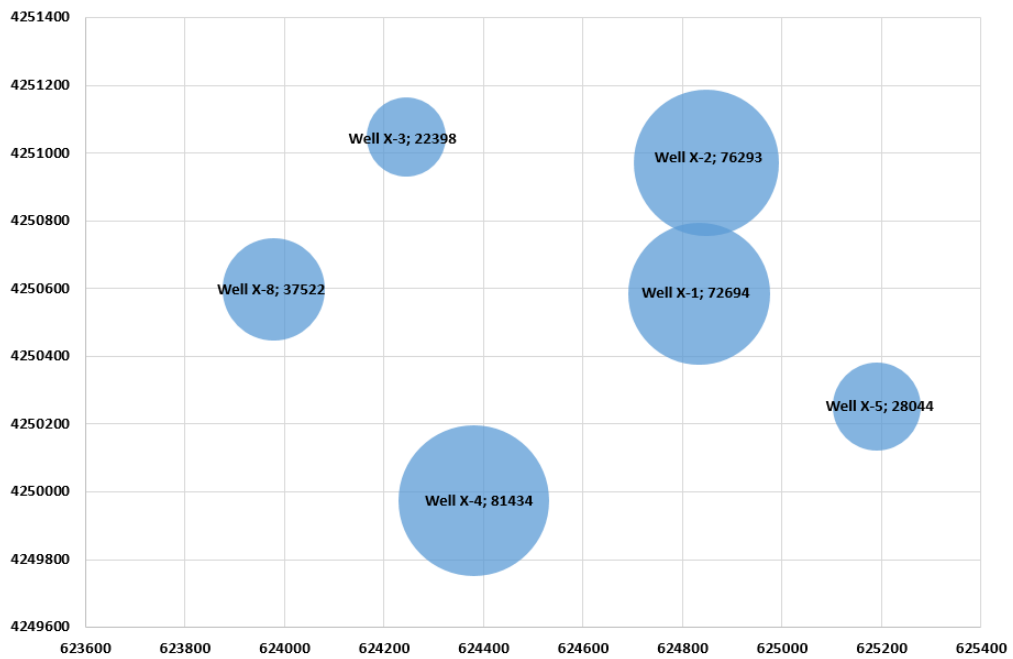
Figure 33: Fracture pore volume of tracer NTS 1,3,6

55
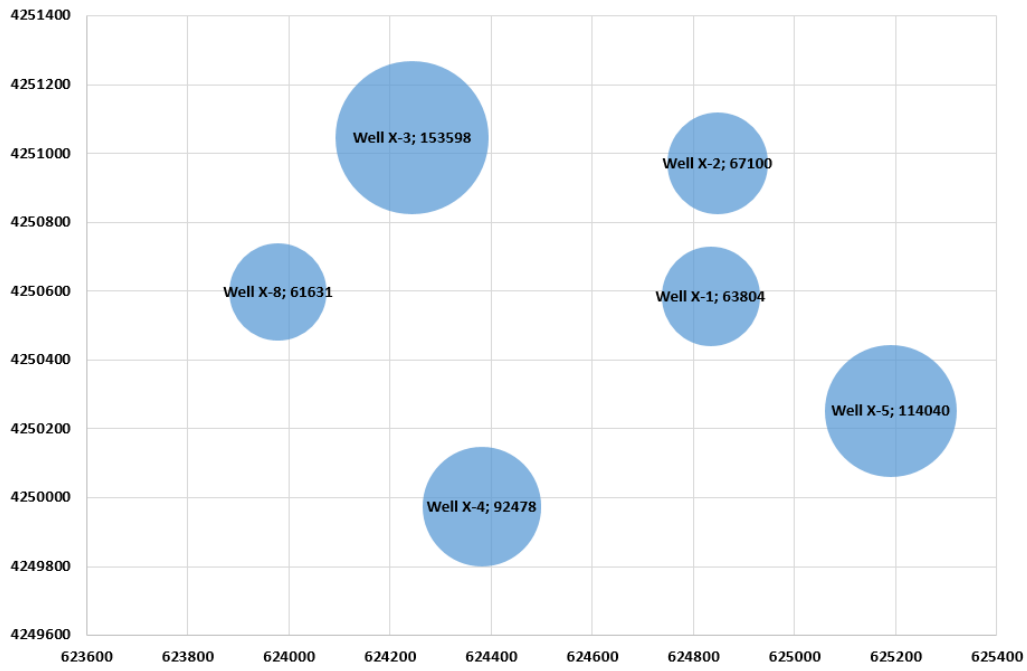
Figure 34: Fracture pore volume of tracer NDS 1,6
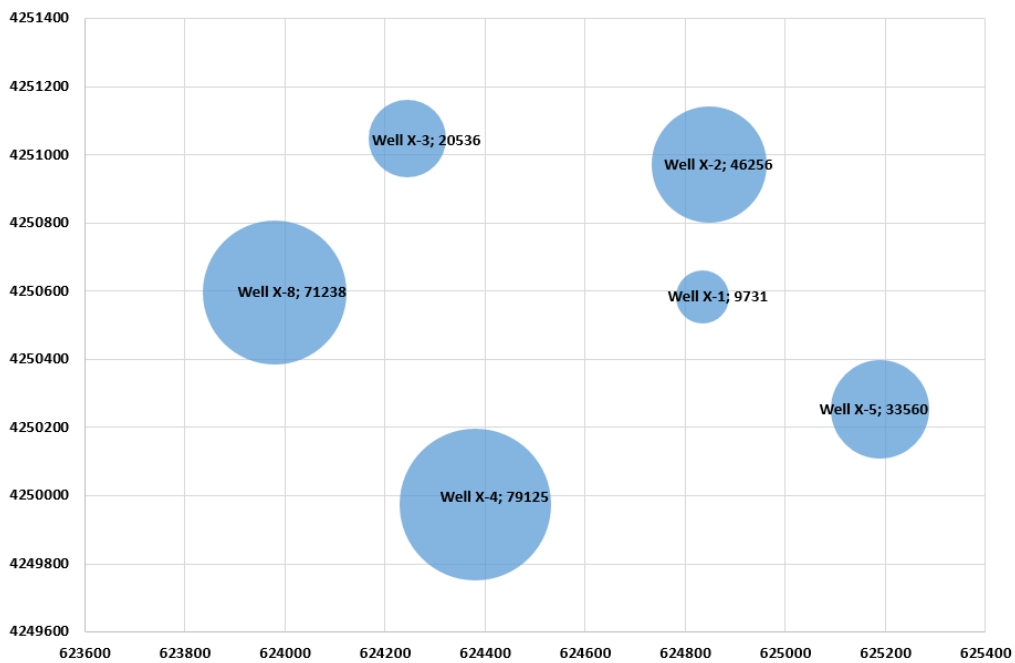
Figure 35: Fracture pore volume of tracer ns 2

6.3 Pressure Transient Test

Pressure transient test is an indirect method to obtain the reservoir characteristics. The test can be conducted in a single well or a set of wells. The concept of single well test is to create pressure disturbance by changing flow rate in a well while pressure values are continuously recorded in the same well. In multi well test, pressure disturbance is created and recorded in more than one well. Based on the goal of the test, there are several types of transient tests. Kamal et al., (1995) reported reservoir characteristic properties that can be obtained from various transient tests (Table-15).

Table 15: Types of Pressure Transient Tests (Kamal et al. 1995)

	DSTs	Wireline Formation Test	Drawdown Test	Buildup Test	Step Rate Test	Falloff Tests	Interference and Pulse Tests
Fluid Samples	√	√					
Permeability	√		√	√	√		
Skin	√		√	√	√	√	
Fracture Length	√		√	√		√	
Reservoir Pressure	√			√		√	√
Reservoir Limit	√		√			√	
Boundaries	√		√	√			
Pressure profile		√					
Reservoir Behaviour			√	√			√
Formation parting pressure					√		
Communication between wells							
Porosity							√
Interwell Permeability							√

Several well test interpretation methods have been developed. Straight line method, type curve matching and pressure derivative analysis are the most widely used techniques. Computer-aided well test analysis has become famous and time saving with nonlinear regression. Horne, (1990) discusses the advantages and limitations of these interpretation methods in detail.

In Alaşehir geothermal field, pressure buildup tests were conducted in most of the wells. Prior to buildup test, a static pressure − temperature test and a short term flow test were conducted to identify major feeding zones and for clean out purposes.

Once clean flow is observed, well flow rate is adjusted to desired constant rate. Due to mud pit size limitation, flow duration was usually limited to 2-3 hours.

After that PT (pressure, temperature) tool was run into well to a desired depth for pressure recording. Flow control valve was closed in a very short time for pressure buildup. However, electronic PT tool has temperature dependent time limitation at the downhole, therefore most of the buildup tests were limited to 3-6 hours. However, in some wells mechanical pressure gauges was used which enable us to extend the test duration.

Well test analysis was performed by using Saphir which is a module of Kappa's Ecrin software (Houze et al. 2013). The software has automatic type curve matching for pressure derivative curve and some special straight line techniques to estimate reservoir parameters. In Saphir, by performing nonlinear regression reservoir characteristics are estimated with a certain confidence interval. However, it is important to select a proper well model, reservoir model and boundary conditions for test interpretation. In addition, Saphir has some options to identify the proper model and for initial estimation of reservoir parameters. To illustrate, wellbore storage has unit slope in initial time of log-log plot, in semi-log graph transmissivity value is obtained at infinite acting radial flow time interval which can be found as a flat line in middle time of log-log plot (Figure-36). In late time of log-log plot, special lines with different magnitude of slopes are available for boundary types. Alaşehir geothermal field has highly fractured and vuggy reservoir which developed secondary porosity. The reservoir limits are mostly graphite-schist filling sealing faults. In this study, all wells are assumed to be vertical and the reservoir model is considered as double porosity behavior with intersecting fault boundary. By using automatic type curve matching and performing nonlinear regression, reservoir parameters are estimated with a confidence interval in which error is less than 10%. Results obtained from log-log analysis are confirmed with special straight line analysis in semi-log plot. Results of pressure buildup tests are provided in (Table-16). Spatial distribution of the transmissivity is given in (Figure-39). It was observed that transmissivity of the South-West of the field is much higher than that of other parts of the field. The lowest transmissivity was found in North of the field.

A multi-well interference test was conducted in Alaşehir geothermal field. Akin (2015) designed and implemented an interference test which included four wells to assess the reservoir characteristics.

He reported that there is a good communication between wells and result of the test is given in (Table-17). The storativity of the Well-1 was found smaller than others and the transmissivity in between Well-3 and Well-4 was found as several order higher than in between other wells. It was also found from the analysis of the buildup test that order of magnitude of transmissivity was several orders higher than that of the interference test. The reason may be that in interference test large volume of the reservoir is tested while in buildup test a small drainage volume near the well is tested. Buildup test was not long enough to investigate the deeper section of the reservoir and it was limited with the several meters near to the wellbore which shows usually higher transmissivity. Yet another reason explaining the discrepancy between the results may be buildup test was conducted in the wells which are targeted to the North-south direction fault. This fault represented as the youngest and the most conductive one. In these wells, reservoir pay zone is penetrated few meters up to 200 m with total drilling fluid loss which is a good indication of transmissivity.
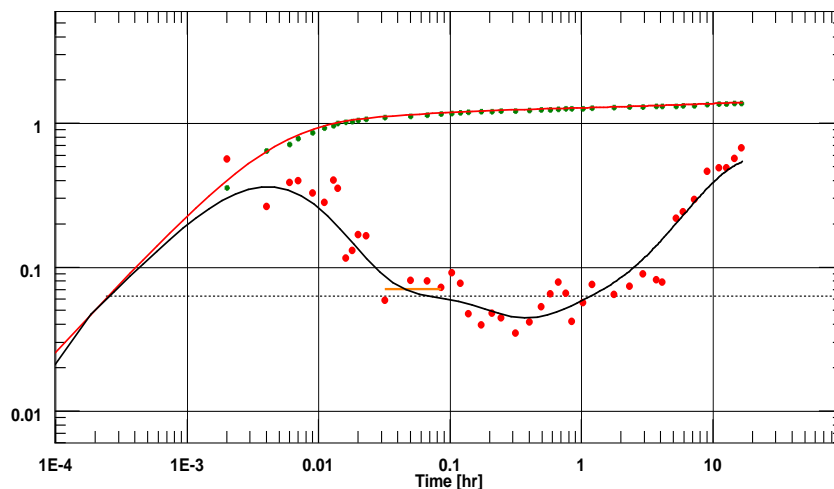
Figure 36: Log-log Plot of well X-1 Pressure Buildup

Semi-Log plot: p [bara] vs Superposition Time
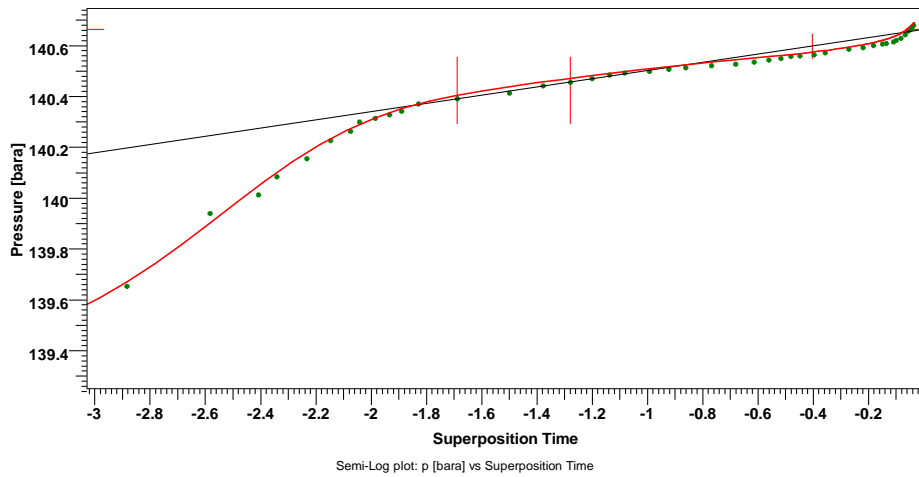
Figure 37: Semi log Plot of Well X-1

History plot (Pressure [bara], Liquid rate [STB/D] vs Time [hr])
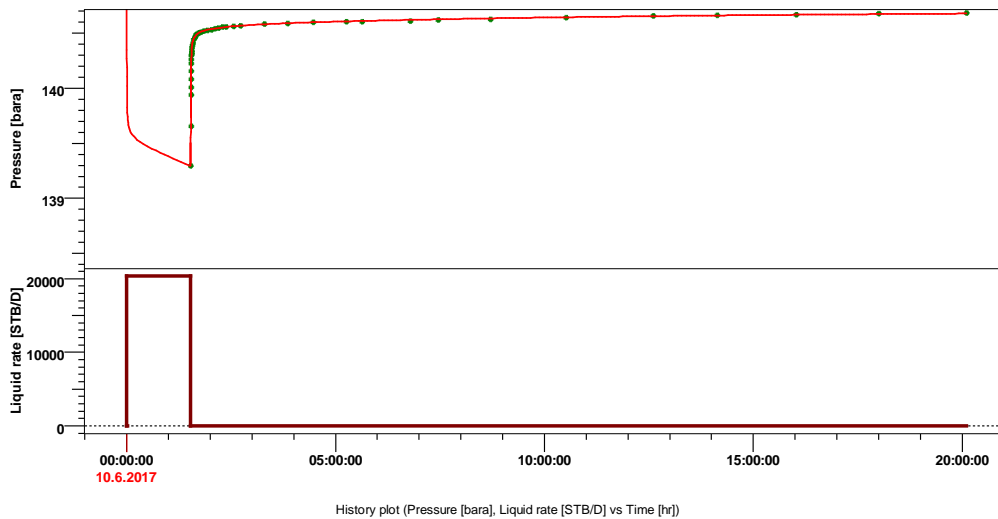
Figure 38: History Match of Well X-1

Table 16: Pressure Buildup Test Results

Parameters/Well ID	X-1	X-2	X-3	X-4	B-1	K-3	Units
Wellbore Storage, C	0.639	0.171	0.436	0.1	0.97	0.3	m³/Bar
Skin Factor	1.59	1.27	1	3.07	-3.6	-3.6	Dimensionless
Permeability*thickness kh	96.5	35.5	278	570	34	0.88	Darcy*m
Omega	0.286	0.00753	0.00194	0.011	0.0155	6.50E-05	Dimensionless
Lambda	1.10E-07	1.23E-07	4.98E-08	3.98E-08	1.57E-05	4.80E-05	Dimensionless

60

Table 17: Interference Test Results (Akin, 2015)

Parameter	W-1	W-2	W-3	W-4
Wellbore storage coefficient, C, m^3/Pa	4.35×10^{-11}	9.64×10^{-10}	4.78×10^{-8}	2.37×10^{-6}
Wellbore storage coefficient ratio, C_i/C_f	0.0424	0.0928	0.01	5.52
Alpha	1.1	32	45.6	7.43
Skin	-17.6	-16.0	-7.44	-17.1
Permeability – thickness, kh, m^3	5.63×10^{-13}	6.04×10^{-16}	1.64×10^{-12}	7.23×10^{-12}
Porosity – c_t -h, 1/Pa	1.34×10^{-6}	2.39×10^{-4}	5.61×10^{-4}	6.08×10^{-4}
Omega	4.27×10^{-4}	1.31×10^{-9}	8.62×10^{-9}	0.0265
Lambda	2.98×10^{-4}	0.00867	1.52×10^{-6}	0.00152
kx/ky	1.21×10^{-7}	5.3×10^{-4}	0.180	0.27
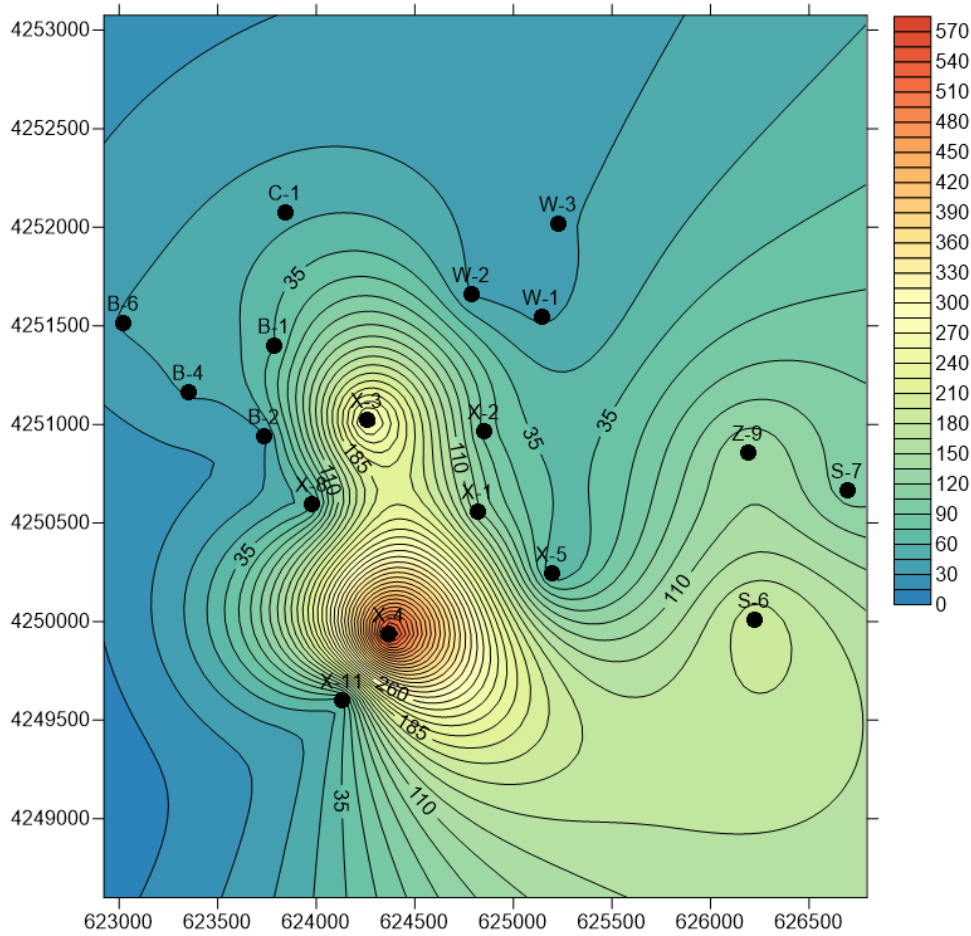
Figure 39: Transmissivity Distribution

CHAPTER 7

RESULTS AND DISCUSSIONS

- Fracture pore volume calculated in DFN modeling for each well is in good agreement with tracer swept pore volume calculated from moment analysis.
- Fracture porosity was calculated as ranging from 1.5 % to 3 % in DFN modeling. However, average porosity of outcrop analysis changed from 3 % to 12% in Gurel et al. (2016). The reason of discrepancy may be due to that overburden and confining pressure at reservoir conditions is higher than that of outcrops on surface. Outcrops of reservoir rock may also be exposed to weathering, which may develop secondary porosity.
- Fracture aperture was found to change between 1 mm to 2 mm in DFN modeling. However, Akin (2013) used cubic law in drilling mud loss data and calculated fracture aperture as ranging from 0.3 to 0.4 mm. FracMan7.6 has a convergence problem in performing mesh operation if volumetric fracture density is higher than 0.08. Thus, fracture aperture was increased to higher than 1 mm to obtain a match with actual test data. FMI logging is a very useful method to measure fracture aperture, fracture density, dip direction and dip amount. However, in conventional geothermal wells, FMI log is rarely taken in Turkey. There was no reported FMI log data for Alaşehir Geothermal field.
- There was no compartmentalization fracture set in DFN modeling. Tracer test, geochemical components and interference test also agree with this claim.
- Transmissivity obtained in buildup tests was found to be somewhat larger than that of interference test results. In interference test, Akin (2013) included 4

wells in test design and they were put on production at the same time. Therefore, a much larger volume of the reservoir was tested. However, buildup tests were conducted individually and typical test duration was not long enough to test deeper sections of reservoir. Therefore, it can be concluded that transmissivity decreases as distance from wells increases.

- In buildup test analysis, positive skin was observed in some wells which is not very common in geothermal wells. Since flow rate of wells are higher than 300 tons/hour, skin effect may be due to rate dependent turbulence effect near wellbore. Another reason would be that drilling mud loss may plug near wellbore.

- In DFN dynamic analysis, shortest flow paths between wells were significant. Early tracer concentrations observed in tracer test is probably related with these shortest flow paths.

- Detachment fault and high angle normal faults were found as intersected from tracer test.

CHAPTER 8

CONCLUSION AND RECOMMENDATIONS

Discrete Fracture Network (DFN) was conducted to characterize Alaşehir geothermal field. The study was populated with several data sources for further characterization, namely, drilling mud loss analysis, outcrop analysis, geochemical analysis, seismic analysis, well test analysis and tracer test. FracMan7.6 software was used to model fracture network in ten wells. Static model was constructed and dynamic model calibration was performed by matching simulation results with actual well test data to estimate unknown parameters. Chi square method was used to test goodness of matches and it was found that model data was matched with actual test data with 95 % significant confidence.

It was found that all wells are interconnected through intersected faults and fault related fractures. There is no compartmentalization observed in the study area. Spatial distribution of carbon dioxide (CO_2) concentration was used to identify preferential flow directions.

FMI log should be taken to confirm fracture properties that are found in DFN modeling. Results of this study can be used as basis to a numerical reservoir simulation.

REFERENCES

Akin, S. (2001). *Analysis of Tracer Tests with Simple Spreadsheet Models*. Computer and Geosciences, 27,2, 171-178

Akin, S. (2013). *Estimating Natural-Fracture Permeability from Mud-Loss Data*. 38th Workshop on Geothermal Reservoir Engineering Stanford University, Stanford, California.

Akin, S. (2017). *Alaşehir Geothermal Field Tracer Test (in Turkish.* Unpublished report, 25 May 2017.

Akin, S. (2017). *Geothermal Resource Assessment of Alaşehir Geothermal Field*, 42nd Workshop on Geothermal Reservoir Engineering Stanford University, Stanford, California,

Andersson, J. A., (1984). *Stochastic Model of a Fractured Rock Conditioned by Measured Information*. Water Resources Research, 1984; 20(1), pp. 79–88.

Andersson, J. and Dverstorp, B. (1987). *Conditional Simulations of Fluid Flow in Three-Dimensional Networks of Discrete Fractures*. Water Resources Research, 23(10) pp.1876–1886

Andersson, J.A. 1984. *Stochastic model of a fractured rock conditioned by measured information.* Water Resources Research, 20(1): 79-88

Ardislamova, D., Salimgareeva, E. and Gallyamova, D. (2015). *Integrated Approach to Modelling Naturally Fractured Carbonate Reservoirs* Journal of Society of Petroleum Engineering, SPE-176639.

Arnorsson, S. (2000). *Isotopic and Chemical Techniques in Geothermal Exploration, Development and Use. Sampling Methods, data Handling and Interpretation*, International Atomic Energy Agency, Vienna, 351pp

Babadagli, T. (2000). *Evaluation of Outcrop Fracture Patterns of Geothermal Reservoirs in Southwestern Turkey*, World Geothermal Congress, Beppu-Morioka, Japan

Babadagli, T. (2000). *Fractal Analysis of 2-D Fracture Networks of Geothermal Reservoirs in South-Western Turkey*. Journal of Volcanology and Geothermal Research 112(2001) pp. 83-103

Bareblatt, G.I., Zheltov, I.P. and Kochina, I.N., (1960) *Basic Concepts in the Theory of Seepage of Homogeneous Liquids in Fissured Rocks*, PMM-Soviet Applied Mathematics and Mechanics, Vol. 24, No, 5, pp.852-864

Barenblatt, G.I., Zheltov, I.P., and Kochina, I.N., 1960. *Basic concepts in the theory of seepage of homogeneous liquids in fissured rocks: Journal of Applied* Mathematics, v. 24, 1286-1303.

Bauer, J.F., Krumbholz, M. and Meier, S. (2017*). Predictability of Properties of a Fractured Geothermal Reservoir: The Opportunities and Limitations of An Outcrop Analogue Study*. Geotherm Energy, Springer Berlin Heidelberg.

Beggs, H. D. and Brill, J. P. (1973). *A Study of Two-Phase Flow in Inclined Pipes* Journal of Petroleum Technology. AIME. 255 SPE-4007-PA.

Beven, K. and Germann, P. (1981). *Water Flow Soil Macropores. II: A combined flow model,* Journal of Sci., 32, 15-29.

Bourdet, D. and Cubiit, J. (2002). *Well Test Analysis: The Use of Advanced Interpretation Models*, Netherlands: Elsevier, pp. 426. ISBN-10: 0444549889.

Chesnaux R, Allen DM, and Jenni S. (2009) *Regional Fracture Network Permeability Using Outcrop Scale Measurements*. Engineering Geology 108(3-4) pp.259-271

Ciftci B.N. (2007). *Geological Evolution of the Gediz Graben, SW Turkey: Temporal and Spatial Variation of the Graben*. Thesis of the Degree of Doctor Philosophy in Geological Engineering, Middle East Technical University.

Davy, P., Bour, O., Dreuzy, J.R. (2006). *Discrete Fracture Network for the Forsmark Site*. Itasca Consultants, Swedish Nuclear Fuel and Waste Management

Dershowitz, W. S. and Einstein, H. H. (1987). *Three-Dimensional Flow Modelling in Jointed Rock Masses*. Proc. of 6th Cong. ISRM, Vol. 1, pp. 87–92, Montreal Canada. Dershowitz, W.S, Einstein, H.H. (1988). *Characterizing Rock Joint Geometry with Joint System Models*. Springer Rock Mechanics and Rock Engineering, vol.21, n1, pp.21-51.

Dershowitz, W.S, Lee, G., Geier, J., Foxford, T., LaPointe, P. and Thomas, A. (1998). *FracMan Version2.6 Interactive Discrete Feature Data Analysis, Geometric Modeling, and Exploration Simulation, user documentation*, Report 923-1089, Golder Associates Inc, Seattle, Washington

Dershowitz, W.S., Cottrell, M.G., Lim, D.H., and Doe, T.W. 2010. *A discrete fracture network approach for evaluation of hydraulic fracture stimulation of naturally fractured reservoirs.* 44th Rock Mechanics Symposium, Salt Lake City, U.S.

Dershowitz, W.S., Foxford, T. and Doe, T. (1998). *Fractured Reservoir Discrete Feature Network Technologies.* Research report, Fracture Data Analysis Technology, BDMOklahoma, U.S. Department of Energy. Prepared by Golder Associates Inc. Redmond, Washington.

Doe, T.W., Uchida, M. and Dershowitz, W. (1990). *Simulation of Dual-Porosity Flow in Discrete Fracture Networks*, Petroleum Society of Canada, Annual Tecnical Meeting, Calgary, Alberta

Dowd, P. and Xu, C. 2010. *A new computer code for discrete fracture network modelling*. Computer and Geosciences 36 (3): 292-301

Drummond, J.M. (1964). *An Appraisal of Fracture Porosity*. Bull. Can. Pet. Geol., 12, 226.

Einstein, H.H and Baecher, G. 1983. *Probabilistic and statistical methods in engineering geology - Specific methods and examples part I: Exploration.* Rock Mechanics and Rock Engineering 16(1):39-72

Elsworth, D. (1986). *A Hybrid Boundary-Finite Element Analysis Procedure for Fluid Flow Simulation in Fractured Rock Masses. International Journal for Numerical and Analytical Methods in Geomechanics*, 10(6) pp.569–584.

Endo, H. K., (1984) *Mechanical Transport in Two-Dimensional Networks of Fractures*. Ph. D. Thesis, University of California, Berkeley.

Endo, H. K., Long, J. C. S., Wilson, C. K. and Witherspoon, P. A. (1984). *A Model for Investigating Mechanical Transport in Fractured Media*. Water Resources Research, 20(10) pp.1390–1400.

Ferrandon, J.:*Les lois de l'écoulement de filtration*, Génie civil, 125, No. 2, 24–28 (1948)

Fournier, R.O. (1985). *Application of Water Geochemistry to Geothermal and Reservoir Engineering*, U.S. Geological Survey, 1985

Fournier, R.O. (1989). *Lectures on Geochemical Interpretation of Hydrothermal Waters*. UNU Geothermal Traninig Programme, Reykjavik, Iceland

Fournier, R.O. and Potter, R.W. (1982) *A Revised and Expanded Silica (quartz) Geothermometer.* Geothermal Resource Council, Transactions volume: 6

Gaillot, P., Brewer, T., Pezard, P. and En-Chao Yeh. (2007). *Borehole Imaging Tools Principles and Applications*, Scientific Drilling, No. 5.

Geier, J.E., Lee, L., Dershowitz, W.S. (1989). *Field Validation of Conceptual Models for Fracture Geometry*. Unpublished Monograph. Golder Associates Inc., Washington.

Gislason, G., Ivarsson, G., Gunnlaugsson E., Hjartarson, A., Björnsson, G. and Benedikt Steingrimsson. (2005). *Production Monitoring as a Tool for Field Development a Case History from the Nesjavellir Field, Iceland*, World Geothermal Congress, Antalya, Turkey.

Gould, T. L. (1974). *Vertical Two-Phase Steam-Water Flow in Geothermal Wells*. Journal of Petroleum Technology, pp. 883-842.

Gürel, E. (2016). *Uncertainty Quantification by Using Stochastic Approach in Pore Volume Calculation for Geothermal Reservoir*, Thesis of Master of Science in Petroleum and Natural Gas Engineering, Middle East Technical University.

Gurel, E., Akin, S. and Conskuner Y.B. (2016). *Fractal Modeling of Outcrop Fracture Patterns in Alasehir Geothermal Reservoir Turkey*. 41st Workshop on Geothermal Reservoir Engineering, Stanford University.

Haizlip, J.R., Stover, M.M., Garg, S.K., Haklidir, F.T. and Nicholas Prina. (2016). *Origin and Impacts of High Concentration of Carbon Dioxide in Geothermal Fluids of Western Turkey*. 41st Workshop on Geothermal Reservoir Engineering, Stanford University.

Haizlip, J.R., Tut Haklidir, F., and Garg, S.K. (2013). *Comparison of Reservoir Conditions in High Noncondensable Gas Geothermal Systems*. 38 th Workshop on Geothermal Reservoir Engineering, Stanford University.

Hartle, L. and Roberts, D. (2013). *Summary of Discrete Fracture Network Modelling as Applied to Hydrogeology of the Forsmark and Laxemar Sites*, AMEC.

Homuth, S. (2014). *Outcrop Analogue vs. Reservoir Data: Characteristics and Controlling Factors of Physical Properties of the Upper Jurassic Geothermal Carbonate Reservoirs of the Molasse Basin, Germany*, Stanford University, Stanford, California.

Horne, R.N. (1990). *Modern Well Test Analysis: A computer Aidad Approach*, Stanford Universty

Horne, R.N. (2007). *Inferring Well to Well Connectivity Using Nonparametric Regression on Well Histories*, Stanford Geothermal Workshop, Stanford University.

Houze, O., Viturat, D., Fjaere, O.L., Trin, S., Allain, O., Tauzin E. 2013. *Dynamic Data Analysis: The Theory and Practice of Pressure Transient, Production Analysis, Production Logging and The use of data from Permenent Downhole Gauges. Kappa ver 4.12.03*

Howell, J.A., Martinius, A.W. and Good, T.R. (2018). *The Application of Outcrop Analogues in Geological Modelling: A Review, Present Status and Future Outlook*. Geological Society, London, Special Publications, 387.

Howell, J.A., Matinius, A.W., Good T.R. (2018). *The Application of Outcrop Analogues in Geological Modelling a Review, Present Status and Future Outlook.* Geological Society London Special Publications 387(1) pp.1-25

Howell, J.A., Martinius, AW., Good TR. (2014). *The Application of Outcrop Analogues in Geological Modelling: A Review, Present Status and Future Outlook.* Geol Soc Lond Spec Publi.

Huang, J. and Griffiths, D.V. (2011) *Characterization Natural-Fracture Permeability from Mud-Loss Data*, Journal of Society of Petroleum Engineers SPE-139592

Huang, J., Griffiths D.V., Wong, S.W. (2011). *Characterizing Natural-Fracture Permeability from Mud-Loss Data*. SPE Journal, SPE 139592-PA

Hull, C.L. and Clemo, T.M., 1987. *Effects of using a continuum representation to stimulate discrete fracture networks*. Geothermal Resources Council Vol 11

Jing, L. and Stephansson, O. (2007). *Developments in Geotechnical Engineering* Volume 85, pp. 1-545

Kamal, M.M., Freyder, D.G., Murray, M.A. (1995*). Use of Transient Testing in Reservoir Management*, SPEJournal Paper, SPE 28008-PA

Kazemi, H., (1969). *Pressure Transient Analysis of Naturally Fractured Reservoirs with Uniform Fracture Distribution*, Society of Petroleum Engineers Journal 9 (4), 451-461.

Kazemi, H., Merrill L.S., Porterfield, K.L., Zeman P.R. 1976. *Numerical Simulation of Water-Oil Flow in Naturally Fractured Reservoirs*. Society of Petroleum Engineers, SPE 5719

Kissling W.M and White, S.P. (1996). *Modelling Chloride and CO_2 Chemistry at the Wairakei Geothermal Field, New Zealand*. 21st Workshop on Geothermal Reservoir Engineering, Stanford University.

Kuchuk, F., Biryukov, D. and Fitzpatrick, T. (2015). *Fractured-Reservoir Modeling and Interpretation*, Journal of Society of Petroleum Engineering, SPE-176030-PA.

Lee, C.H., Deng, B.W., Chang, J.L., 1995. *A Continuum approach for estimating permeability in naturally fractured rocks.* Engineering Geology 39 (1995) 71-85

Lee, J., Choi, S. and Cho, W. (1999). *A comparative study of Dual-Porosity Model and Discrete Fracture Network Model*, KSCE Journal of Civil Engineering

Liang Z., Feng Z., Guangxiang X. (2012). *Comparison of Fractal Dimension Calculation Methods for Channel Bed Profiles*. International Conference on Modern Hydraulic Engineering.

Liang, Z. (2012). *Comparison of Fractal Dimension Calculation Methods for Channel Bed Profiles*, International Conference on Modern Hydraulic Engineering, Nanjing Chaina.

Lietard, O., Unwin, T., Guillot, D., Hodder, M.H. (1999) *Fracture Width Logging While Drilling and Drilling Mud/Loss-Circulation-Material Selection Guidelines in Naturally Fractured Reservoirs.* SPE Drill & Compl 14 (3), pp.168-177.

Long J.C.S., Remer, J.S., Wilson. C.R. and Witherspoon, P.A., (1982). *Porous Media Equivalents for Networks of Discontinuous Fractures*, Water Resources Research 18(3) pp.645-658

Long, J. C. S. 1982. *Porous media equivalent for a network of discontinuous fractures.* Geophys. and Reservoir Eng., Geosci. p 24-27

Long, J. C.S., and P.A. Witherspoon, 1985. *The Relationship of the degree of interconnection to permeability in fracture networks*. J.Geophys. Res., 90 no: B4, pp. 3087-3098

M. Karimi-Fard, L. J. Durlofsky, and K. Aziz. (2004). *An Efficient Discrete Fracture Model Applicable for General Purpose Reservoir Simulators*, SPE Journal, SPE-88812-PA, vol. 9, no. 02, pp. 227 – 236.

Majidi, R., Miska, S.Z., Yu, M., Thompson, L.G. (2008*). Quantitative Analysis of Mud Losses in Naturally Fractured Reservoirs: The effect of Rheology*. SPE 114130, SPE Western Regional and Pacific Section AAPG Joint Meeting, Bakersfield.

Malate, R.C.M. (1990). *Modelling of Chemical and Thermal Changes in Well PN-26, Palinpinon, Philippines*, Fifteenth Worksop on Geothermal Reservoir Engineering, Stanford Universty.

Meehan, D. N. (1980). *Estimating Water Viscosity at Reservoir Conditions*. Petroleum Eng. Vol:52(8), pp.117-18.

Miao, T. (2015). *A Fractal Analysis of Permeability for Fractured Rocks*, International Journal of Heat and Mass Transfer (81) pp. 75–80

Oda, M. 1986. *An equivalent continuum model for coupled stress and fluid flow analysis in jointed rock masses*. Water Resources Research, 22, 1845-1856.

Padilla, E.K. and Carlos, J.E. (2016). *Interpretation of Geochemical Production Monitoring Data from Well SJ4-1, San Jacinto, to Indicate Reservoir Response to Production*, 41st Workshop on Geothermal Reservoir Engineering Stanford Universty.

Philipp, SL., Reyer, D. and Meier S. (2010). *Strukturgeologische Geländestudien in Aufschlussanaloga und Permeabilitätsentwicklung in Potentiellen Geothermischen Reservoiren*. Z Geol Wiss.

Robinson, P. C. (1984). *Connectivity, Flow and Transport in Network Models of Fractured Media*. Ph.D. Thesis, St. Catherine's College, Oxford University, UK.

Rogers, S.F. (2011) *Understanding Hydraulic Fracture Geometry and Interactions in Pre-Conditioning through DFN and Numerical Modeling*. ARMA 11-439

Sanfillippo, F., Brignoli, M., Santarelli, F.J., Bezzola, C. (1997). *Characterization of Conductive Fractures While Drilling*. Journal of Society of Petroleum Engineers, SPE 38177, SPE European Formation Damage Conf, The Hague, Netherlands.

Shook, M.G. (2003). *A Simple, Fast Method of Estimating Fractured Reservoir Geometry from Tracer Tests*. Geothermal Resource Council, Vol.27, pp.407-411

Smith, L. and Schwartz, F. W. (1984). *An analysis of the influence of fracture geometry on mass transport in fractured media*. Water Resources Research, 20(9) PP.1241–1252.

Snow, D.T. (1965). *A Parallel Plate Model of Fractured Permeable Media*. Ph. D. dissertation, University of California, Berkeley.

Snow, D.T., 1968. *Rock fracture spacings, openings and porosities*. Jour. Soil Mech. and Foundation Div., Amer. Soc. Civil Eng., 94, 1.

Soltanieh, A. (2015*) Discrete Fracture Network Modeling and Gel Injection Simulationin Fractured Carbonates*, M.S. Thesis. Middle East Technical Universty.

Staub, I., Anders, F. and Nils, O. (2002). *Strategy for a Rock Mechanics Site Descriptive Model R-02-02*. Golder Associates AB

Tavakkoli, M. (2009). *Deterministic versus Stochastic Discrete Fracture Network (DFN) Modeling, Application in a Heterogeneous Naturally Fractured Reservoir*. Journal of Society of Petroleum Engineering, SPE 127086

Versluys, J., 1915. *De onbepaalde vergelijking der permanente beweging van het groundwater. Verk. Geol-Mijnbouw*. Genoot. Ned. en Kolonien. Geol. Serie 1 : 349-360.

Waren, J.E. and Root, P.J. (1963). *The Behaviour of Naturally Fractured Reservoirs*, Gulf Research & Development, Pittsburgh, PA.

Warren J. E., and Root P. J., 1963, *The behavior of naturally fractured reservoirs*. SPEJ, 245–255.

Zimmerman, R. W. and Bodvarsson, G. S. (1996) *Effective transmissivity of two-dimensional fracturenetworks*. International Journal of Rock Mechanics and Mining Sciences and Geomechanics 33(4) pp.433–436.

APPENDIX A

TRACER RESULTS AND PLOTS
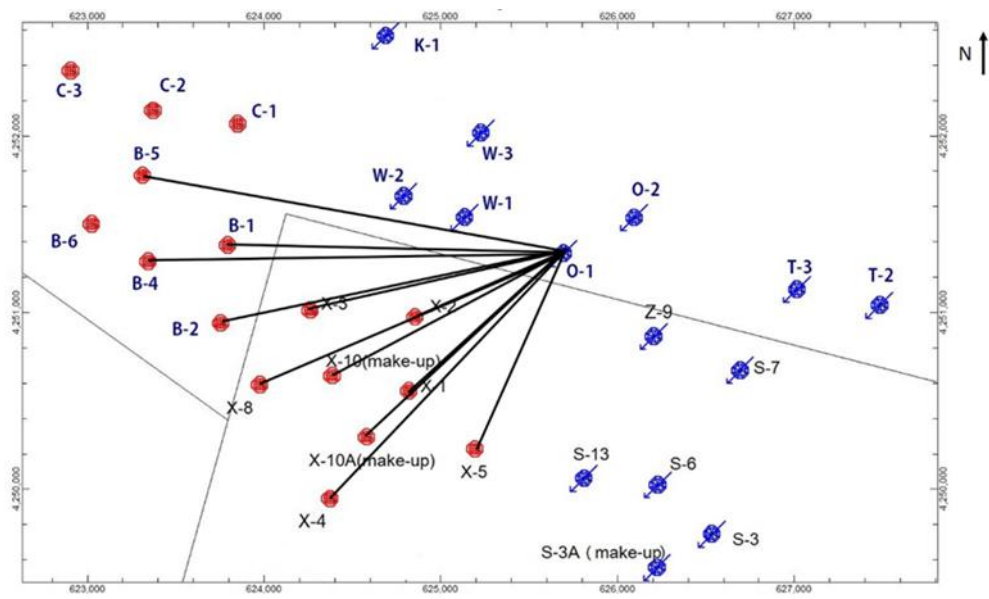
Figure 40: Communication between O-1 and Production Wells
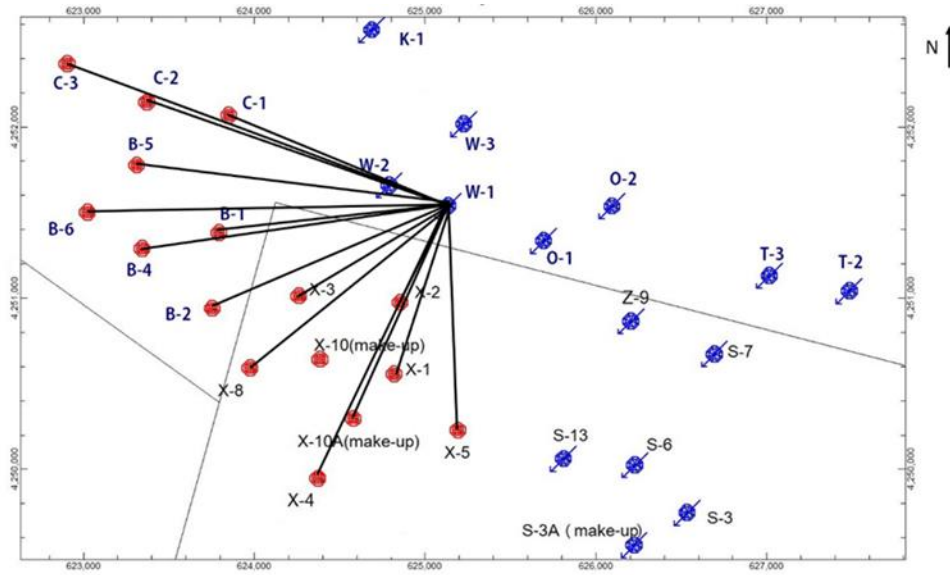
Figure 41: Communication between W-1 and Production Wells
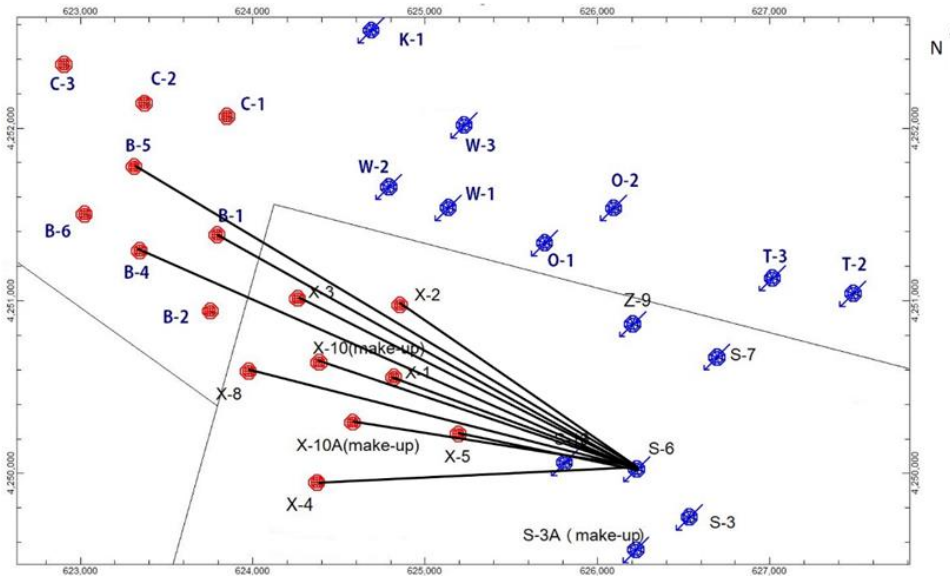
Figure 42: Communication between S-6 and Production Wells

APPENDIX B

DFN FRACMAN RESULTS AND MATCH PLOTS
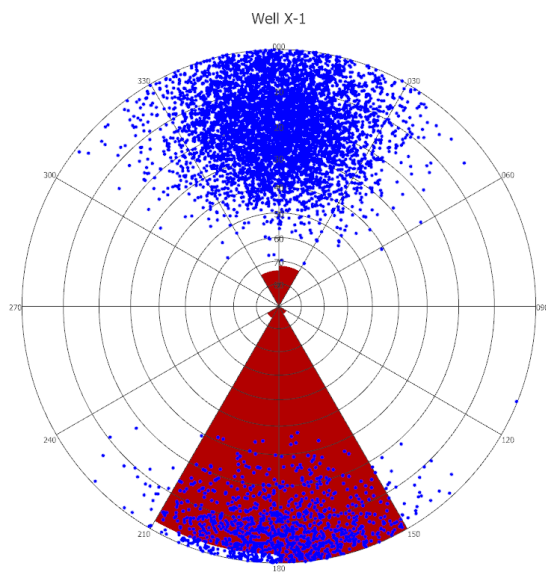
Figure 43: Fractures Orientation for Well X-1
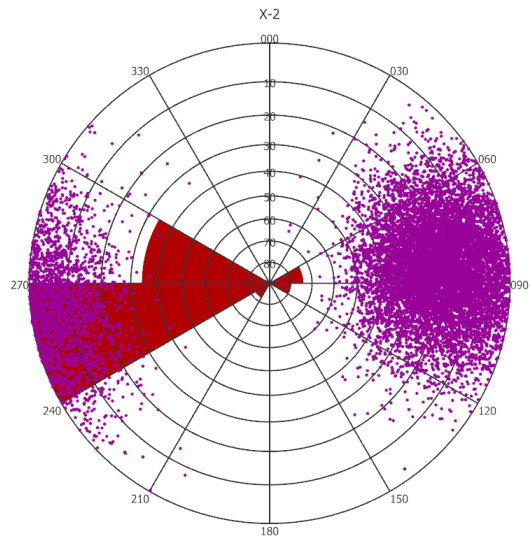
Figure 44: Fractures Orientation for Well X-2
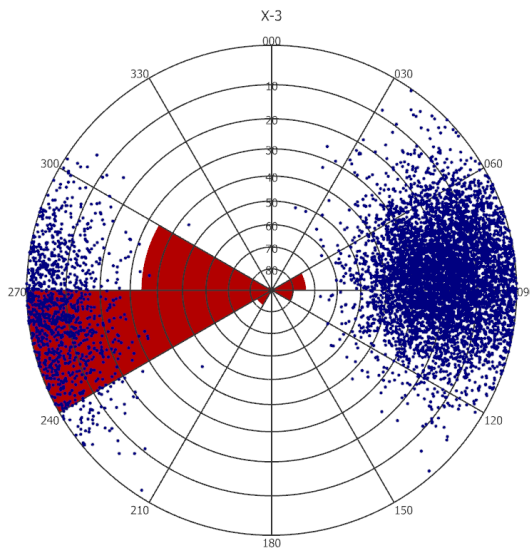
Figure 45: Fracture Orientation for Well X-3
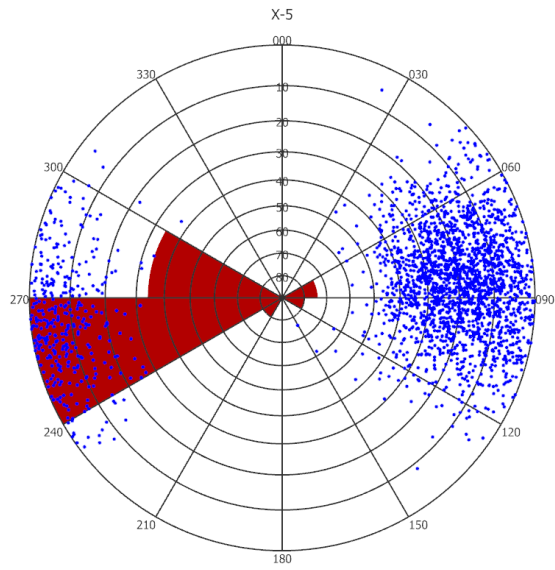
Figure 46: Fracture Orientation for Well X-5
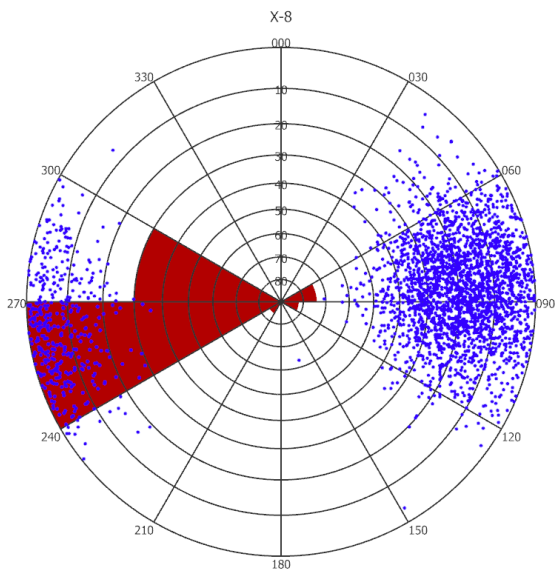
Figure 47: Fracture Orientation for Well X-8

81
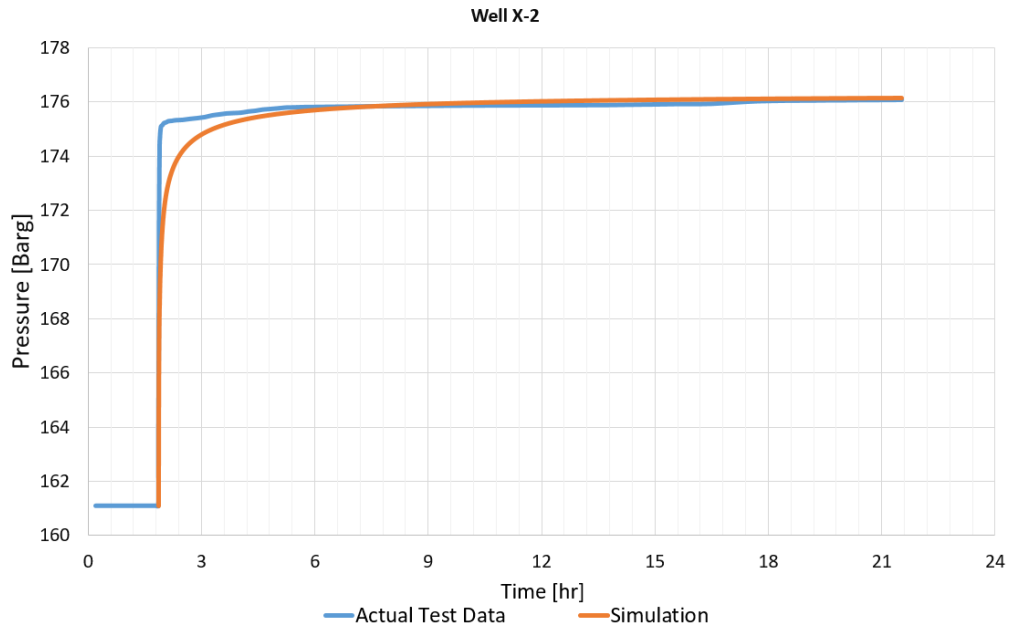
Figure 48: Simulation Calibration for Well X-2
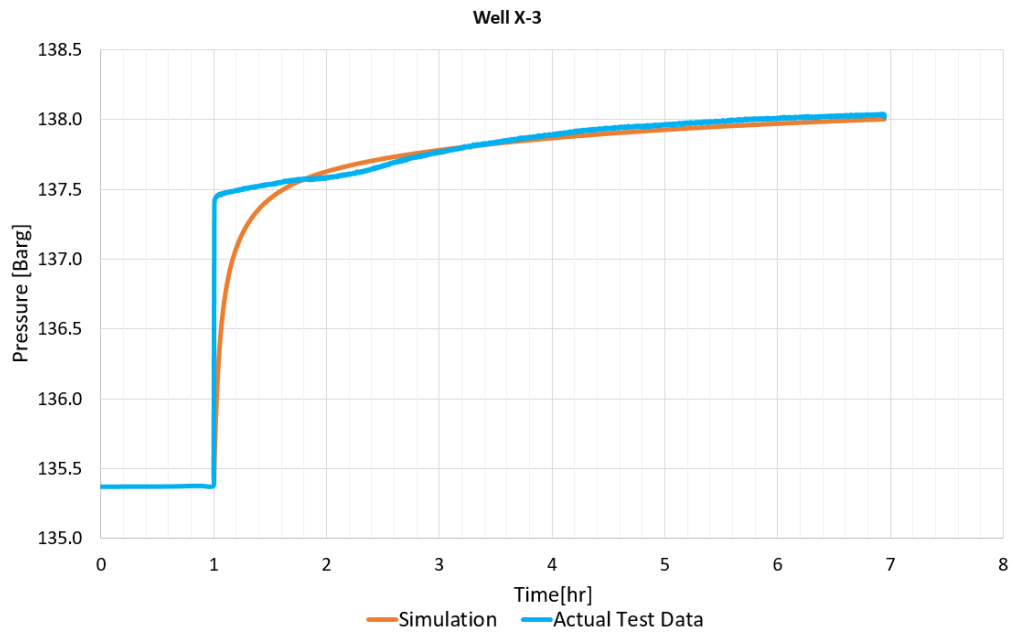
Figure 49: Simulation Calibration for Well X-3
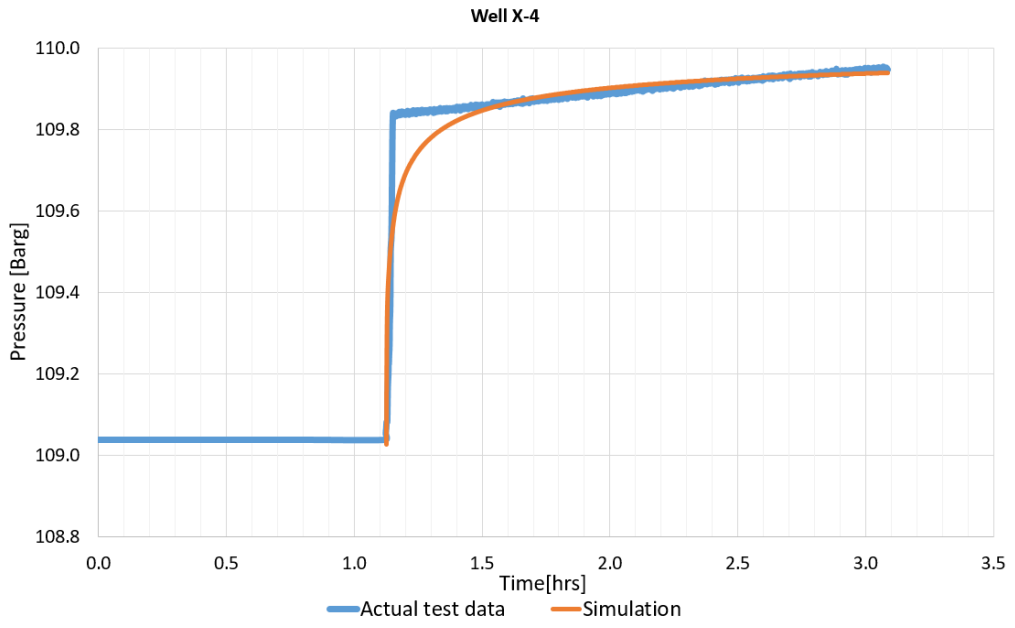
Figure 50: Simulation Calibration for Well X-4
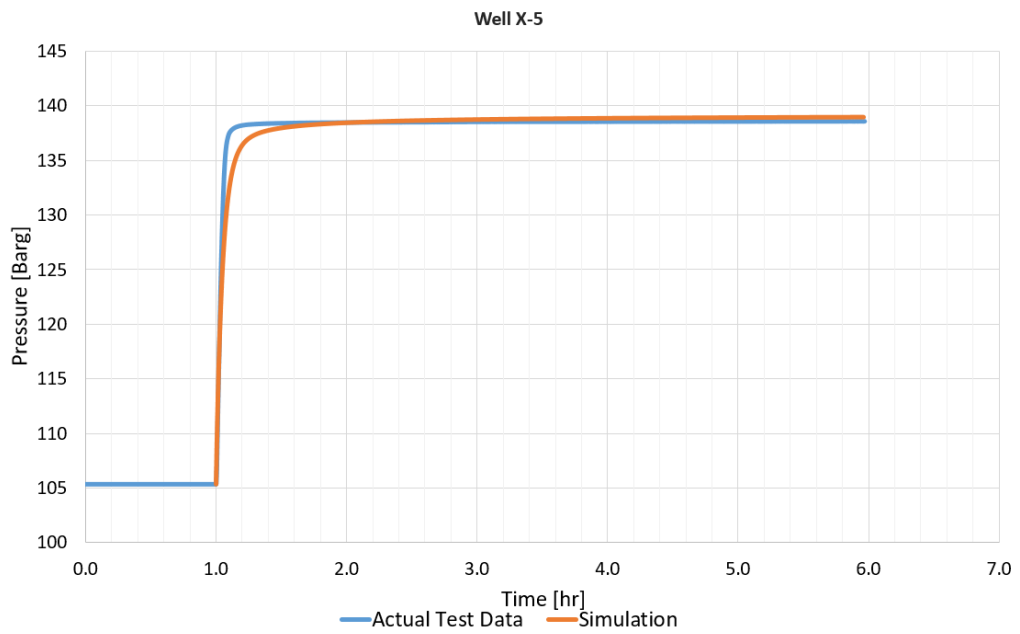
Figure 51: Simulation Calibration for Well X-5
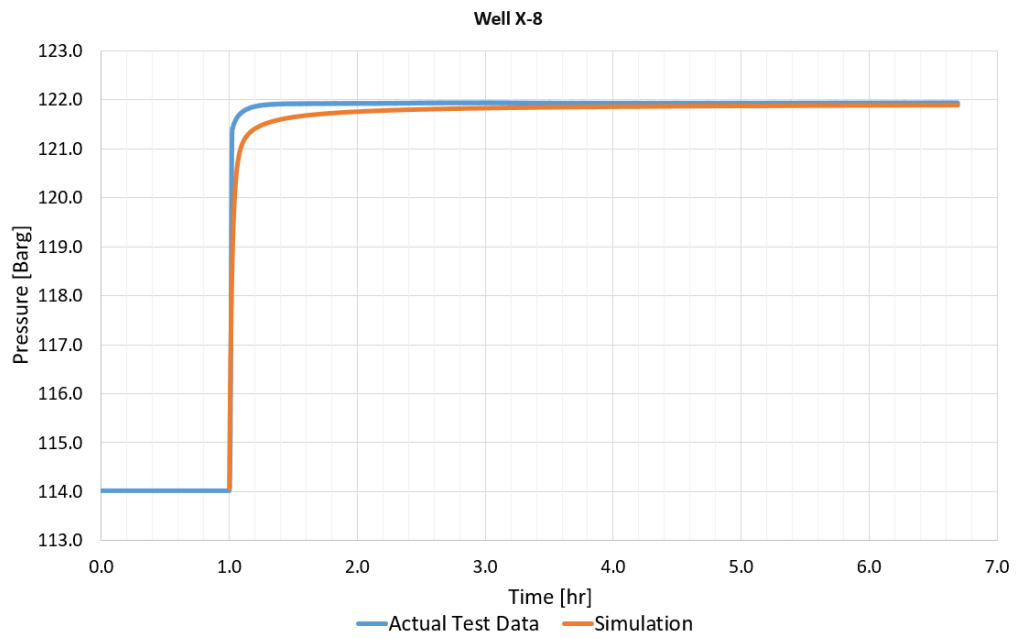
Figure 52: Simulation Calibration for Well X-8
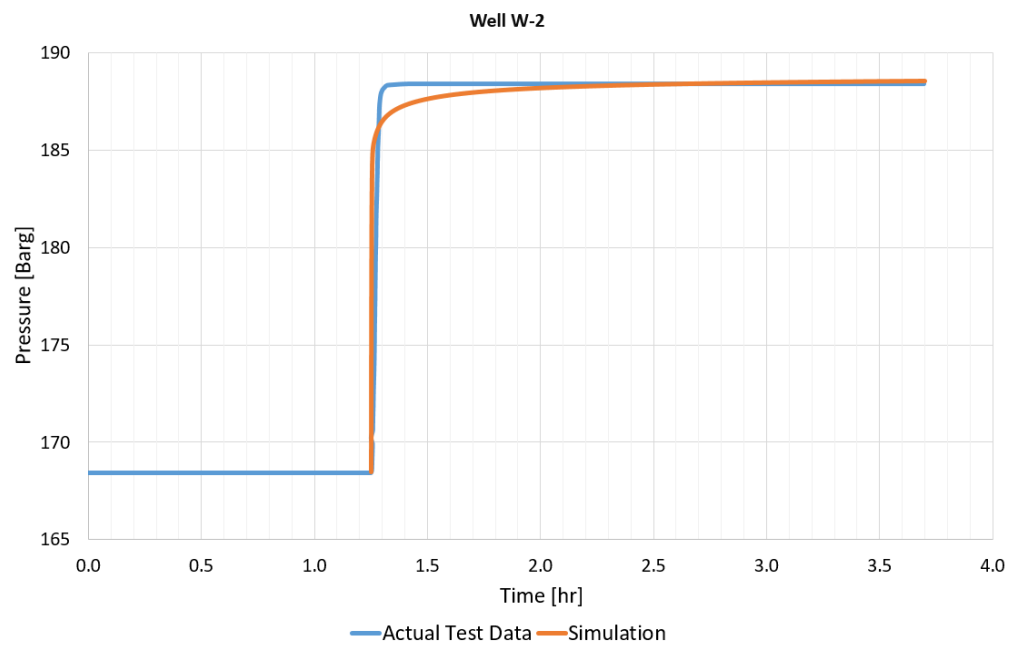
Figure 53: Simulation Calibration for Well W-2
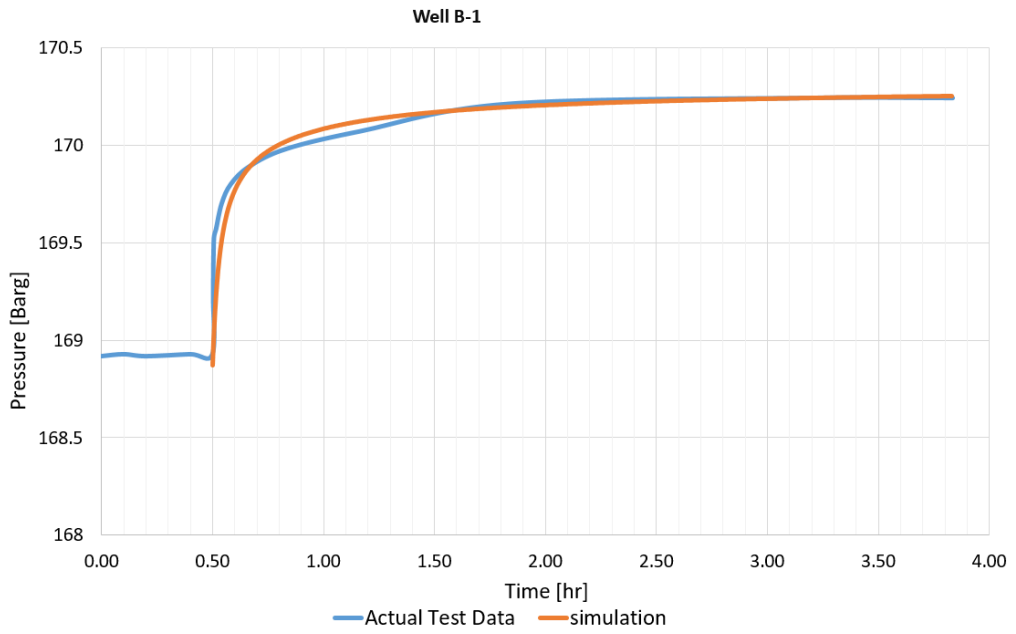
Figure 54: Simulation Calibration for Well B-1
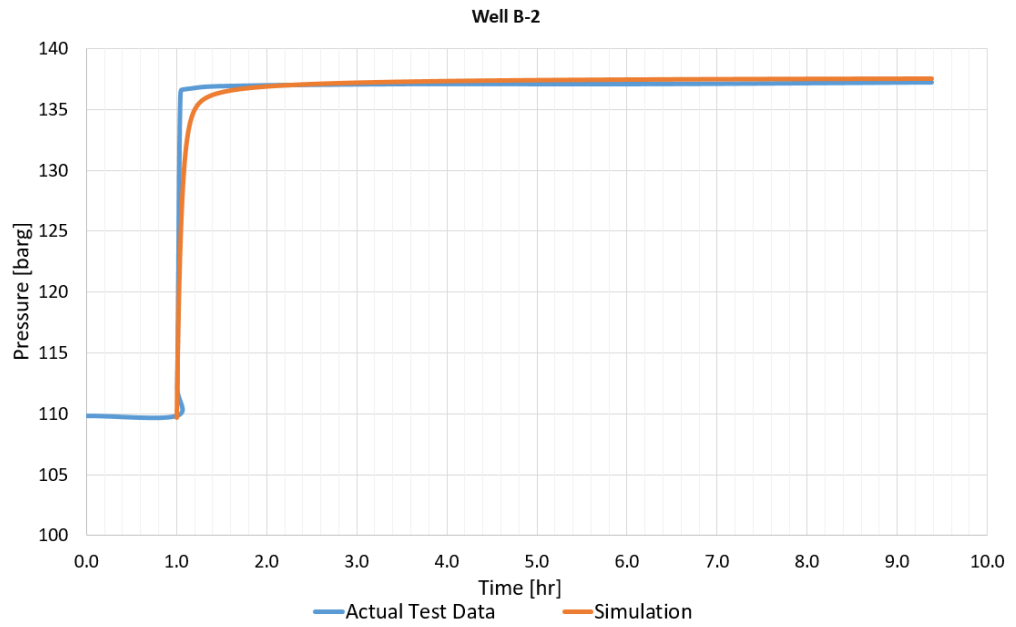
Figure 55: Simulation Calibration for Well B-2
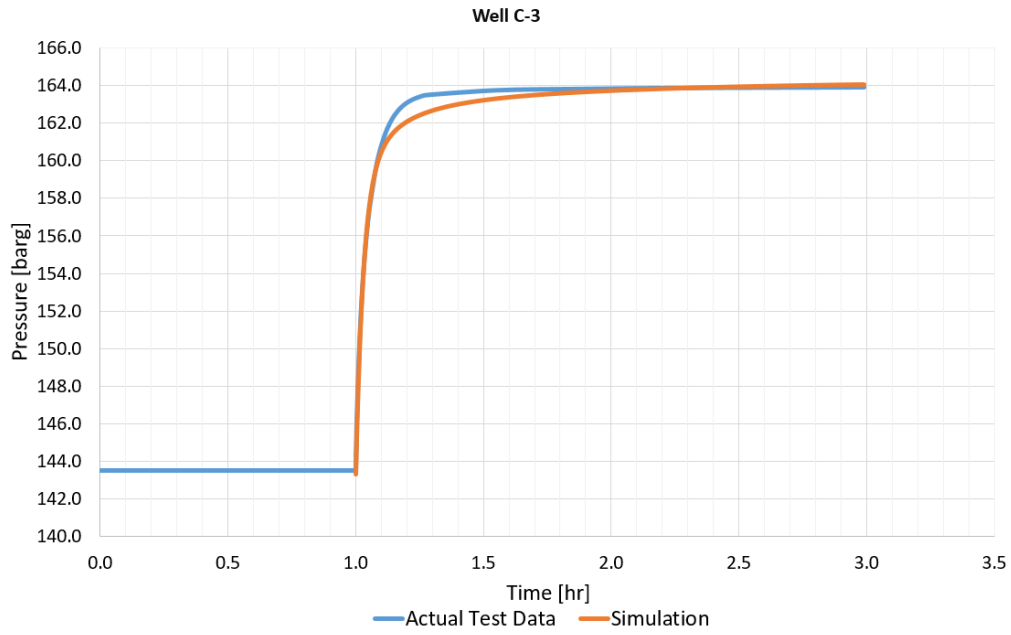
Figure 56: Simulation Calibration for Well C-3
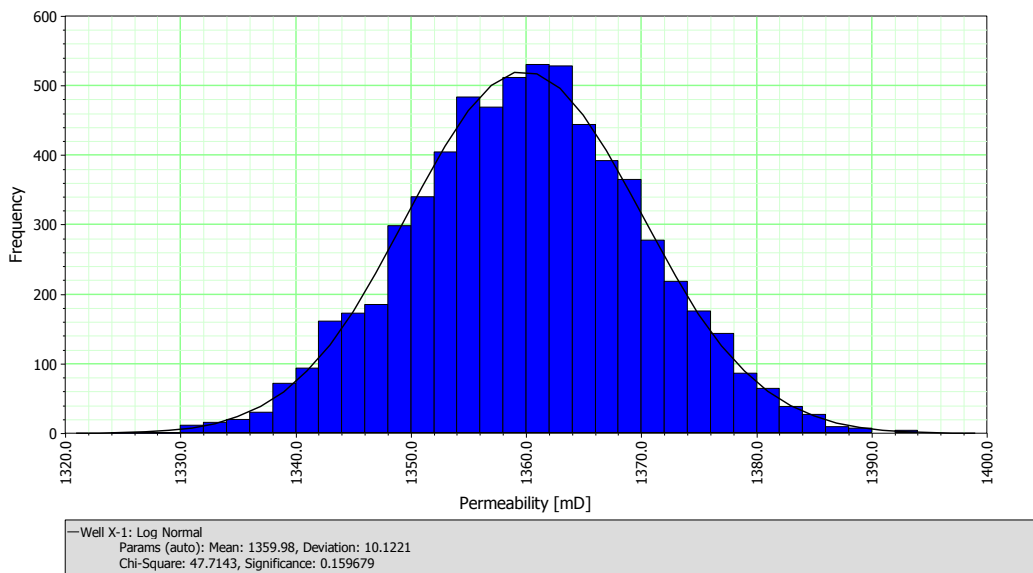
Figure 57: DFN Permeability Distribution for WellX-1
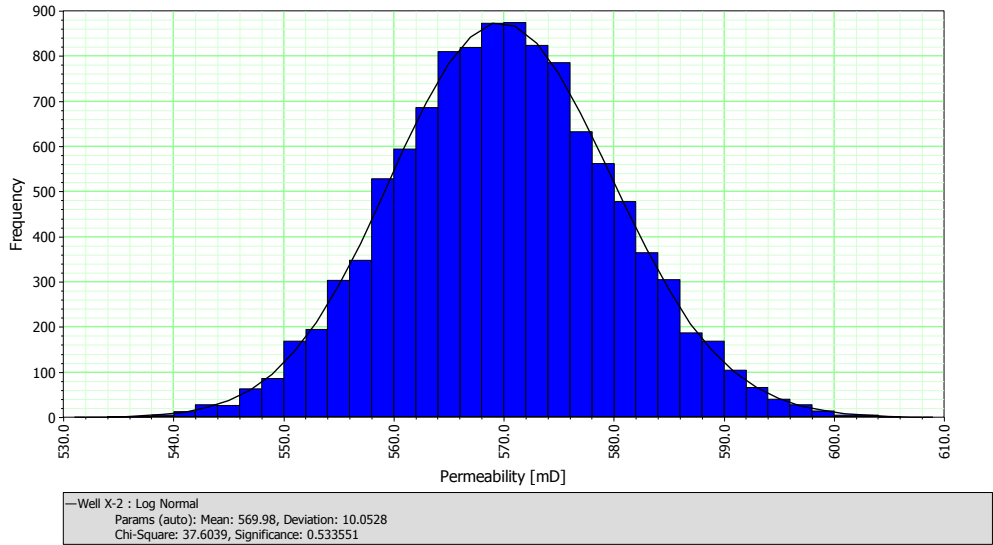
Figure 58: DFN Permeability Distribution for Well X-2
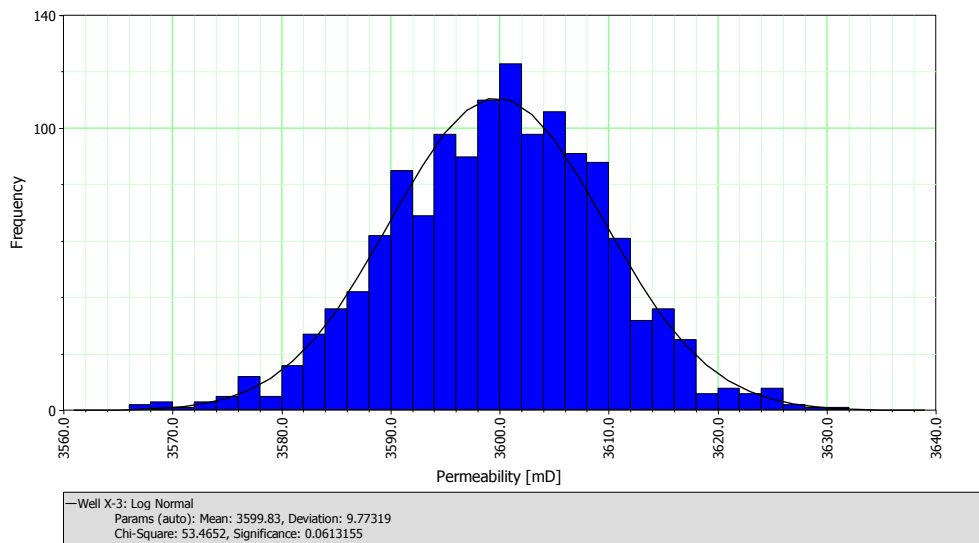
Figure 59: DFN Permeability Distribution for Well X-3
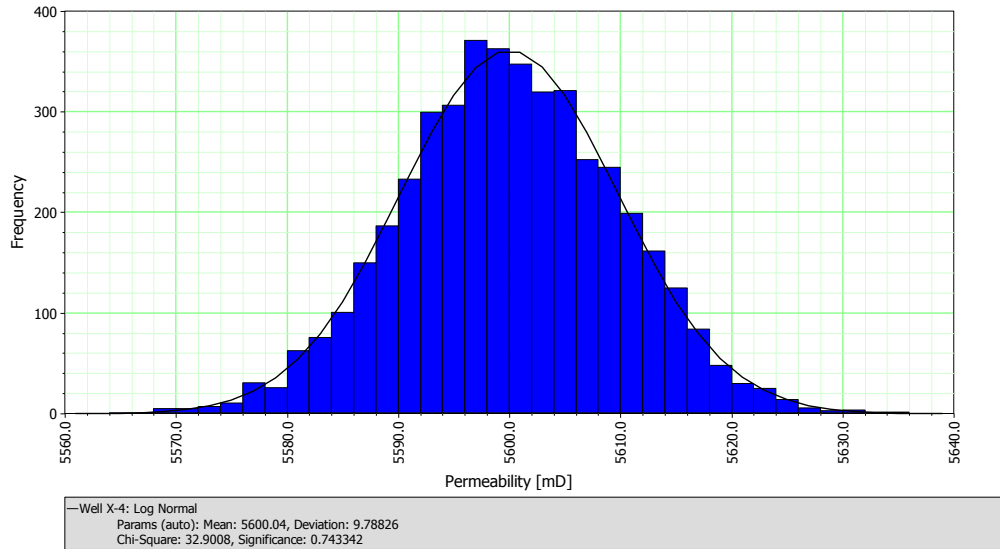
Figure 60: DFN Permeability Distribution for Well X-4
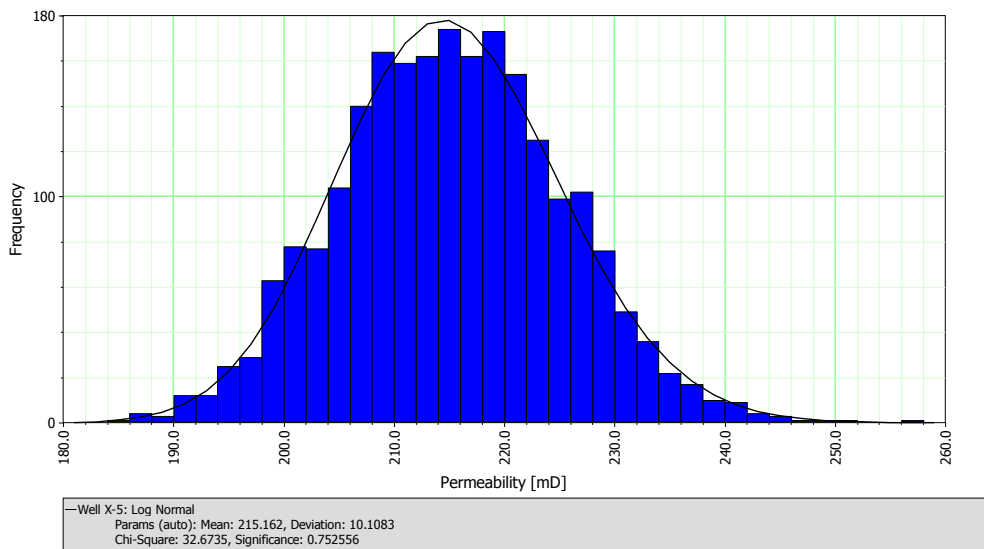
Figure 61: DFN Permeability Distribution for Well X-5
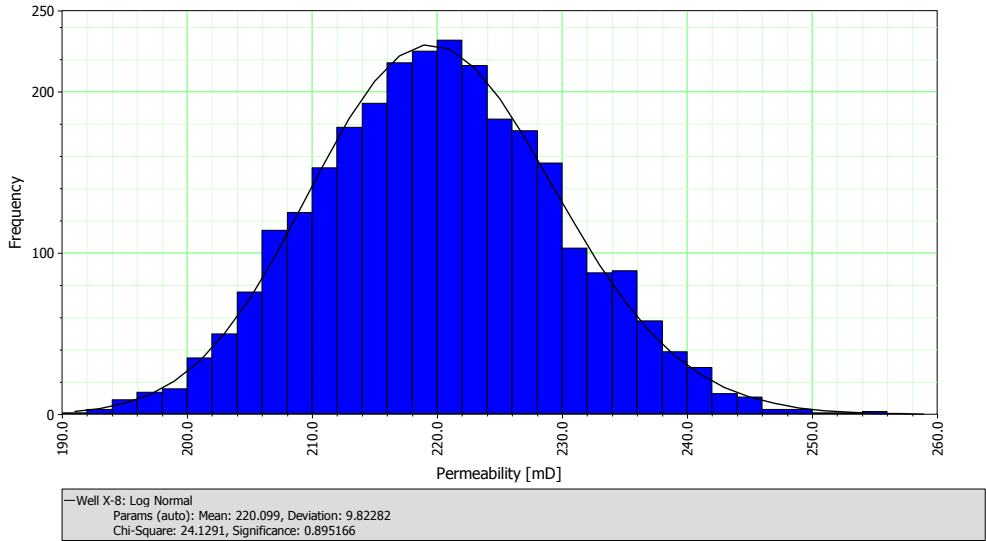
Figure 62: DFN Permeability Distribution for Well X-8
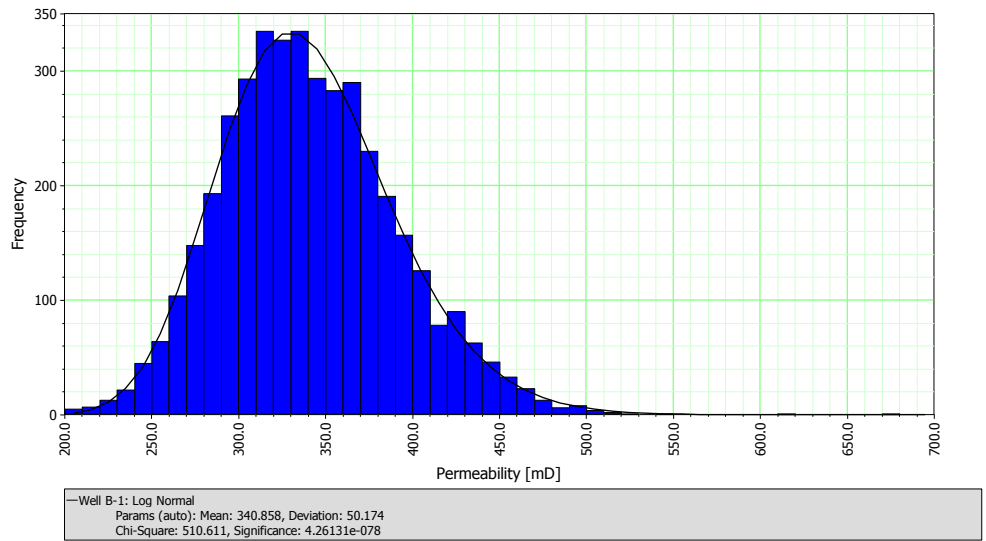
Figure 63: DFN Permeability Distribution for Well B-1
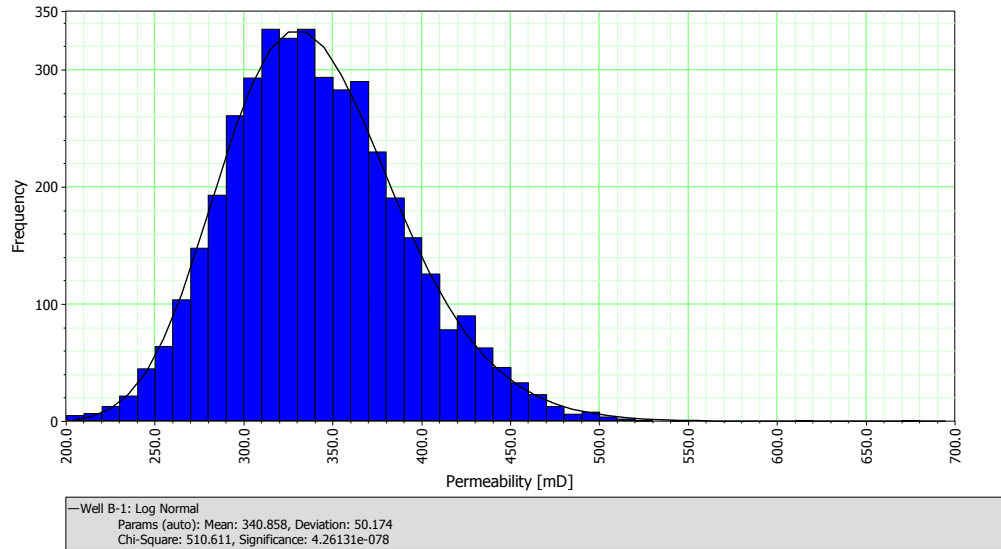
Figure 64: DFN Permeability Distribution for Well B-2
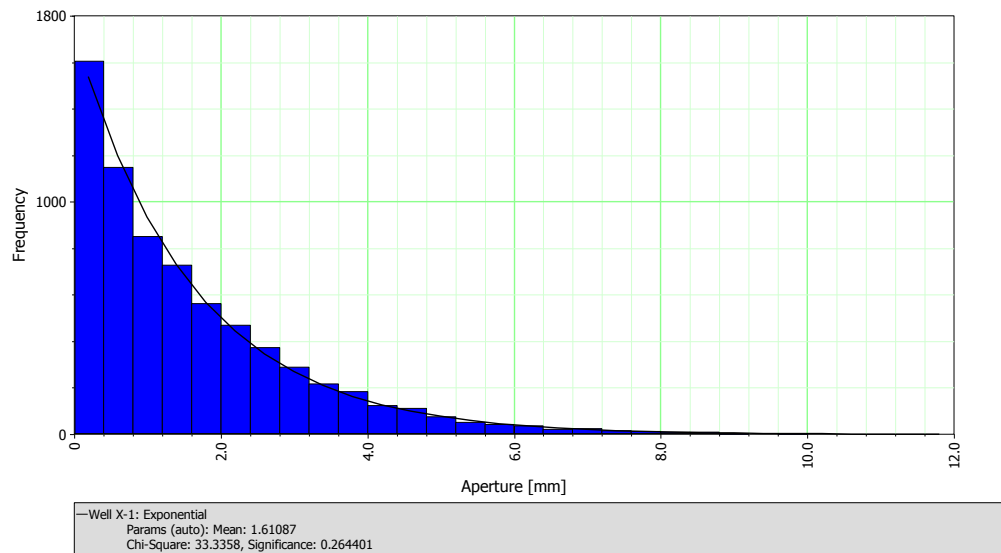
Figure 65: DFN Aperture Distribution for Well X-1
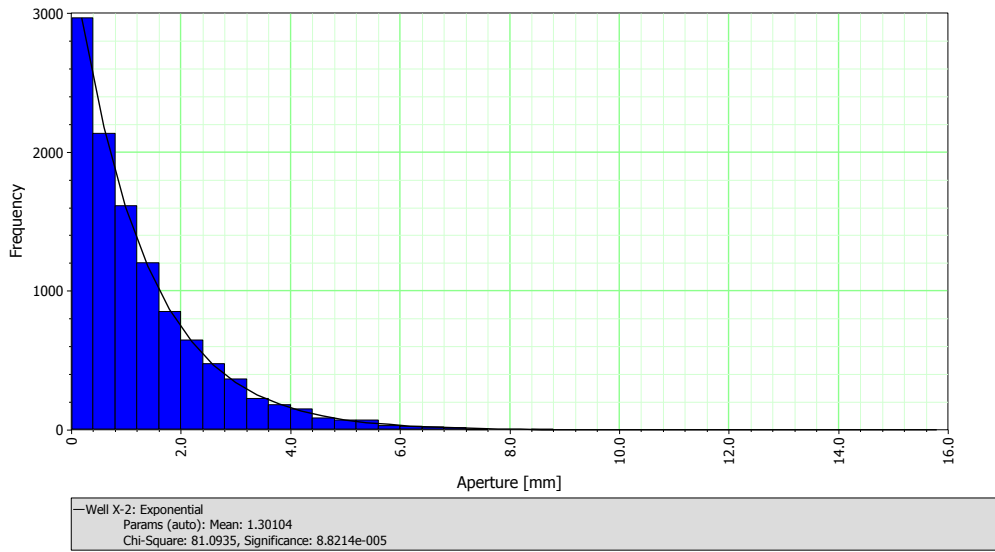
Figure 66: DFN Aperture Distribution for Well X-2
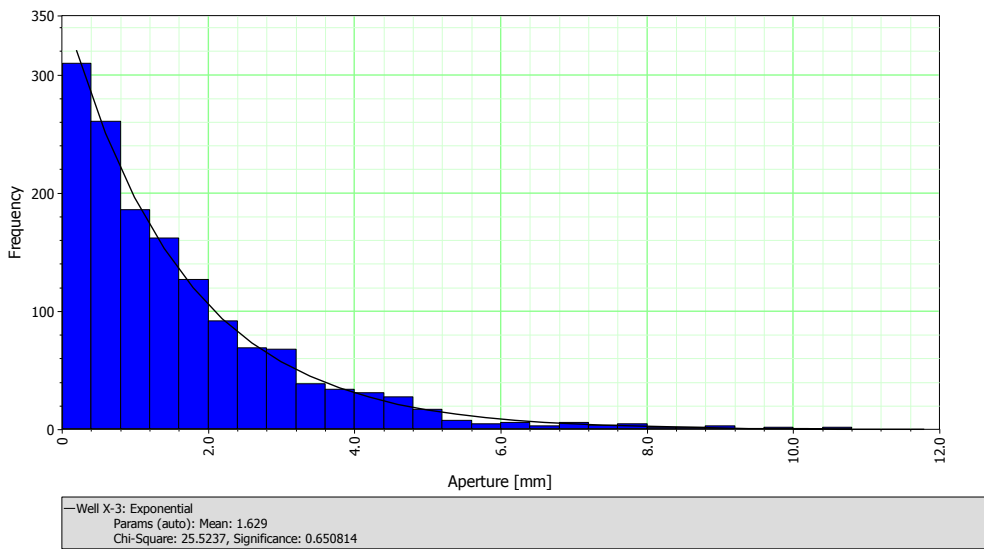
Figure 67: DFN Aperture Distribution for Well X-3
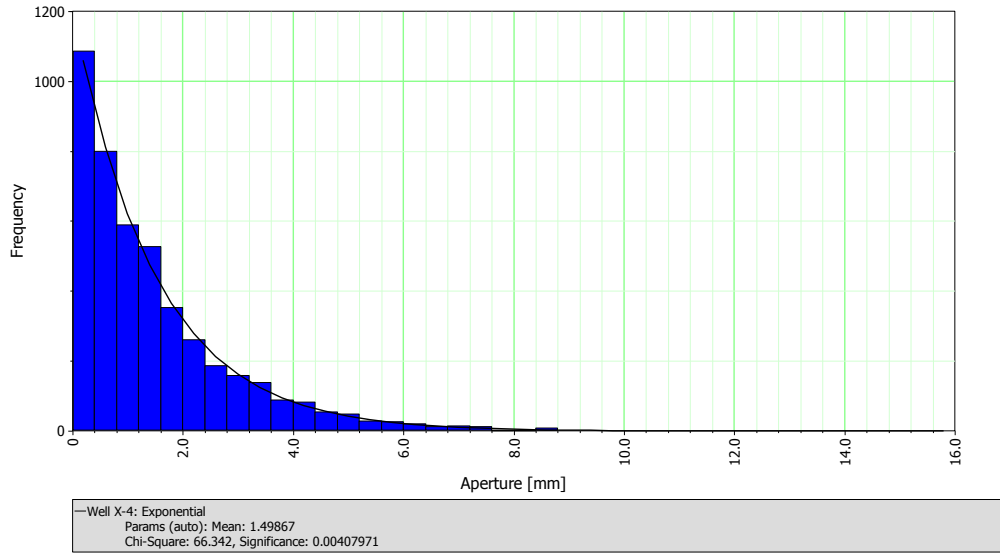
Figure 68: DFN Aperture Distribution for Well X-4
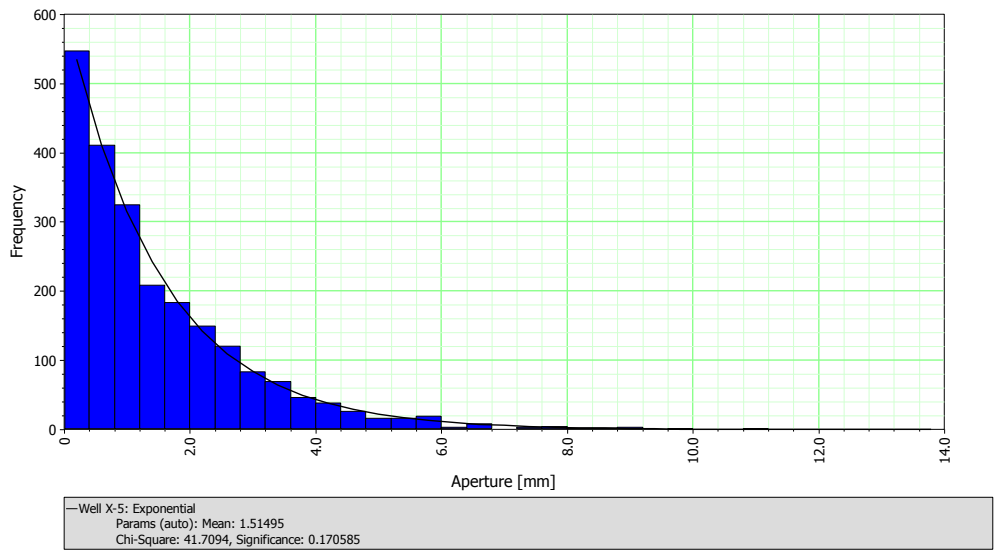
Figure 69: DFN Aperture Distribution for Well X-5
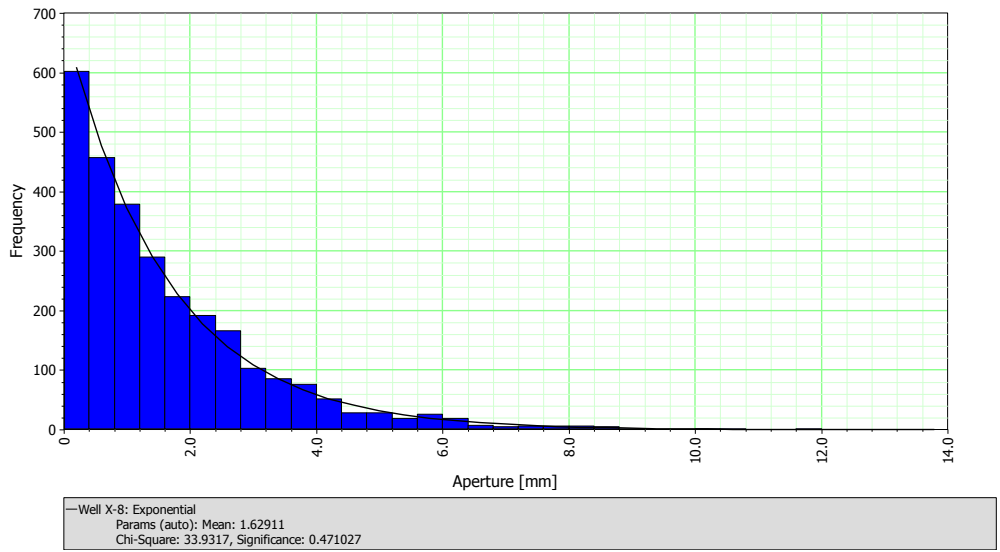
Figure 70: DFN Aperture Distribution for Well X-8
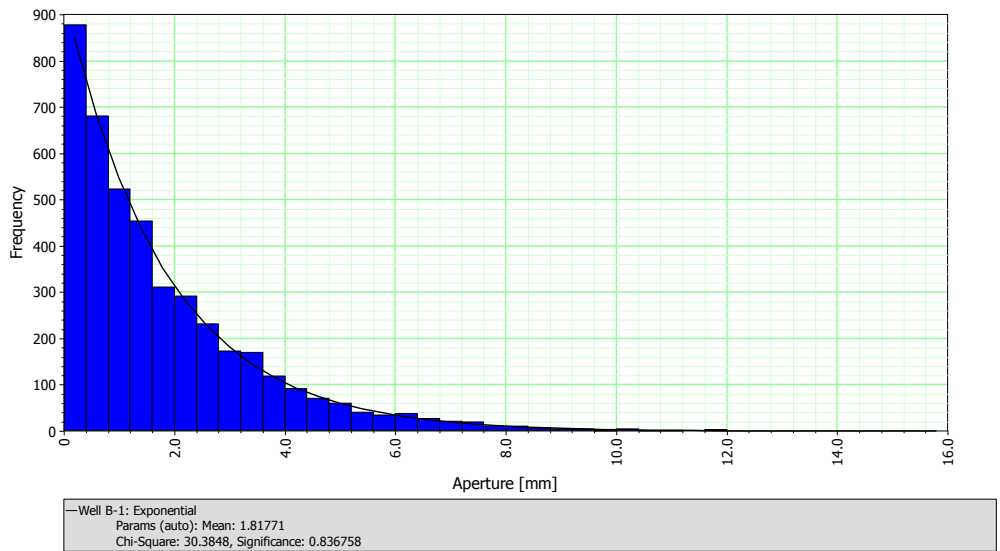
Figure 71: DFN Aperture Distribution for Well B-1
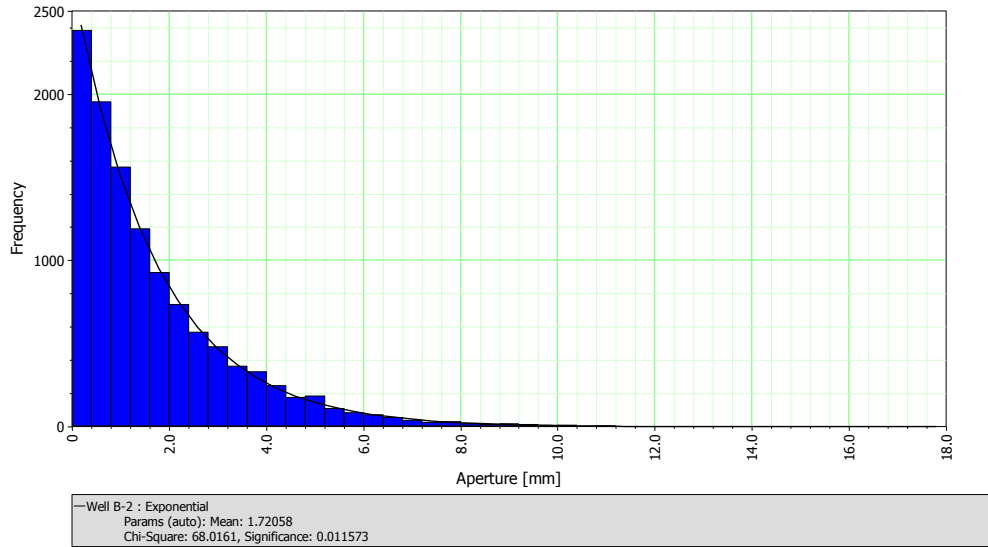
Figure 72: DFN Aperture Distribution for Well B-2
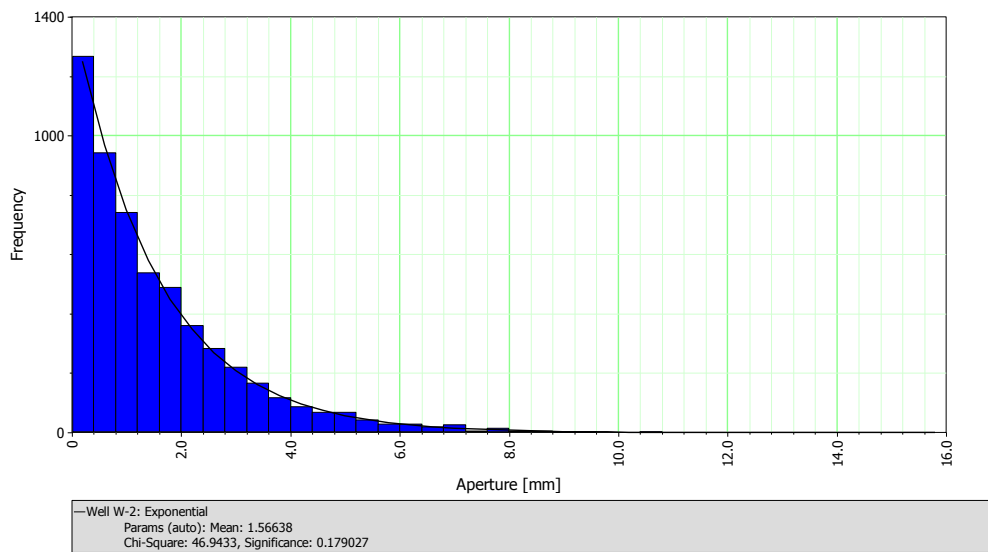
Figure 73: DFN Aperture Distribution for Well W-2
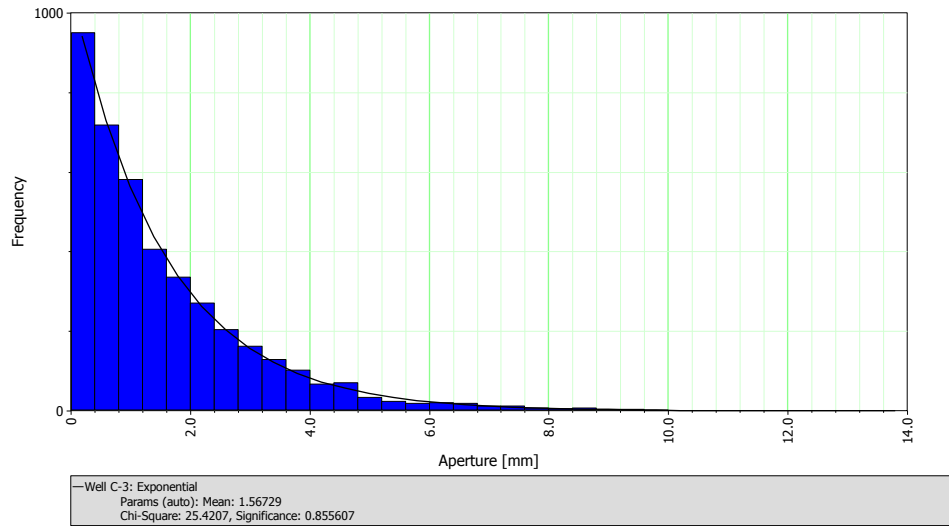
Figure 74: DFN Aperture Distribution for Well C-3

PRESSURE TRANSIENT TEST PLOTS
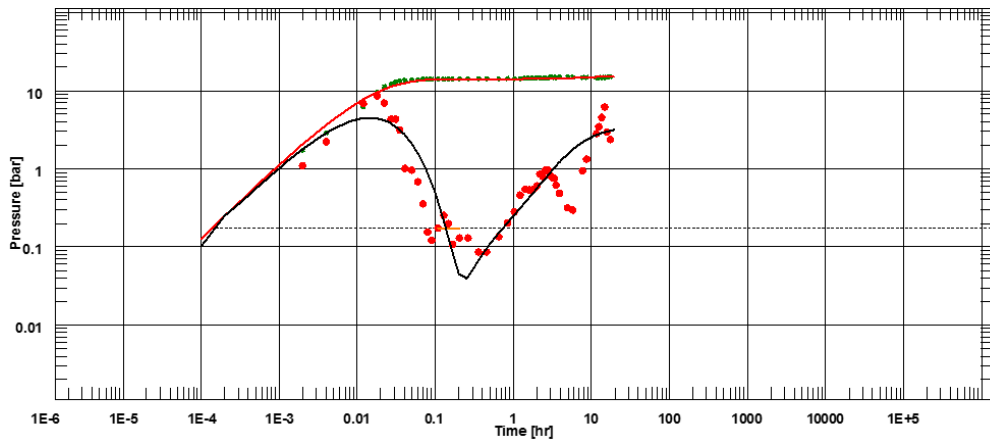
Figure 75: Log-log Plot of Well X-2 Pressure Buildup

Semi-Log plot: p [bara] vs Superposition Time
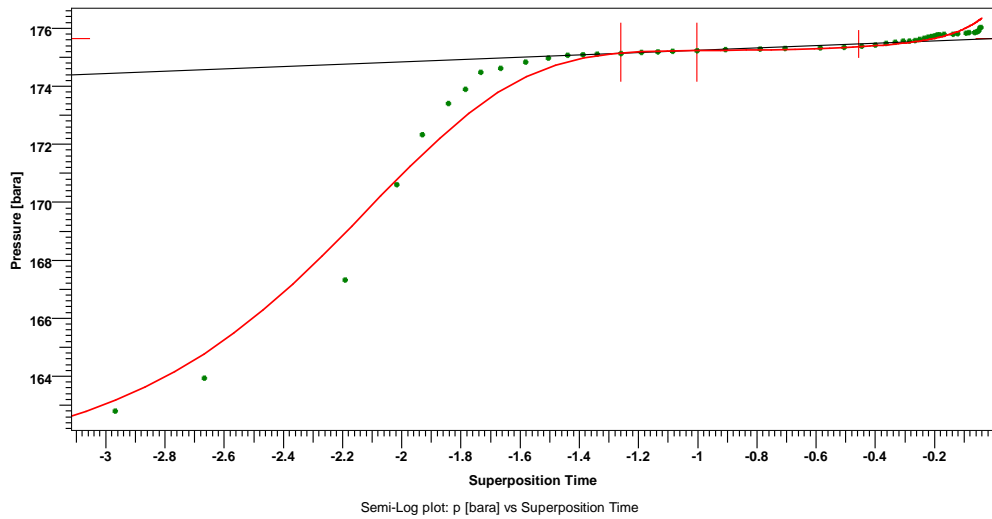
Figure 76: Semi-log Plot of Well X-2
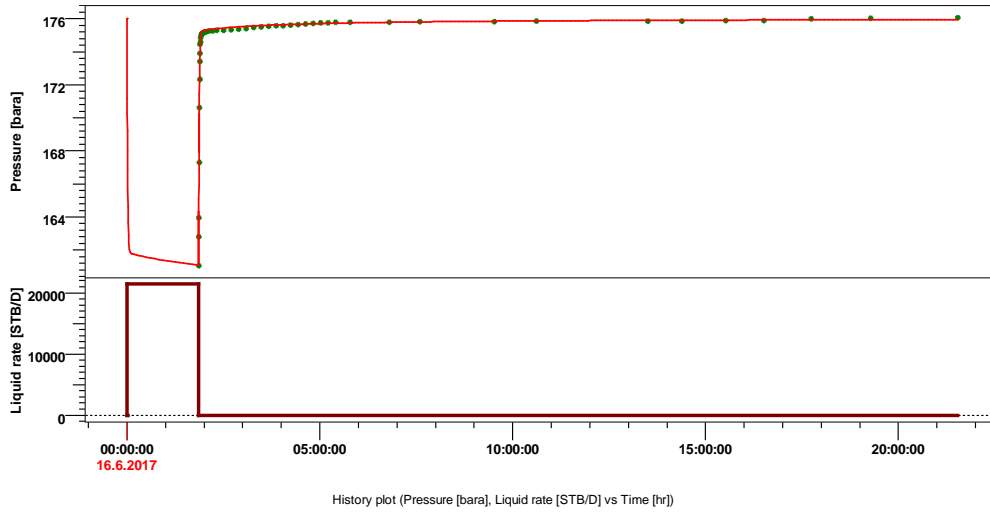
Figure 77: Pressure History Match of Well X-2
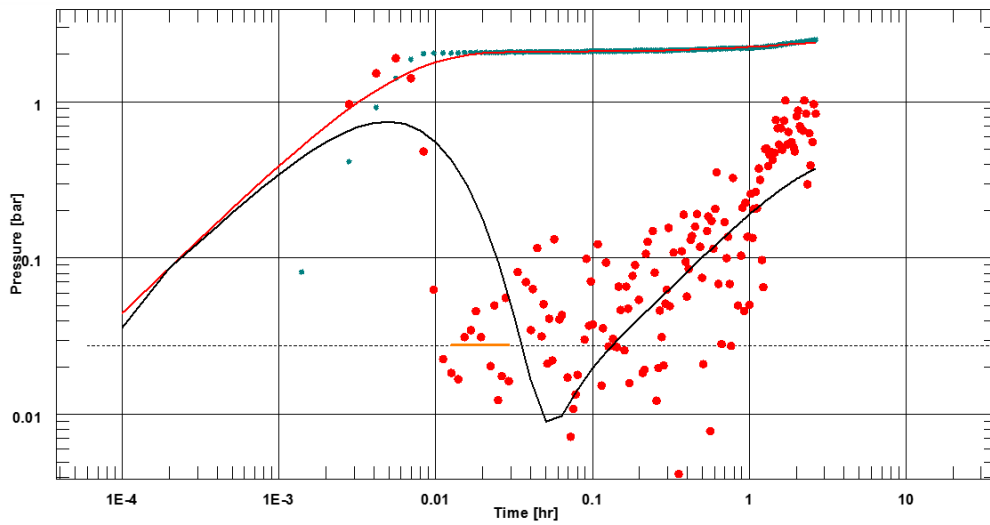
Figure 78: Log-log Plot of Well X-3 Pressure Buildup
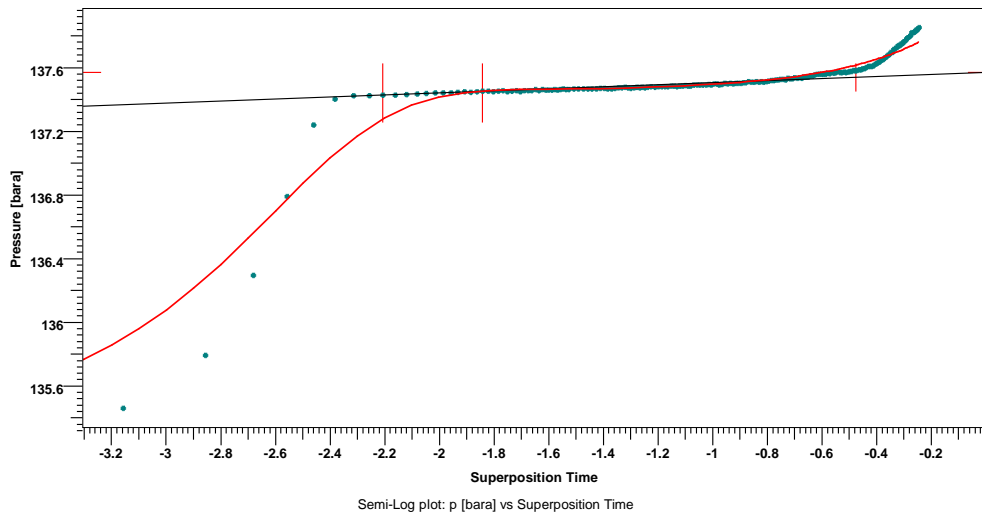
Figure 79: Semi-log Plot of Well X-3
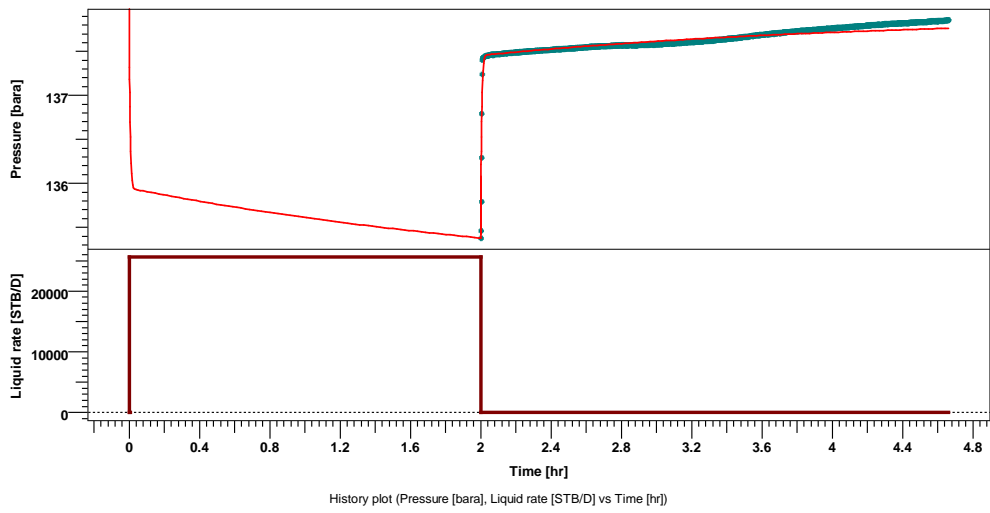
Figure 80: Pressure History Match of Well X-3
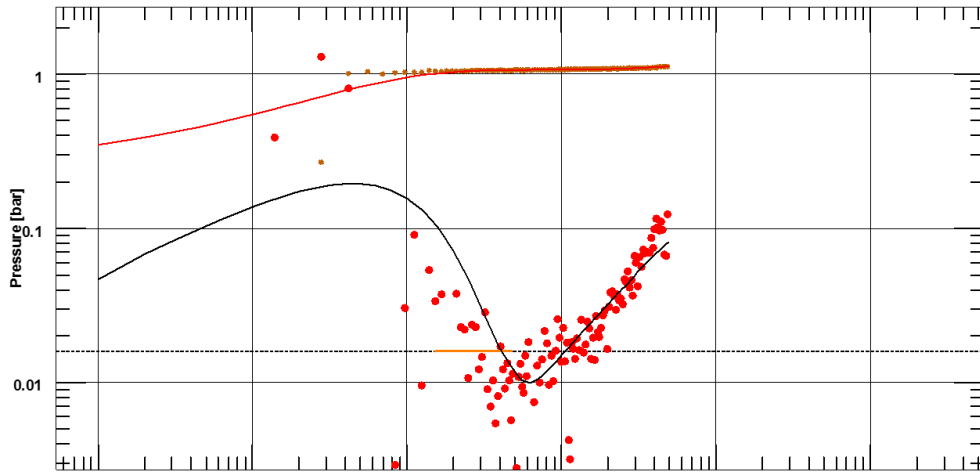
Figure 81: Log-log Plot of Well X-4 Pressure Buildup

Semi-Log plot: p [bara] vs Superposition Time
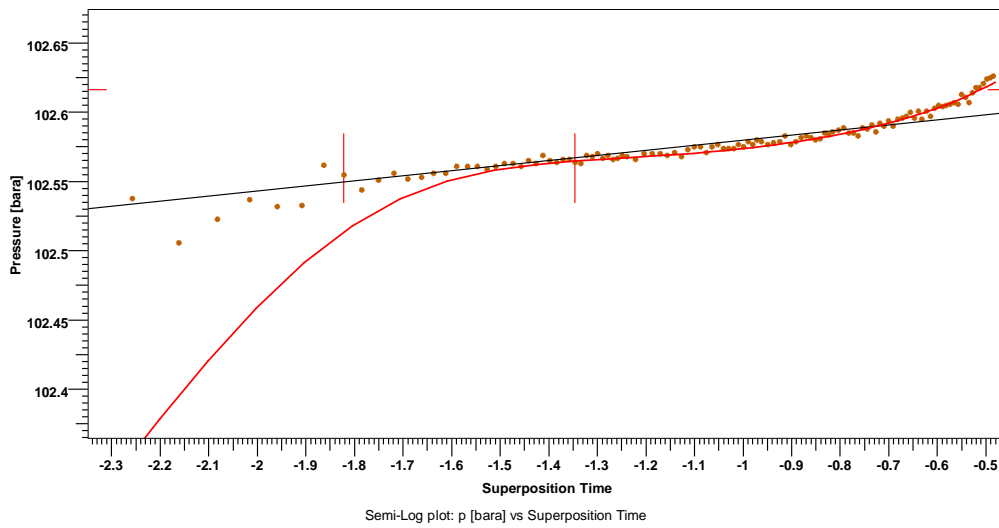
Figure 82:Semi-log Plot of Well X-4
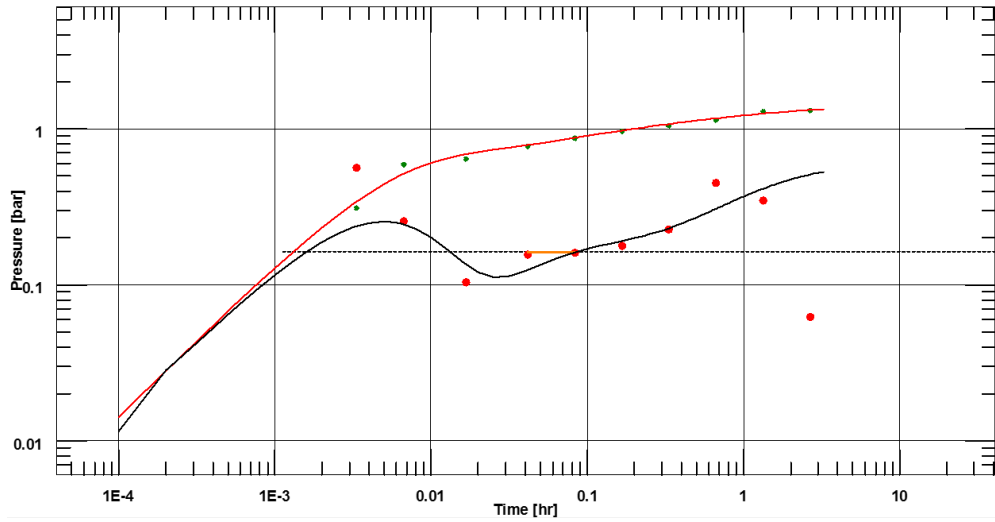
Figure 83: Log-log Plot of Well B-1 Pressure Buildup

History plot (Pressure [bara], Liquid rate [STB/D] vs Time [hr])
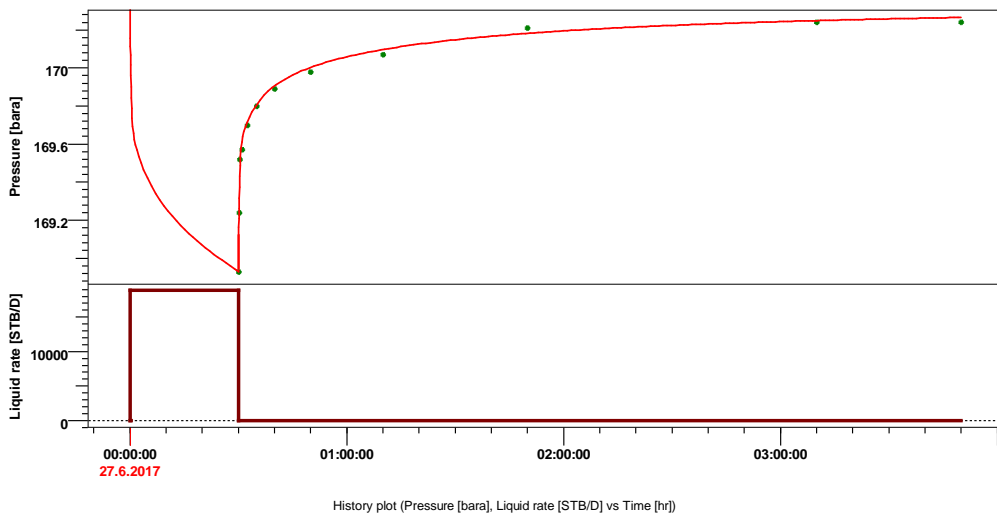
Figure 84: Pressure History Match of Well B-1
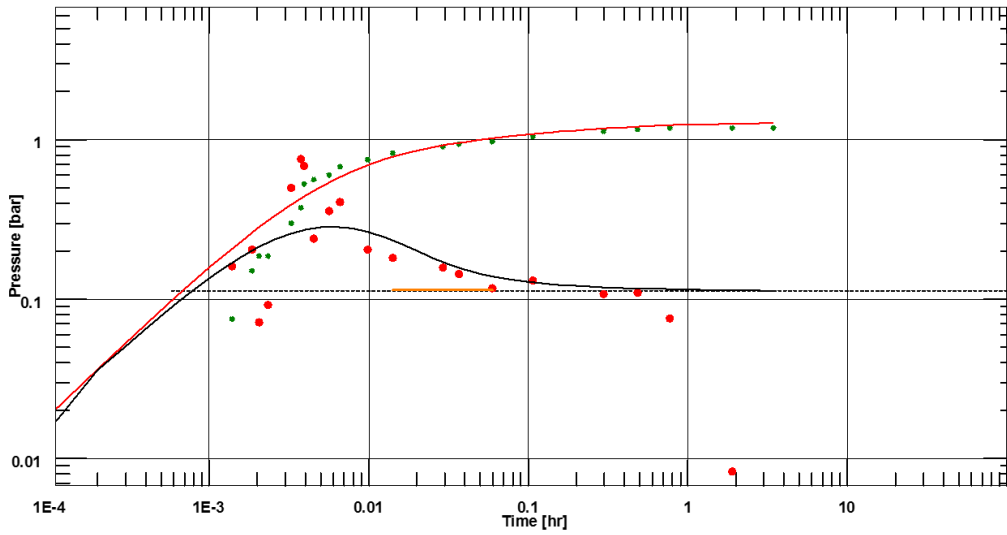
Figure 85: Log-log Plot of Well C-1 Pressure Buildup
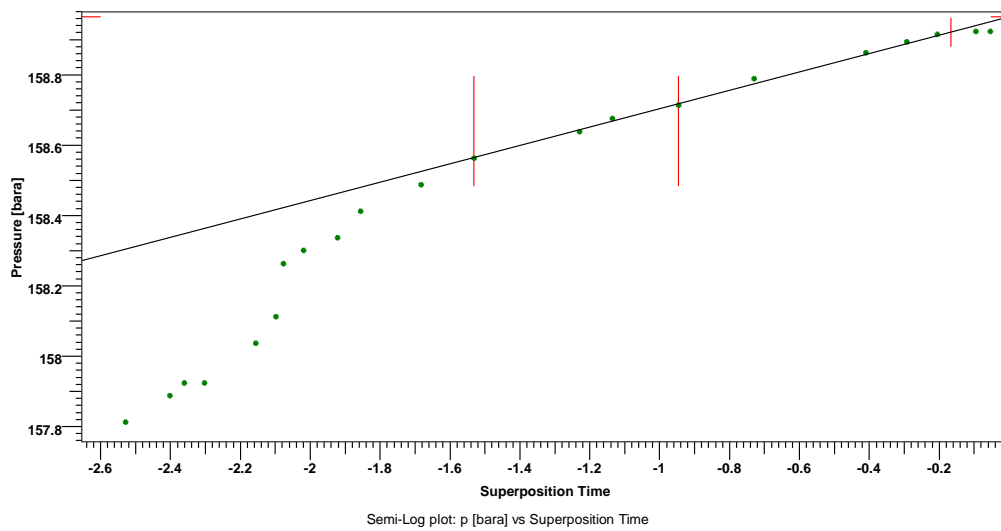
Figure 86: Semi-log Plot of Well C-1
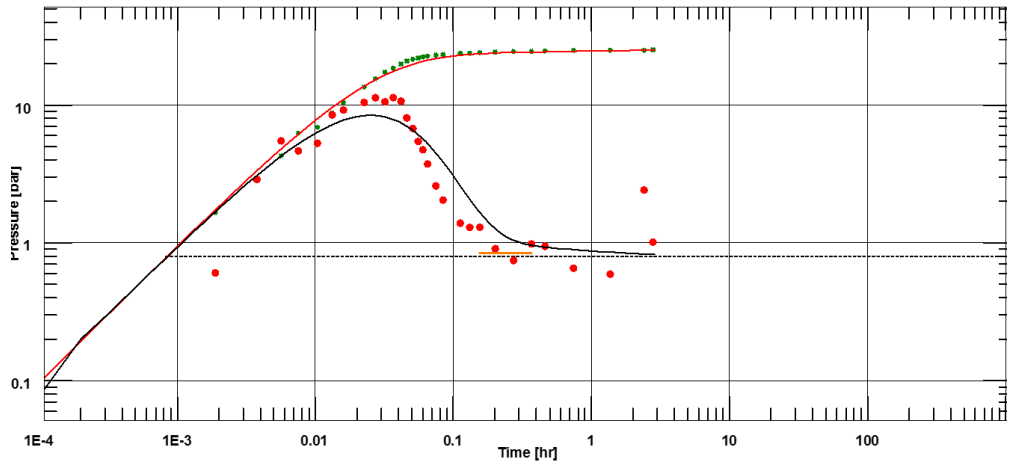
Figure 87: Log-log Plot of Well K-1 Pressure Buildup

Semi-Log plot: p [bara] vs Superposition Time
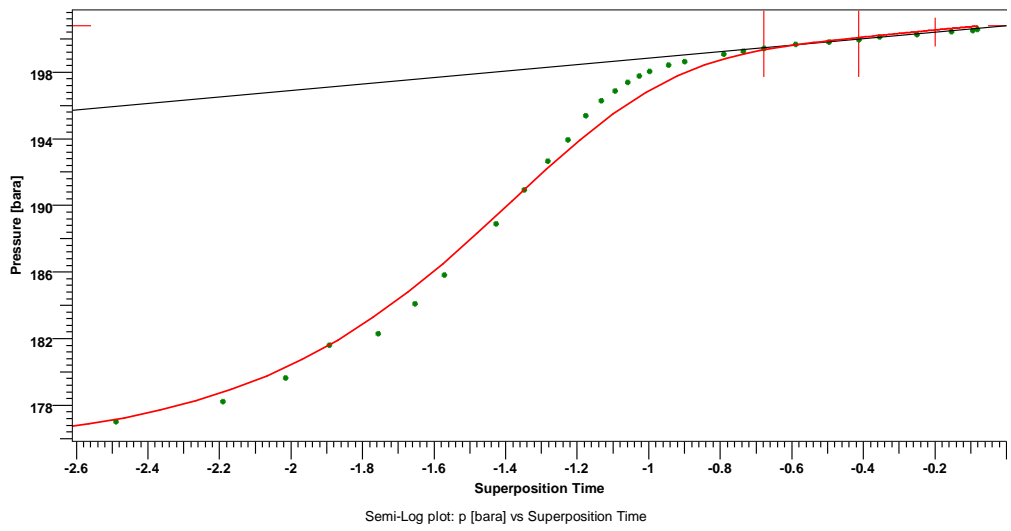
Figure 88: Semi-log Plot of Well K-1

103
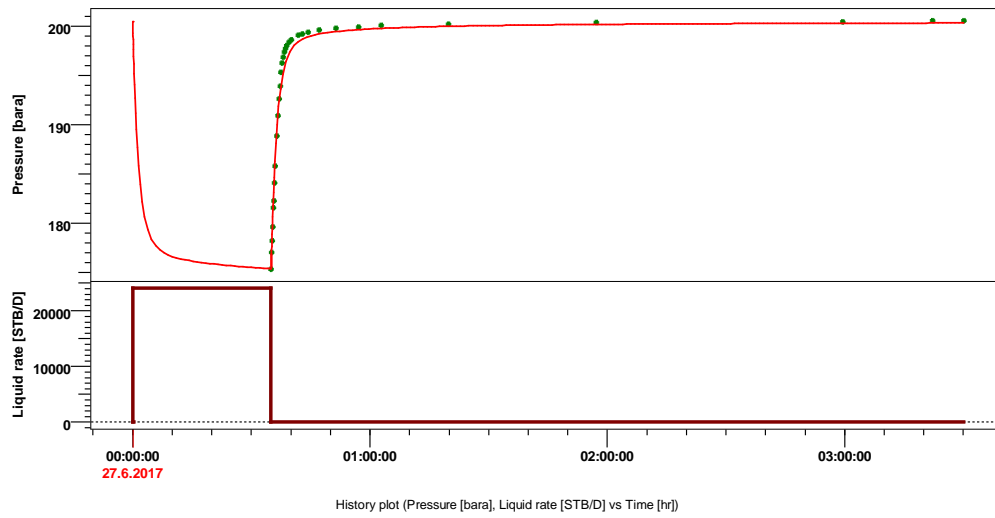
Figure 89: Pressure History Match of Well K-1
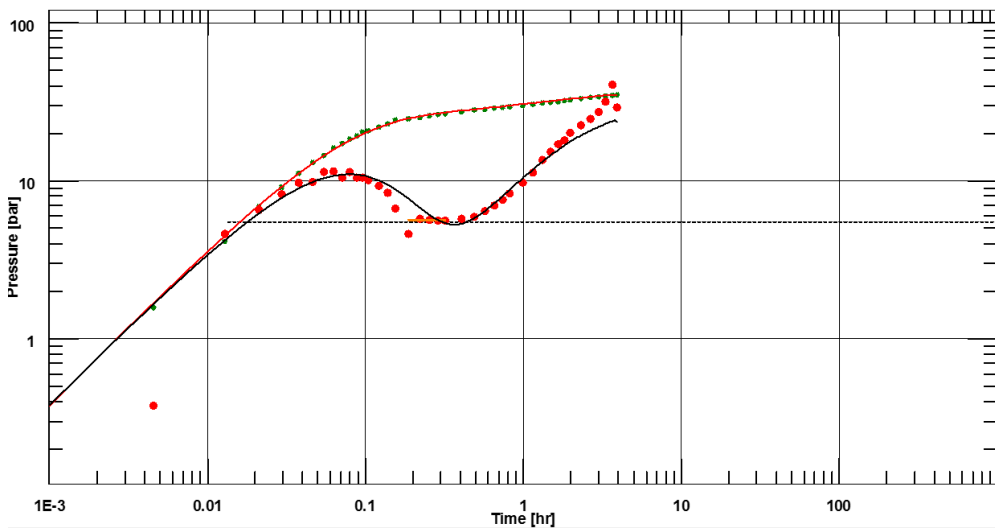


Figure 90: Log-log Plot of Well K-3 Pressure Buildup

Semi-Log plot: p [bara] vs Superposition Time
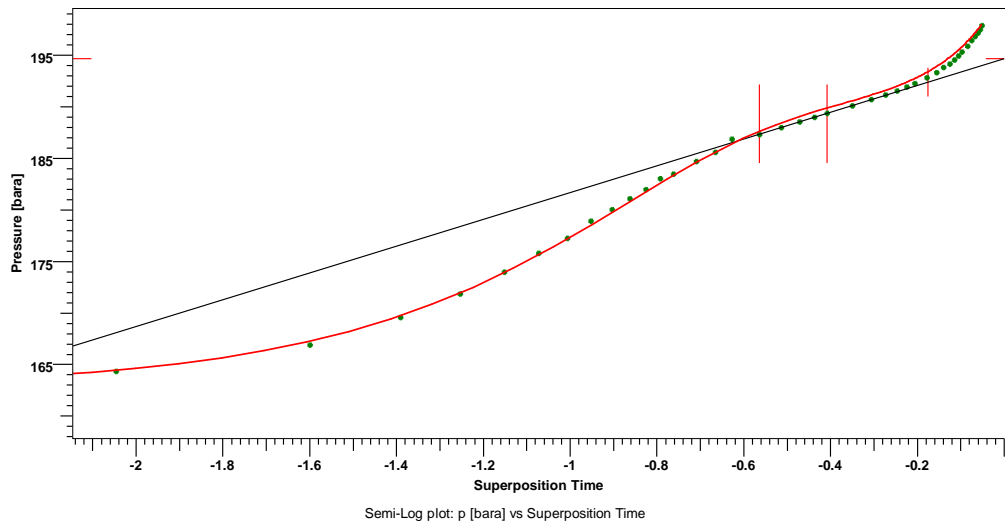
Figure 91: Semi-log Plot of Well K-3

History plot (Pressure [bara], Liquid rate [STB/D] vs Time [hr])
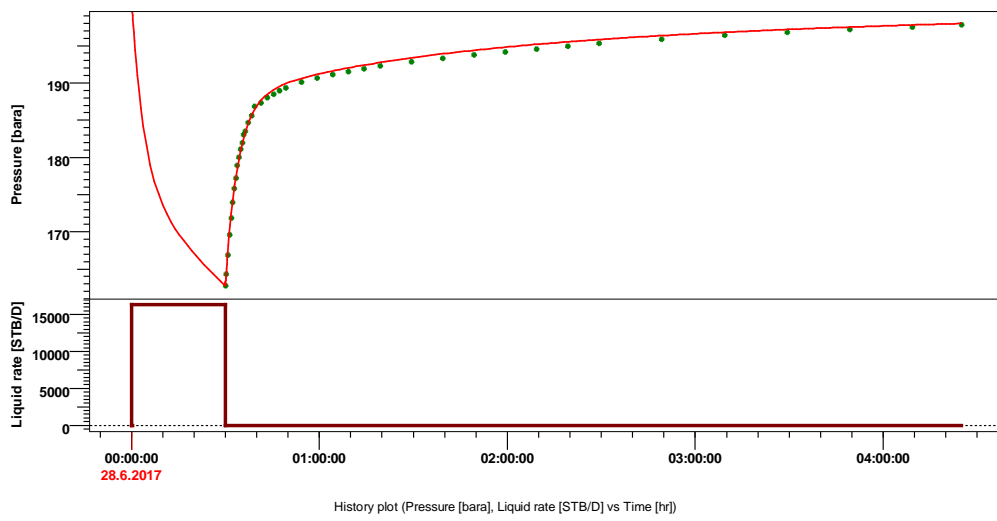
Figure 92: Pressure History Match of Well K-3
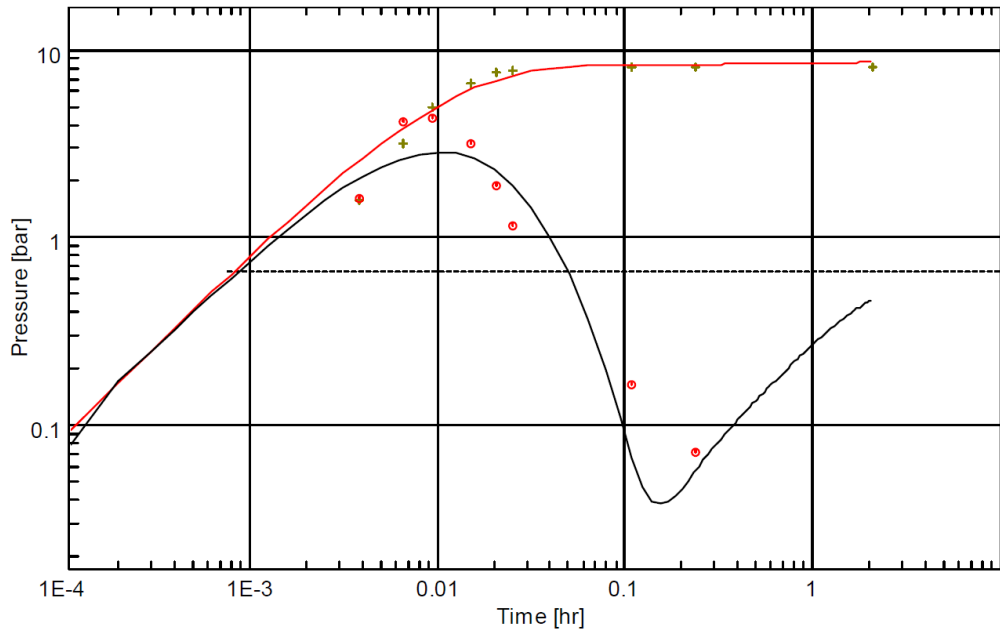
Figure 93: Log-log Plot of Well B-6 Pressure Buildup
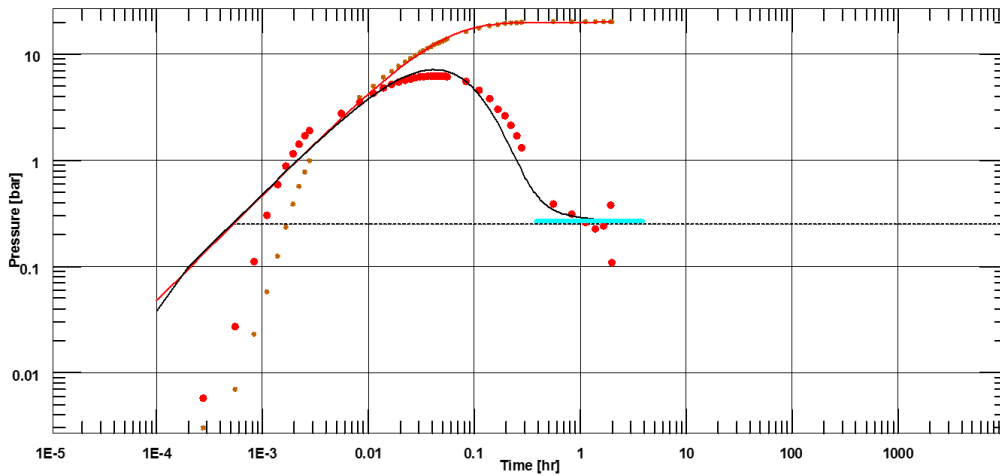
Figure 94: Log-log Plot of Well C-3 Pressure Buildup

106

Horner plot: p [bar] vs log(tp+dt)-log(dt)
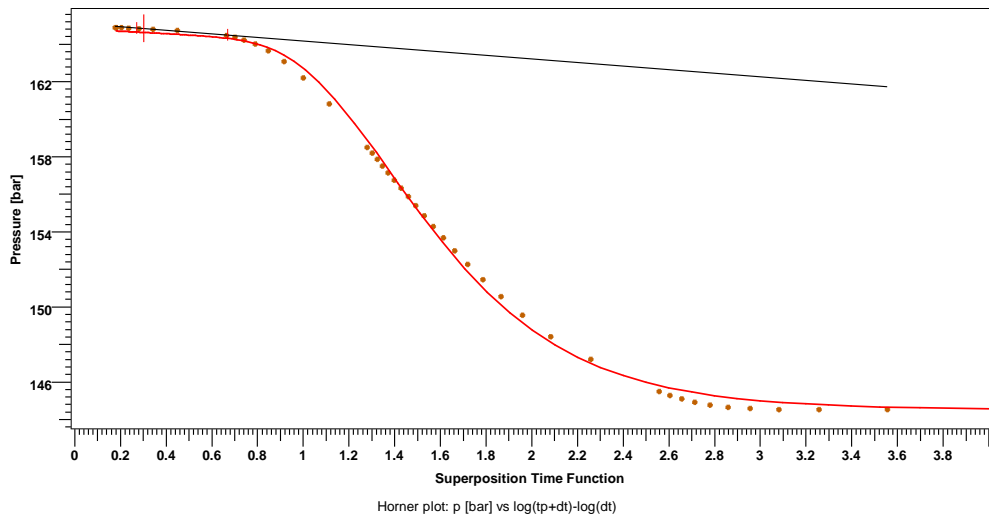
Figure 95: Semi-log Plot of Well C-3


History plot (Pressure [bara], Liquid rate [m3/hr] vs Time [hr])
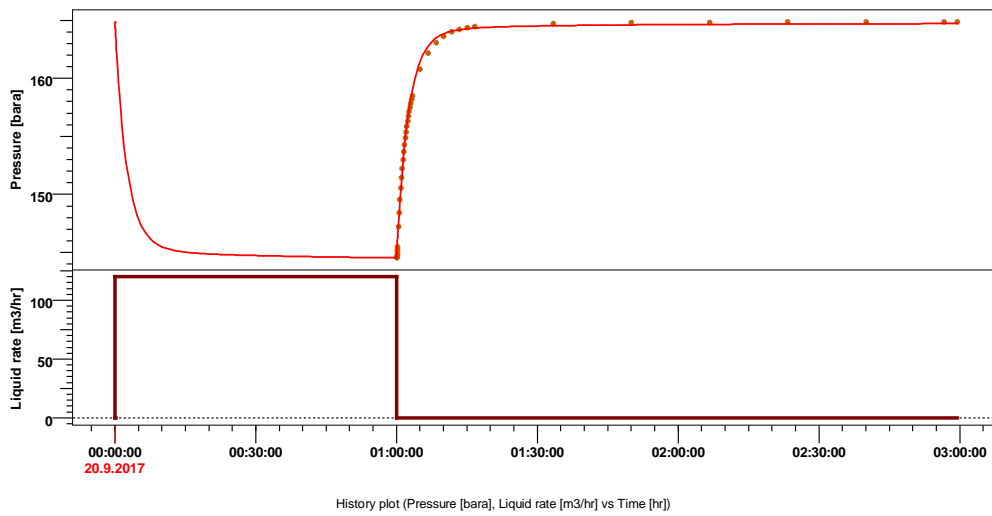
Figure 96: Pressure History Match of Well C-3